AN NMR INVESTIGATION OF THE ORGANIZATION AND DYNAMICS OF CHOLESTERYL ESTERS IN LIPOPROTEINS AND MEMBRANES

by

Walter Dale Treleaven

B.Sc., Simon Fraser University, 1977

THIS THESIS IS SUBMITTED IN PARTIAL FULFILLMENT

OF THE REQUIREMENTS FOR THE DEGREE OF

DOCTOR OF PHILOSOPHY

in the Department

of

Chemistry

APPROVAL

Name: Walter Dale Treleaven

Degree: Doctor of Philosophy

Thesis Title: An NMR Investigation of the Organization and Dynamics of Cholesteryl Esters in Lipoproteins and Membranes.

Examining Committee:

Chairman: Dr. T. N. Bell

Dr. R. J. Cushley
Senior Supervisor

Dr. E. Kiehlmann

Dr. K. Colbow

Dr. I. D. Gay

Dr. G. G. Shipley
Biophysics Department,
Boston University,
Boston

Date Approved: 7 February 1985

PARTIAL COPYRIGHT LICENSE

I hereby grant to Simon Fraser University the right to lend my thesis, project or extended essay (the title of which is shown below) to users of the Simon Fraser University Library, and to make partial or single copies only for such users or in response to a request from the library of any other university, or other educational institution, on its own behalf or for one of its users. I further agree that permission for multiple copying of this work for scholarly purposes may be granted by me or the Dean of Graduate Studies. It is understood that copying or publication of this work for financial gain shall not be allowed without my written permission.

Title of Thesis/Project/Extended Essay

"An NMR Investigation of the Organization and Dynamics of Cholesteryl Esters in Lipoproteins and Membranes"

Author: _____
(signature)

Walter D. (Dale) Treleaven
(name)

_____
(date)

Abstract

Cholesteryl oleate, deuterated at selected acyl chain positions has been incorporated into fresh human low density lipoprotein (LDL). Deuterium longitudinal relaxation times increase progressively between C8 and the methyl terminus indicating increased motion near the end of the acyl chain.

Temperature dependence of the ^2H NMR spectra was investigated between 15 °C and 45 °C. The linewidths generally decrease with increasing temperature. At chain positions 2, 5, and 8 the linewidths remain approximately constant above 35 °C indicating completion of the phase transition, while linewidths at positions 14 to 18 did not become constant at 35 °C indicating distal chain positions are less sensitive to phase behaviour. The ^2H NMR spectra at the C2 and C5 chain positions contain superposed broad and narrow signals. This was attributed to the coexistence of two ester regions of different order within the LDL core. At 15 °C, which is below the onset of the transition detected by differential scanning calorimetry, and at 45 °C which is above the transition temperature, both spectral components are observed for the C2 labelled ester. The ratio of the relative intensity of broad:narrow signals is ~60:40 and remains approximately constant over the temperature range studied. The C–^2H bond order parameters, S_{CD}, are ~0.20

for the more ordered region and 0.04-0.06 for the less ordered region.

Selectively deuterated palmitic acid was incorporated into the outer monolayer of LDL. The NMR spectra indicate two regions of different order, S_{CD} ~0.31 and ~0.05-0.07, which may reflect a non-uniform distribution of phospholipid, cholesterol, and protein at the LDL surface.

The location of cholesteryl esters within phospholipid bilayers was investigated by monitoring the effect of spin labels, placed at various positions in the ester molecule, on the ^{13}C spin-lattice relaxation times. The spin label induced relaxation rates, $1/T_{1,SL}$, of the phospholipid acyl chains indicate the C5 position of the ester acyl chain is located near the C1-C2 region of the phospholipid chain while the D-ring of the sterol rests near the C8 position of the phospholipid chains. These observations are consistent with the cholesteryl ester existing in a "horseshoe" conformation.

A greater spin label induced enhancement of relaxation rate was observed for the inner vesicle layer than for the outer one. This is attributed to higher ester incorporation and/or tighter packing in the inner layer.

To Sharon

ACKNOWLEDGEMENTS

The author wishes to express sincere gratitude to Dr. R. J. Cushley for his constant interest and guidance during the course of these investigations. Additionally the author wishes to extend his gratitude to Dr. E. Kiehlmann, and Dr. K. Colbow for the effort they have put forth as members of the supervisory committee and to thank Dr. S. Aronoff for the use his ultra-centrifuge.

The author further acknowledges his indebtedness to the other members of the research group, in particular Mr. Y. Parmar and Mrs. J. Thewalt, for the many helpful and provocative discussions.

Finally, the author wishes to thank Mr. F. Wick, who in spite of my lack of skill as a draughtsman, manufactured the racks in which the spectrometer is now located.

Financial support from the National Research Council of Canada and the British Columbia Heart Foundation in the form of research grants to Dr. R. J. Cushley, as well as the support of Simon Fraser University are gratefully recognized.

Table of Contents

LIST OF TABLES

LIST OF FIGURES

Chapter 1

Introduction

Membranes are complex arrays of lipids and proteins plus small amounts of carbohydrate. The relative proportion of each component is governed by specific membrane function. For example, myelin, of nerve tissue, contains 80% lipid while the inner mitochondrial membrane contains more than 75% protein (92,143). Frequently these membrane components display an asymmetric distribution throughout the membrane. In human erythrocytes, phosphatidylserine is preferentially located on the cytoplasmic side of the membrane, while 75% of the phosphatidylcholine is located on the outer half of the membrane. This uneven lipid distribution parallels a similar asymmetric distribution of protein in the erythrocyte (215).

Singer and Nicolson (185) described the macroscopic organization of biomembranes as a "fluid mosaic". According to this model, amphiphilic phospholipids are arranged in bilayers with hydrophilic regions exposed to the aqueous environment, while the hydrophobic acyl chains extend from the polar interface toward the central region of the membrane. Extrinsic proteins interact with membrane lipids only near the surface, while intrinsic proteins may extend through the bilayer. Rapid

lateral diffusion of membrane-bound proteins, in the plane of the bilayer, may result in collisions between proteins and thereby facilitate enzymatic processes.

Cellular metabolism is coordinated by biological membranes. This coordination is a consequence of compartmentalization of different organelles within a single cell, coupled with vectorial transport, through the membrane, brought about by membrane-bound proteins. Additionally, some membranes may promote enzymatic reactions by serving as a matrix in which specific proteins are embedded.

Model Membranes

Our present perception of membranes has been acquired predominantly through the study of model membranes. A review of model membranes has recently been published by Quinn (157). Model membranes offer the advantage of ease of preparation in relatively large quantities. Secondly, in contrast to natural membranes, their composition can be rigidly controlled, thus reducing the complexities of natural membranes.

In the presence of excess water (>40%), phosphatidylcholine, a phospholipid common to most natural membranes (100), readily forms lamellar bilayers (34). Consequently, phosphatidylcholine bilayers are frequently employed as models of natural membranes. The validity of this analogy is supported

by a variety of experimental evidence.

Natural membranes from several sources have been examined by X-ray diffraction (220). In each case, the diffraction pattern demonstrates the existence of a phospholipid bilayer. Furthermore, as in the case of model membranes (130), the bilayer thickness in A° is determined, for the most part, by the length of the fatty acyl chains present in the phospholipid. Maximum membrane thickness is observed below the phase transition temperature, and individual fatty acyl chains appear to be separated by approximately 4.15 A°. Above the transition temperature, membrane thickness is reduced while the acyl chain separation is increased to approximately 4.5 A°. In the case of phospholipid bilayers, a similar decrease in bilayer thickness, below the transition temperature, has also been reported in the presence of increased surface charge density (102). The physiological significance of this observation is not understood at the present time.

Comparative studies of molecular motion in phospholipid bilayers and biological membranes further illustrate the fidelity of lipid bilayers as model membranes. Nuclear magnetic resonance (NMR) techniques have demonstrated a characteristic similarity in the orientational order of lipid bilayers and bacterial membranes (67,201). More recently, investigators have reported that the orientational order of cholesterol in erythrocyte ghosts is the same as in model membranes (115).

The liquid crystalline components of membranes are characterized by their tendency to display regular long-range periodicity while, at the same time, as a consequence of molecular motion, appearing disordered at short-range. When heated, liquid crystals undergo a transition through one or more mesophases (34,193). Interest in the thermotropic phase behaviour of liquid crystals stems from the idea that different mesomorphic states may be biologically significant.

Differential scanning calorimetric (DSC) investigations of synthetic phosphatidylcholines reveal two transitions. The sharp, reversible, gel-to-liquid crystalline transition indicates a cooperative "chain melting" within the bilayer (34). In general, the temperature at which this transitition occurs, is dependent on the length and degree of unsaturation of the acyl chains (34,105). The nature of the olefinic bond also affects the transition temperature: a trans-unsaturated phospholipid will display a higher transition temperature than a cis-unsaturated phospholipid of the same chain length (34). Furthermore, the positional isomers of mixed acid phosphatidyl-cholines, containing acyl chains differing in length by just two methylene residues, display different gel-to-liquid transition temperatures. Generally, for each isomeric pair, the lipid with the longer acyl chain at the sn-1 position is characterized by the lower transition temperature (117,181). The much broader "pretransition" observed in these studies has been associated

with the formation of a "rippled" gel phase (105,181). Recent studies have shown this transition is not totally reversible, except after prolonged storage at temperatures considerably below the temperature where the pretransition is expected (181).

Calorimetric studies have been augmented by infrared spectroscopy. Infrared spectroscopy is sensitive to atomic vibrational modes such as bond stretching and scissoring, which, in turn, reflect conformation and dynamics of phospholipid acyl chains (49). Infrared spectra of fully hydrated dipalmitoyl-phosphatidylcholine demonstrate that the crystal lattice, below the pretransition temperature, is not rigid. Slightly below the pretransition temperature the acyl chains are in the all-trans conformation (32). As the temperature is reduced to -60 °C, the acyl chains tilt progressively more, with respect to the bilayer surface, and distort the hexagonal chain packing arrangement detected at higher temperatures by X-ray diffraction (107).

At the molecular level, the mobility and organization of model membrane constituents have been investigated using fluorescence (3,224), electron paramagnetic resonance (EPR) (30,44,48,99,161,173,208), and NMR spectroscopy. Since phospholipids are neither intrinsically fluorescent nor paramagnetic, these techniques are possible only after a suitably labelled probe has been incorporated into the model membrane. Fluorescence and EPR spectroscopy can detect as little as

0.1 - 1.0 umoles of a suitable probe; however, because such probes are frequently bulky, they perturb the environment being studied. Qualitatively the orientational order in lipid bilayers, as reflected by EPR and NMR are similar. However, investigators have demonstrated quantitative discrepancies between the results of EPR and NMR experiments (174,196,211). These differences have been ascribed to a disruption of the organization due to the bulky nature of the large spin label.

A major advantage of NMR is the fact that it is a non-perturbing technique. As a consequence, a great deal of our present understanding of the dynamic characteristics of lipids in model membranes has been obtained from a variety of ^{1}H (16, 140), ^{31}P (28,46), ^{13}C (11,18,38,69,70,116,131,167,169,214) and ^{2}H (172,175,176,196,202,203,211) NMR investigations.

Protons display a high natural abundance (99%) and a large magnetic moment, therefore the sensitivity of the nucleus is very high. However, the range of chemical shifts is small, and as a result the resolution is generally quite poor, due to the partially overlapping signals. Moreover, ^{1}H relaxation data are frequently difficult to interpret, since the relaxation rate may contain contributions from spin diffusion (142), as well as a combination of inter- and intramolecular dipolar interactions (68). Interpretation of proton relaxation data is further complicated, in model membranes, by the fact that the spin lattice relaxation rate is sensitive to both the radius of

curvature and the number of bilayers in the liposome (205).

Although ^{31}P is a very sensitive technique, it is of limited utility since the phosphorus nuclei are confined only to the phospholipid headgroup.

The natural abundance of ^{13}C is low (1.1%), and therefore ^{13}C is a less sensitive technique than ^{1}H NMR. However, through the use of Fourier transform (FT) NMR techniques this problem is readily overcome. ^{13}C NMR offers three important advantages over the use of ^{1}H NMR. Firstly, the ^{13}C nuclei display a wide range of chemical shifts (~200 ppm) resulting in much higher resolution than ^{1}H NMR (116). Secondly, the dominant relaxation mechanism is via intramolecular dipole-dipole interactions (129,197). Finally, unlike ^{1}H NMR, ^{13}C spin lattice relaxation rates are insensitive to the radius of curvature of the model membrane system, since the spin lattice relaxation time, T_1, of both multilamellar liposomes and unilamellar vesicles agree, within experimental error (167,169). This combination of increased resolution and lack of competing relaxation mechanisms make ^{13}C NMR a useful method by which to study rates of motion in phospholipid bilayers.

Natural abundance ^{2}H NMR is generally not practical, due to the low natural abundance (0.016%) and the small magnetic moment of the deuterium nucleus ($u_D = 0.25\ u_H$) (171). Selective replacement of a ^{1}H with its ^{2}H isotope plus the use of FT NMR techniques defeat this limitation. Indeed, the requirement for

selective labelling can be an advantage, since the ^2H resonance can then be immediately and unambiguously assigned. The dominant ^2H relaxation mechanism is the electric-quadrupolar interaction. Therefore interpretation of ^2H relaxation is less complicated than ^1H relaxation. The notable feature of ^2H is the fact that ^2H spectra are sensitive to both the rate of molecular motion as well as the orientational order at the site of the ^2H nucleus. This is important, since the ^2H spectrum then represents a convenient means of directly measuring the orientational order.

A frequently studied model membrane system is the unilamellar vesicle formed by ultrasonic irradiation of multilamellar liposomes (98). NMR spectra of vesicles are characterized by sharp resonance signals and increased resolution (16,59,167,202). This enhanced resolution observed in sonicated vesicles has been the subject of considerable debate. Several authors argue that the decrease in linewidth is the consequence of a decrease in the orientational order of the bilayer due to the high degree of curvature of the vesicle surface (132,133,152,166,179), while others contend the reduced linewidths can be explained by the increased tumbling rate of the vesicle (~250 A° diameter) and the order within the vesicle bilayer is unchanged (16,58-60,140,203). Attempts to resolve this controversy using DSC have served only to augment the debate. Sturtevant (207) reported the gel-to-liquid

crystalline phase transition, in vesicles, occured at a lower temperature and was accompanied by a lower enthalpy change than was observed in multilamellar liposomes. By way of contrast, De Kruijff et al. (46) were unable to detect either a decrease in the transition temperature or the enthalpy during the phase transition. The most recent evidence (152) points to a reduced orientational order in vesicles compared to liposomes. In view of this evidence, vesicles may not be the best general model of membrane structure or organization. Nevertheless, they do represent an excellent model of membrane regions which characteristically possess a high degree of curvature, such as the inner mitochondrial membrane, presynaptic vesicles, and coated pits near protein receptors. In addition, vesicles may be considered an approximate representation of the outer shell of low density lipoprotein (LDL). In this case, the analogy is particularly good since both unilamellar vesicles and LDL have approximately the same diameter.

Cholesteryl Esters in Model Membrane Systems

Cholesteryl esters comprise a second important class of membrane components which currently are the object of intense research activity. Experimentally, the link between atherosclerosis and the localized accumulation of cholesteryl esters has been well documented.

Atherosclerosis is characterized by the deposition of lipids in the walls of coronary arteries. The early stages of atherosclerosis are characterized by a general increase in the total lipid content of the aortic intima. These lipid deposits develop into fatty streaks, and in later stages, form fibrous plaques which protrude into the lumen of the aorta and restrict blood flow, thus leading to the condition known as ischemia (194). Lipids isolated from these lesions are, for the most part, cholesteryl esters (35). Lipid analysis of fatty streaks, isolated at autopsy, indicates cholesteryl esters constitute 77%-79% of the total lipid content of this type of lesion (112), and the majority of the cholesteryl esters are localized in oily droplets where they may represent as high as 95% of the total lipids present (127). Fibrous plaques are structurally more complicated, and various lipid components may separate into discrete phases. However, within the oily droplet phase, similar to fatty streaks, cholesteryl esters account for approximately 90% of the lipids (112,113).

Initial investigations of the phase behaviour and organization of cholesteryl esters in phospholipids employed a combination of optical and calorimetric techniques (104,106). In general, the solubility of cholesteryl esters in phospholipid is dependent on both the degree of hydration and the liquid crystalline state of the phospholipid. Maximum solubility of the unsaturated ester cholesteryl linolenate, in egg phospha-

tidylcholine, (egg PC) is reported to be 4.5 mol% over the range 15%-30% water by weight (104). As the degree of hydration is increased from 30% to 42%, the ester solubility decreases to a approximately 3 mol%, and remains unchanged upon further hydration. From X-ray diffraction patterns Janiak et al. (104) concluded that above 20% water by weight, cholesteryl linolenate existed in a "horseshoe" conformation such that the carbonyl of the ester was near the lipid-water interface, and both the steroid and fatty acyl moieties were essentially parallel to the phospholipid acyl chains. In the case of cholesteryl myristate, in dimyristoyl phosphatidylcholine (DMPC), at 37 °C, maximum solubility, ~5 mol%, was observed at 20% hydration. Below the phospholipid solid to liquid-crystalline transition temperature, 23 °C, cholesteryl myristate is insoluble in DMPC (106).

Surface pressure-molecular area studies of lipid monolayers have shown generally similar results with a wider range of cholesteryl esters (190-192). At surface pressures approximating pressures found in natural membranes, 30-35 mN/metre, cis-unsaturated cholesteryl esters displayed low solubility in dioleoyl phosphatidylcholine while both trans-unsaturated and saturated esters were insoluble.

Several magnetic resonance techniques have been employed to study molecular motion and conformation of cholesteryl esters. EPR studies of 1 mol% 5-doxyl cholesteryl palmitate, in oriented multilayers, reflect restricted motion in this region of the

acyl chain, with the nitroxide label displaced from the bilayer normal by of 47 degrees (79). Similar studies with 16-doxyl cholesteryl stearate indicate nearly isotropic motion near the methyl terminus of the acyl chain. These observations were interpreted as support for the "horseshoe" conformation proposed by Janiak et al. (104). At concentrations exceeding 1 mol% 16-doxyl cholesteryl stearate, EPR spectra resemble a superposition of two spectra, one originating from ester in a nearly isotropic environment, and the other from microdomains of solid ester (78).

The coexistence of "dissolved" and "solid" cholesteryl ester in egg PC liposomes has also been demonstrated by ^{2}H NMR (77,215). Moreover, the quadrupole splitting profile of selectively labelled cholesteryl esters lends further support to the proposed horseshoe conformation of cholesteryl esters. Analogous experiments with sonicated vesicles are consistent with the horseshoe conformation, however, cholesteryl esters appear to be more soluble in vesicles than in liposomes (39,76).

Phosphorus NMR experiments have demonstrated the differential effect of saturated and unsaturated cholesteryl esters on phospholipid vesicles. Incorporation of up to 5 mol% cholesteryl palmitate in vesicles at 33 °C significantly increased the permeability of the vesicles to praseodymium and EDTA ions, while cholesteryl linoleate appeared to have no effect on membrane permeability. These experiments demonstrate the

significance of the thermotropic state of the ester in model membranes, (64) since cholesteryl palmitate is in the gel state while cholesteryl linoleate is in the liquid crystalline state at this temperature.

Low Density Lipoproteins

Cholesteryl esters are transported throughout the body by lipoproteins, and of the four major classes of lipoproteins, low density lipoprotein (LDL) is the principal carrier (24,94). Elevated serum concentrations of LDL are known to correlate positively with the development of atherosclerosis (128,198, 221). Immunofluorescence techniques have illustrated a pattern of LDL accumulation that parallels the progressive development of atherosclerosis (95,96). In normal aortic tissue, no specific immunofluorescence was observed. On the other hand, fatty streaks and fibrous plaques did display immunospecific fluorescence. Tissue analysis indicates that increasingly more LDL is bound to the atherosclerotic lesion as the severity of the lesions progress (195). LDL isolated from normal tissue was of similar lipid composition to plasma LDL, while that found in atherosclerotic lesions displayed a reduced cholesteryl ester content (93).

LDL is derived intravascularly by the enzymatic structural reorganization of very low density lipoprotein (VLDL). The

in vivo conversion of VLDL involves several lipolytic enzymes. Current evidence suggests that as VLDL is degraded, apo-C, triglycerides and some phospholipids are transferred from VLDL to high density lipoprotein (HDL) while apo-B and the remaining core remnants are selectively retained, thus forming intermediate density lipoprotein (IDL) which is in turn rapidly converted to LDL (53-56,146,200). Analysis of chemical composition reveals that, on average, LDL contains 21% protein, 22% phospholipid, 37% cholesteryl esters, 11% triglyceride and 8% free cholesterol (162).

From the point of view that IDL can be isolated as a discrete entity within the density range 1.006-1.019, IDL may be considered a separate class of lipoprotein. However, experiments in man indicate that this lipoprotein species is only short lived, and therefore IDL is generally considered only as a precursor of LDL.

In normal humans, VLDL appears to be the only source of LDL (54). However in patients suffering from the homozygous form of hypercholesterolemia (198) or diabetics displaying hypertriglyceridemia (155) direct hepatic secretion of LDL may be important. Normal subjects too may secrete LDL directly, however if this does occur, the amount of LDL produced by this mechanism is so low as to escape detection (74).

The uptake of LDL has been characterized primarily as a result of studies of several cultured cell lines (22-24,63,71,

73,145,180). In the presence of calcium ions LDL binds electrostatically to a high-affinity LDL receptor located on the cell surface in regions known as coated pits (81). Cultured cells from patients suffering from familial hypercholesterolemia have been shown to possess either no high-affinity LDL receptor (receptor-negative) or receptors of impaired function (receptor-defective)(74,75). As a result, the biological half-life of LDL, in these patients, rises from the usual 3-4 days reported in normal humans (128,184) to more than six days (198). More recently, the importance of the high affinity receptor has been demonstrated, in vivo, in humans. Uptake of LDL by this receptor accounts for 30-50% (25,184) of the total daily LDL uptake. The remainder of the daily uptake of LDL is thought to come about by a low-affinity LDL receptor (63,71,145). Recently, in two cell lines previously classified as receptor-negative, a low affinity LDL receptor has been reported (180).

The currently accepted structural model of LDL has grown from the results of a variety of experimental techniques. Negative staining electron microscopy indicated LDL is an approximately spherical particle with a characteristic diameter of 200 to 250 A° (66). At very high magnification, in addition to the apparent fine structure on the LDL surface, fine serrations were evident on the edge of individual particles.

Small-angle X-ray scattering experiments confirm the electron microscopy investigations, and extend these studies to

present a more detailed understanding of the interrelationship between individual LDL constituents (7,8,42,43,124,138,210). Polar phospholipids, free cholesterol and apoprotein-B are confined to the outer shell of the LDL particle while the apolar triglycerides and cholesteryl esters are localized within the core of the particle (7,8,124,138,210). Tardieu and coworkers (138,210) report that the polar shell is convoluted, and protein is distributed over the surface in apparently tetrahedral symmetry. Similarly, neutron scattering experiments indicate a phospholipid monolayer surrounds a core of cholesteryl esters and triglycerides with the protein protruding 5 to 10 A° above the phospholipid head groups (126,206). A recent freeze-etching electron microscopy study also reports the existence of small globules, presumably protein, on the surface of LDL (80).

Molecular organization within the core of LDL is still the subject of disagreement. Luzzati et al (138) contend the cholesteryl esters form small micelle-like domains of ~16 A° diameter which are arranged in a cubic matrix within the LDL core. Alternatively, several experimenters (7,8,42,43,124) assert that at temperatures near 10 °C the cholesteryl esters and triglycerides form two concentric spheres within the core, while a less orderly geometry is predicted at temperatures near 45 °C. Each model of the LDL core depends heavily on the specific assumptions made by their respective proponents. Final resolution of this controversy awaits further experimentation.

Figure 1 shows a schematic representation of LDL as proposed by Deckelbaum and coworkers.

Cholesteryl esters with unsaturated acyl chains predominate in LDL, with cholesteryl linoleate and cholesteryl oleate typically accounting for ~50% and ~25% of the ester content of human LDL (162). In monkeys, diets rich in saturated fats elevate the transition temperature of LDL (209)(see below). Furthermore, it has been reported that increased levels of saturated cholesteryl esters closely parallel the development of atherosclerosis in these animals (209). From these findings, it is evident that the phase behaviour of LDL is important.

Phase behaviour of human LDL has been investigated by differential scanning calorimetry (DSC) (4,43). Between 0 °C and 60 °C native LDL displays a broad reversible transition beginning at ~ 20 °C and ending at ~40 °C. Synthetic mixtures containing cholesteryl esters and triglycerides, in proportions aproximating those in LDL, display similar transitions. No thermal transitions are observed within this temperature range when triglycerides, cholesterol, or phospholipids, isolated from LDL, are investigated. Therefore, this transition is associated solely with a phase transition of the cholesteryl esters. This phase transition is associated with an enthalpy change of 0.69 cal/g of ester (42), while in cholesteryl esters isolated from LDL the associated enthalpy change is 1.01 cal/g of ester. Deckelbaum et al (42) suggest the reduced enthalpy change may be

Figure 1. Model of low density lipoprotein structure

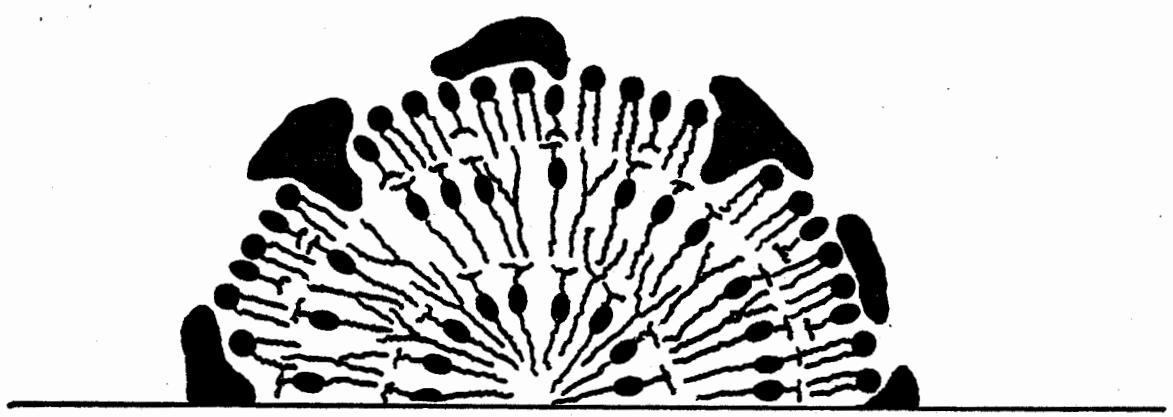

PROTEIN

CHOLESTEROL

CHOLESTERYL ESTER

PHOSPHOLIPID

TRIGLYCERIDE

related to structural constraints within the LDL core. Two observations appear to support this hypothesis. Firstly, while thermally denatured LDL displays a broad transition extending from ~10 °C to ~40 °C the enthalpy of this transition is 0.89 cal/g of ester. Secondly, upon cooling from 50 °C to 17 °C, thermally denatured LDL undergoes an additional transition at 17 °C, while no such exothermic transition is displayed in native LDL. A similar transition, associated with cholesteryl ester crystallization, has been demonstrated in isolated cholesteryl esters or cholesteryl esters containing small amounts of triglycerides (43).

Thermal transitions within the LDL have also been studied by circular dichroism (188). When cholesteryl cis-parinarate (see p.128) is incorporated into the core of LDL, the magnitude and the sign of the induced circular dichroism vary with temperature. The variation of the circular dichroism parallels closely the DSC transition recorded on the same labelled LDL sample. It should be indicated however, that the incorporation of cholesteryl cis-parinarate into LDL did depress the DSC transition by 10-15 °C from that observed in native LDL (188). Thorough understanding of the circular dichroism behaviour is not possible at this time and awaits future development of a complete theoretical description of this phenomenon.

Within the LDL core, molecular motions have been probed using fluorescence spectroscopy (189). Throughout the

temperature range 2 °C to 30 °C, cholesteryl cis-parinarate exhibits two distinct fluorescence lifetimes indicating the coexistence of two discrete environments within the LDL core. The relative proportion of the short- and long-lived components is strongly temperature dependent. Sklar et al. assert that core lipids are highly immobilized as indicated by the extraordinarily high value (~.78) of the order parameter they measure (189). Furthermore, they reported that the order parameter is relatively insensitive to temperature over the range 1.8 °C to 30 °C. This observation is difficult to reconcile with similar experiments reported by Sklar et al. (188) showing that a thermal transition does occur in this temperature range as evidenced by both DSC and circular dichroism.

Data measured by EPR experiments are not in complete agreement with evidence exhibited by fluorescence techniques (114,119). In accord with fluorescence data, EPR experiments indicate the coexistence of domains of substantially differing degrees of molecular motion (114). However, in sharp contrast to fluorescence data, EPR spectra of spin labelled cholesteryl stearate, in LDL, suggest molecular order in the LDL core is very low (114). Also, in agreement with calorimetry experiments, EPR results provide evidence that a thermal transition occurs in the LDL core near 30 °C (119). Moreover, the Arrhenius-type plot presented by Keith et al. (114) alludes to a complex pattern of phase behaviour within the LDL core.

While both fluorescence and EPR spectroscopy are very sensitive and useful techniques, for reasons already discussed earlier in this chapter, they are not without their limitations. NMR spectroscopy, on the other hand does not suffer from such impediments. As a consequence, NMR spectroscopy is particularly well suited to the study of both molecular motion and structural organization in LDL. The structural arrangement of phospholipid headgroups in LDL has been investigated using ^{31}P NMR. Similar experiments using sonicated phosphatidylcholine vesicles, in the presence of paramagnetic shift reagents, clearly demonstrate the existence of a bilayer structure in the vesicles (64). Analogous experiments with LDL in the presence of lanthanide (226) or manganese ions (90) reveal that 100% of the observable phosphorus signal is shifted or broadened by the paramagnetic ions. Corroborating evidence has been presented by ^{1}H NMR experiments which demonstrate that all the observable $N(CH_3)_3$ protons are shifted upfield in the presence of ferricyanide ions (61). However, when manganese ions are chelated with ethylenediaminetetraacetic acid (EDTA) (Mn^{2+}:EDTA = 1:2.2) only 50% of the LDL phosphorus signal is broadened (90). Yeagle et al. calculated that the observable phosphorus signal accounts for only 80% of the phosphorus nuclei present in the LDL (225) while the remaining 20% are thought to be immobilized such that the resonance is too broad to detect. Taken together, these results demonstrate the complex nature of the LDL surface. On

the basis of the current evidence, it seems likely that the phospholipid exists as a monolayer on the LDL surface such that the phospholipid head groups are exposed at the phospholipid-aqueous interface. Regions of the surface may be covered by protein but small paramagnetic ions appear able to "penetrate" the protein and thereby affect equally the ^{31}P resonance of all phospholipids while large complexes containing paramagnetic ions are blocked by the protein. Ions as large as 9 A° are able to penetrate the protein since the ferricyanide ion is reported to be ~9 A° in diameter (61).

Early investigators, using proton NMR, reported that none of the pholpholipid acyl chains are immobilized in LDL due to the presence of apo-B (199). More recently, the effect of temperature on lipid mobility has been studied by ^{1}H NMR (121). Kroon and Kreiger (121) acknowledged the fact that the fatty acyl chain resonances contain contributions arising from phospholipid, triglycerides, and cholesteryl esters. They contend however, that since cholesteryl esters comprise the most abundant class of lipid (by weight), they will dominate the observed signal. A study of the spectral amplitude of the methylene resonance as a function of temperature, reveals one break at 26 °C and a second, more prominent break at 36 °C. These break points are in harmony with DSC data recorded on the same sample and were therefore interpreted as a manifestation of the onset and completion of a thermal transition within the

LDL core (120).

The greater range of ^{13}C chemical shifts allows some cholesterol resonances to be resolved well away from other overlapping lipid resonances (82,83,122,168). At 50 °C, well above the DSC transition temperature (168), the ^{13}C NMR spectrum of LDL is characterized by several well resolved resonances each displaying relatively narrow linewidth. As the temperature is decreased the sterol resonances broaden and at 10 °C are difficult to detect. Over the same temperature range, the acyl chain methylene resonances broaden significantly less. Parallel experiments using neat esters (168) or mixtures of cholesteryl esters plus triglycerides (84) confirmed this observation. In neat cholesteryl esters, the acyl chain resonances remain narrow until the onset of the smectic phase.

The interpretation of NMR spectra in terms of molecular motion of specific LDL constituents demands an unambigous assignment of the NMR resonances. In the case of both ^{1}H and ^{13}C NMR however, the composite nature of the majority of the resonance signals limits the utility of these techniques. These limitations can be overcome through the use of selectively deuterated compounds.

Objective of the present research

The present research embraces two purposes: firstly, using ^{2}H NMR the orientational order within the core and the outer shell of human LDL_{2} will be studied and secondly, natural abundance ^{13}C NMR experiments will be conducted to investigate the orientation of cholesteryl esters in sonicated vesicles.

The relationship between membranes, cholesteryl esters and low density lipoprotein is well documented. A thorough comprehension of the molecular organization within LDL is an essential prerequisite to the understanding of LDL assembly and its interaction with membranes.

Chapter 2

Materials and Methods

I. Materials

Cholesterol, purified napthalene crystals, certified ACS grade 1,4 dioxane, chloroform and hexadecanoic acid were purchased from Fisher Scientific Co., New Jersey. Cholesterol was recrystallized from benzene before use. Cholesteryl linoleate, triolein, 1,1'-carbonyldiimidazole and deuterium depleted water were purchased from Sigma Chemical Co., St. Louis. Deuterium oxide (99.8% ^{2}H), [5,5,6,6,-$^{2}H_{4}$]hexadecanoic acid, and [11,11,12,12-$^{2}H_{4}$]hexadecanoic acid were purchased from Merck, Sharpe and Dohme Canada, Ltd. Hexadecanoic[16,16,16-$^{2}H_{3}$] acid was purchased from Serdary Research Laboratories, London, Ontario, Canada. Hexadecanoic[2,2-$^{2}H_{2}$] acid was a kind gift from Dr. H. Gorrissen. "Baker analyzed" silica gel, 60-200 mesh, was purchased from J. T. Baker Chemical Company, Philipsburg, New Jersey. Reagent grade ethylene glycol and acetone-free methyl alcohol were purchased from American Scientific and Chemical, Portland, Oregon. Manganous chloride was purchased from General Chemical Division of Allied Chemicals, Morristown, New Jersey, U.S.A. Cholesteryl

[1-^{14}C]Oleate, [1-^{14}C]hexadecanoic acid and liquifluor (NEF-903) were supplied by New England Nuclear, Boston, Mass. Hexadecanoic-[4,4-$^{2}H_{2}$] acid, [2,2-$^{2}H_{2}$]octadecenoic acid, [5,5-$^{2}H_{2}$]octadecenoic acid, [8,8-$^{2}H_{2}$]octadecenoic acid, [14,14-$^{2}H_{2}$]octadecenoic acid, [16,16-$^{2}H_{2}$]octadecenoic acid and [18,18,18,-$^{2}H_{3}$]octadecenoic acids were generous gifts from Dr. A. P. Tulloch, Prairie Regional Laboratory, Saskatoon, Saskatchewan, Canada. The spin label, 5-doxyl palmitic acid (2-(3-carboxypropyl)-2-undecyl-4,4-dimethyl-3-oxazolidinyloxyl) was a gift of Dr. A. K. Grover. The spin labelled acid 16-doxyl stearic acid (2-(14-carboxytetradecyl)-2-ethyl-4,4-dimethyl-3-oxazolidinyloxyl) was purchased from Syva, Palo Alto, California, U.S.A. The spin labelled steroid 1'-hydroxy-3β-di-n-propyl-17,17-aza-17a-D-homo(5α)-androstanoxyl-17a (III) was a generous gift of Dr. A. Rassatt, Grenoble, France. Goat serum antibodies, prepared against human α-proteins, human β-proteins and human albumin, were purchased from Miles-Yeda Ltd., Israel.

II. Methods

A. Isolation of Egg Phosphatidylcholine

Egg phosphatidylcholine (egg PC) was isolated from fresh egg yolks as described by Singleton et al. (186). The crude phospholipid extract was purified by column chromatography on silica gel (159). Fractions containing only egg PC, as determined by thin layer chromatography on Sil G Polygram plates (Brinkmann) in chloroform:methanol:water (65:25:4), were pooled and the solvent was removed by rotary evaporation. Final traces of solvent were removed by vacuum pumping over phosphorus pentoxide. Purified egg PC was made to known concentration, in chloroform, and stored under nitrogen, in the dark, at -30 °C.

B. Preparation of Perdeutero Palmitic Acid

Palmitic acid was perdeuterated under an atmosphere of deuterium over a palladium (5%) on charcoal catalyst, as described by Hsiao.et al. (97). Deuterium gas was generated using a Varian Aerograph model 9652 hydrogen generator. Progress of the reaction was monitored using mass spectral analysis. At completion of the reaction, the extent of deuteration was generally greater than 96%.

C. Cholesteryl ester synthesis

Spin labelled cholesteryl esters were synthesized according to the procedure previously described by Grover and Cushley (78). Deuterium labelled cholesteryl esters were synthesized using a modified form of the procedure. In a typical reaction 1.67 mmol of [2,2-$^{2}H_{2}$]oleic acid was transferred to a pear-shaped flask and dried <u>in vacuo</u> overnight at room temperature. To the dry acid, 1.71 mmol of 1,1'-carbonyldiimidazole was added. The mixture was dissolved in approximately 3 mL of dry benzene and stirred under an atmosphere of nitrogen. After the evolution of CO_{2} had ceased, the solvent was evaporated. Residual benzene was removed by vacuum drying for approximately 45 minutes. To the dry reaction mixture 1.99 mmol of cholesterol was added. The reaction flask was heated to 90 °C, under an atmosphere of dry nitrogen, using an oil bath. At the end of three hours the oil bath was switched off, and the reaction flask was allowed to cool, in the oil bath, to room temperature. The reaction mixture was dissolved in ~20 mL of benzene, 40 mL distilled water was added, and the phases were separated. The aqueous phase was similarly extracted three more times, and the combined organic phase was reduced to approximately 3 mL. The reaction mixture was purified on a 2.5 x 40 cm silica gel column using benzene as eluant. The cholesteryl ester was identified by thin layer chromatography

Figure 2. Deuterated cholesteryl esters

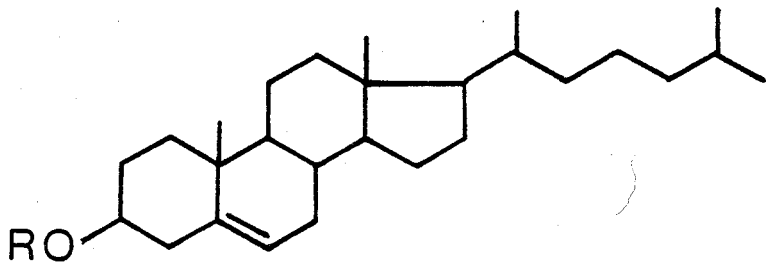

R:

[2,2-$^{2}H_{2}$]oleic acid

[5,5-$^{2}H_{2}$]oleic adid

[8,8-$^{2}H_{2}$]oleic acid

[14,14-$^{2}H_{2}$]oleic acid

[16,16-$^{2}H_{2}$]oleic acid

[18,18,18-$^{2}H_{3}$]oleic acid

Figure 3. Spin labelled cholesteryl esters

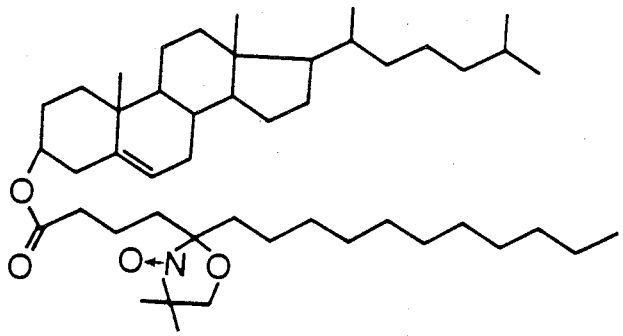

I

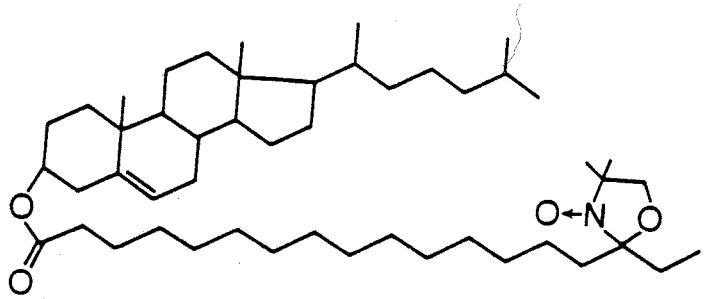

II

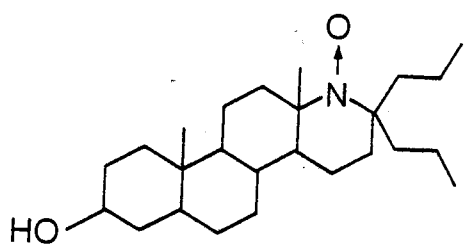

III

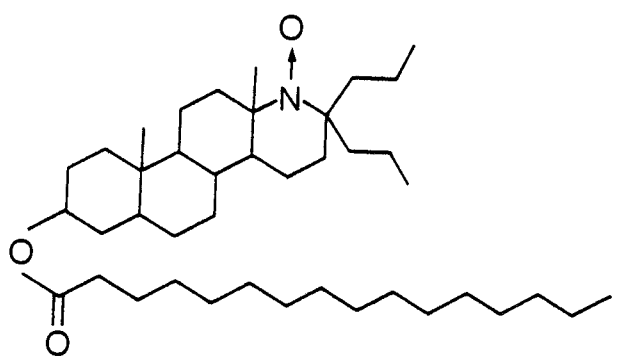

IV

of individual fractions eluted from the column. After exhaustive drying in vacuo 857.5 mg (yield: 78.4%) of the ester was obtained. Figures 2 and 3 illustrate respectively the deuterated and spin labelled esters synthesized.

D. Analysis of Deuterated Cholesteryl Esters

The melting point of each ester was measured using a polarizing light microscope equipped with a heat stage. The instrument was calibrated using azobenzene (mp 60 °C) as a standard. The mass spectral data reported here was obtained using a Hewlett-Packard 5985 GCMS mass spectrometer. The most intense peak observed over the mass to charge (m/e) range 400 to 700 was normalized to 100%. Under conditions of optimum sensitivity, the most abundant peak in this range was generally less than 0.5% of the cholesteryl ion (m/e 386).

Cholesteryl oleate. mp. 51.5-52.5 °C; m/e: 652.9 (20.8% m+2), 651.8 (42.4% m+1), 650.8 (100% m^+.), 649.8 (23.7% m-1), 648.7 (14.4% m-2), 636.7 (16.4%), 645.9 (30.6%)

Cholesteryl [2,2-$^2H_2$]oleate. mp. 51.5-52.5 °C; m/e: 654.7 (20.8% m+2) 653.7 (56% m+1), 652.7 (92.2% m^+.), 651.7 (100% m-1), 650.7 (73.7% m-2), 637.6 (13.5%) 636.6 (19.3%).

Cholesteryl [5,5-$^{2}H_{2}$]oleate. mp. 50.5-51.5 °C; m/e: 654.8 (14.9% m+2), 653.9 (48% m+1), 652.8 (100% m^{+}.), 651.8 (14.5 % m-1), 650.8 (16.2% m-2), 638.8 (13.0%), 637.8 (29.0).

Cholesteryl [8,8-$^{2}H_{2}$]oleate. mp. 52.5-53.5 °C m/e: 654.8 (14.5% m+2), 653.8 (46.7% m+1), 652.8 (100% m^{+}.), 651.8 (16.7% m-1), 650.7 (15.2% m-2), 638.9 (14.3%), 637.9 (28.2%).

Cholesteryl [14,14-$^{2}H_{2}$]oleate. mp. 51.5-52.5 °C; m/e: 654.9 (11.4% m+2), 653.8 (53.6% m+1), 652.8 (100% m^{+}.), 651.8 (26.9% m-1), 650.8 (31.3% m-2), 638.8 (13.4%) 637.8 (29.2%).

Cholesteryl [16,16 $^{2}H_{2}$]oleate. mp. 51.5-52.5; °C; m/e: 655 (15.2% m+2), 654 (46% m+1), 653 (100% m^{+}.), 652 (15.6% m-1), 651 (14.1% m-2), 638 (12.3%), 637 (25.1%).

Cholesteryl [18,18,18-$^{2}H_{3}$]oleate. mp. 51.5-52.5 °C; m/e: 655.9 (12.4% m+2), 654.9 (45.8% m+1), 653.8 (100% m^{+}.), 652.9 (18.6% m-1), 651.8 (15.5% m-2), 639.9 (12.2%), 638.9% (26.7%).

E. Vesicle Preparation

Egg phosphatidylcholine (600 mg) was dispensed volumetrically into a clean round bottom flask. Cholesteryl esters (1.7 mol%), when present, were similarly dispensed and

co-dissolved with the egg PC in chloroform. Solvent was evaporated under a stream of nitrogen, followed by vacuum drying overnight. The lipid was mixed with 3 mL of ^2H_2O using a vortex mixer. The resulting lipid dispersion was sonicated 15-20 minutes at 15 °C under nitrogen, using a Biosonik III probe-type sonicator. Undispersed lipid and titanium particles were removed by centrifugation for 15 minutes in a clinical centrifuge. The vesicles were transferred to an NMR tube, sealed under nitrogen and studied immediately.

F. Preparation of Microemulsions

Cholesteryl ester-rich microemulsions were prepared by a procedure similar to that outlined by Sklar et al (188). In a standard experiment, 27.6 mg of egg PC, 11.5 mg of cholesterol, 25.3 mg of cholesteryl linoleate, 13.8 mg of triolein, and 23.0 mg of the specifically labelled cholesteryl oleate were dispensed into a 15 mm x 25 mm conical tube and codissolved in chloroform. The solvent was gently evaporated under a stream of nitrogen followed by vacuum drying overnight. The dried lipid mixture was dissolved in 6.6 mL of anhydrous 2-propanol, the tube was stoppered and placed in a holder floating in a water bath at approximately 55 °C. The actual water temperature, measured by a copper-constantin thermocouple at mid-height in the water jacket surrounding the Hamilton syringe, was 55 °C.

Three aliquots of 100 uL each were dispensed from a thermostatted syringe into 3.0 mL of rapidly stirring buffer (0.15 M NaCl, 0.2 M Tris-HCl, 0.3 mM EDTA, pH 7.4) at 10 °C. The resulting microemulsion solution was a translucent white. The microemulsions were immediately incubated with plasma without further characterization.

G. Cholesteryl Ester Exchange into Lipoproteins

The donor particles containing 101.2 mg of lipid were added to 240 mL of fresh plasma, and .02% sodium azide (w/w) was added. The plasma-microemulsion solution was transferred to erlenmyer flasks, sealed under nitrogen and incubated at 37 °C for 37 hours. Deuterium labelled cholesteryl esters were exchanged into LDL_2 using human plasma lipid exchange proteins.

H. Isolation of LDL_2

Labelled LDL_2 was isolated by ultracentrifugation between salt densities 1.019 and 1.063 using a Beckman L5-75 ultracentrifuge and a Ti 50.2 rotor (89). The lipoprotein concentration was increased to levels suitable for NMR experiments (25-40 mg/ml) using Millipore CX-30 disposable ultrafiltration units. Deuterium depleted water exchanges (5 to 6) were performed to attenuate the residual ^2HOH resonance. NMR

experiments were conducted immediately following the final solvent exchange. When electrom microscopy was performed, native (unlabelled) LDL_2 was isolated from the same pooled plasma, over the same density range, using an IEC B-60 ultra-centrifuge.

I. Incorporation of Palmitic Acid into LDL_2

Palmitic acid was incorporated into LDL_2 by incubating a lipoprotein solution on a thin film of the appropriately labelled fatty acid (~3-4 mg, representing an excess over 5 mol%) plus a trace of [1-^{14}C]palmitic acid in a round bottomed flask. The solution was gently agitated by hand during the period of incubation. The degree of incorporation was monitored by liquid scintillation counting of aliquots removed from the sample. NMR experiments were conducted immediately.

J. Analytical Procedures

Solubility of cholesteryl esters in egg PC vesicles was determined colorimetrically using the method of Rudel and Morris (160). The amount of egg PC present was determined from measurements of the amount of phosphorus in the same sample (5).

Immunoelectrophoresis of isolated LDL_2 was conducted in sodium barbitol buffer as outlined by Hatch and Lees (88).

Association of either deuterium labelled palmitic acid or cholesteryl esters was demonstrated by column chromatography on Sepharose 6B at 4 °C. The elution solvent was 0.3mM EDTA + 0.02% sodium azide at pH 7.0.

K. ^{31}P NMR

Phosphorus-31 NMR experiments were conducted on a Varian XL 100-15 NMR spectrometer, interfaced to a Nicolet 1080 computer. The free induction decays were recorded at 25 °C in the pulse Fourier transform mode at a frequency of 40.5 MHz, using a ^{19}F field frequency lock. Temperature was controlled using a Varian gas flow temperature controller. Chemical shifts were referenced to an external H_3PO_4 (85%) standard.

L. ^{13}C NMR

Natural abundance ^{13}C NMR experiments, at 25.15 MHz, were conducted on a Varian XL 100-15 spectrometer with a Nicolet 1080 computer and operating in the pulse Fourier transform mode. Spin-lattice relaxation times were measured using the homogeneity-spoiling pulse sequence (139). Broad band proton decoupling was applied continuously. Similar experiments at 100.6 MHz were conducted on a Bruker WH 400 spectrometer. Spin-lattice relaxation times were measured using the inversion

recovery pulse sequence (217).

In experiments investigating the selective broadening effect of Manganese ions, a Bruker WM 400 spectrometer was utilized.

M. ^{2}H NMR

Deuterium NMR spectra were recorded at 38.8 MHz using a homebuilt spectrometer and a Nalorac 5.9 T superconducting magnet. Data collection and Fourier transformation of the resulting free induction decay was performed using a Nicolet BNC-12 computer. In experiments studying deuterium labelled cholesteryl esters in LDL_2, temperature was controlled to +/- 0.5 ^{o}C using a solid state temperature controller. A phase alternating pulse sequence was used during the experiments in order to minimize baseline distortion. Spin-lattice relaxation times were measured using the inversion recovery pulse sequence (217).

The ^{2}H NMR spectra of the methyl labelled cholesteryl esters were recorded at 62 MHz using a Bruker WM-400 spectrometer. Data collection and Fourier transformation was facilitated by an Aspect 2000 computer. Temperature was controlled to +/- 0.5 ^{o}C using a gas flow system.

N. Radioactivity measurements

Radioactivity was assayed by dispensing 50 uL aliquots of sample into 10 mL of scintillation cocktail, and counting the nuclear disintegrations on a Beckman LS-8000 liquid scintillation counter. The scintillation cocktail was made by dissolving 60 g of napthalene, 100 mL of methanol, 20 mL of ethylene glycol, and 42 mL of liquifluor in 600 mL of 1,4 dioxane. After the napthalene had dissolved, the cocktail was diluted to 1 litre with 1,4 dioxane. Ten-mL aliquots were dispensed into new glass scintillation vials and stored in the dark.

O. Electron Microscopy

Electron microscopy was conducted under the tutelage of Mr. Y. I. Parmar. Generally, native and labelled LDL_m (from the same pooled units of plasma) were stained with 2.0% ammonium molybdate at pH 8.0, applied to 200-mesh Formvar carbon-coated grids and air dried. The specimens were examined using a Philips 300 electron microscope at 80 kV.

P. NMR Lineshape analysis

The ^{2}H NMR spectra for the 2, 5, and 8 acyl chain positions of cholesteryl oleate, as well as the selectively deuterated palmitic acids in LDL_{2}, were analyzed using an iterative least squares fit to 6 parameters. The program was generously provided by Dr. K Newman of the Chemistry Department at Simon Fraser University and was run using facilities of the Computing Department at Simon Fraser University. The uncertainties in the calculated linewidths reflect the calculated standard deviations.

Chapter 3

Theory

This chapter will begin with a brief introduction to the theory underlying the NMR experiments used throughout the course of this investigation. Following this general introduction is a discussion of the dipole-dipole relaxation mechanism, which is characteristic of ^{13}C NMR relaxation. For a thorough development of this topic the reader is directed to books by Abragam (1), Slichter (187), or Bovey (17), and the review of NMR applied to membrane systems, by Lee et al. (129).

The latter portion of this chapter is a discussion of quadrupolar relaxation and the additional information available through the use of quadrupole NMR experiments. Several excellent detailed discussions of deuterium NMR and its application to biological systems have been published by Seelig (171), Seelig and Seelig (177), Mantsch et al. (141), and Davis (40).

General

A charged mass rotating about an axis has a magnetic moment, μ, related to the spin angular momentum, $\hbar I$, through the relation

$$\mu = \gamma \hbar I \qquad (3.1)$$

where γ is the magnetogyric ratio, the ratio of magnetic and mechanical moments of the nucleus under investigation, $\hbar$ is Planck's constant divided by 2π and I is the nuclear spin.

According to quantum theory, nuclear spin states, $m_{(I)}$, are quantized and assume (2I+1) values between +I and −I. In the case of nuclei where I = 1/2, such as ^{13}C or protons, $m_{(I)}$ can assume only the values of +1/2 and −1/2.

If an isolated nucleus with a characteristic magnetic moment, μ, is placed at some arbitrary angle θ to a homogeneous magnetic field H_o, which by convention is colinear with the Z-axis, the interaction between the magnetic moment and the field results in a torque applied to the magnetic moment. The torque is directed perpendicular to the plane of both μ and H_o. As a consequence the magnetic moment μ will precess about H_o at the characteristic Larmor frequency, which is determined by the magnitude of both the magnetic moment and the magnetic field as shown by the relation:

$$\nu = -\gamma H_o / 2\pi \qquad (3.2)$$

NMR samples generally contain large collections of nuclei. If the same magnetic field is applied to a collection of nuclei the interaction between the magnetic moments and the field will result in a separation of spin states into (2I + 1) energy levels as shown in Figure 4a for the case of a nucleus of spin 1/2. The energy difference separating these spin states is given by:

$$\Delta E = \gamma \hbar H_o \qquad (3.3)$$

Anticipating future discussion, it will be more convenient to consider not a collection of magnetic moments but rather the bulk or macroscopic magnetization M which is the vector sum of the individual magnetic moments. The relative number of nuclei at each energy level in Figure 4a is determined by a Boltzmann distribution. At equilibrium the Boltzmann distribution favours the lower energy level, consequently, as shown by Figure 4b, M_o is aligned parallel to the magnetic field H_o. Furthermore, if an oscillating voltage is applied to a coil oriented perpendicular to H_o, a (weak) magnetic field H_1 will exist in the plane orthogonal to H_o. This magnetic field, shown in Figure 4b, precesses about H_o in the X-Y plane with a frequency w, and has the magnitude (H_1 cos wt +/- H_1 wt) (17). If w is

Figure 4. Vector addition of magnetic moments

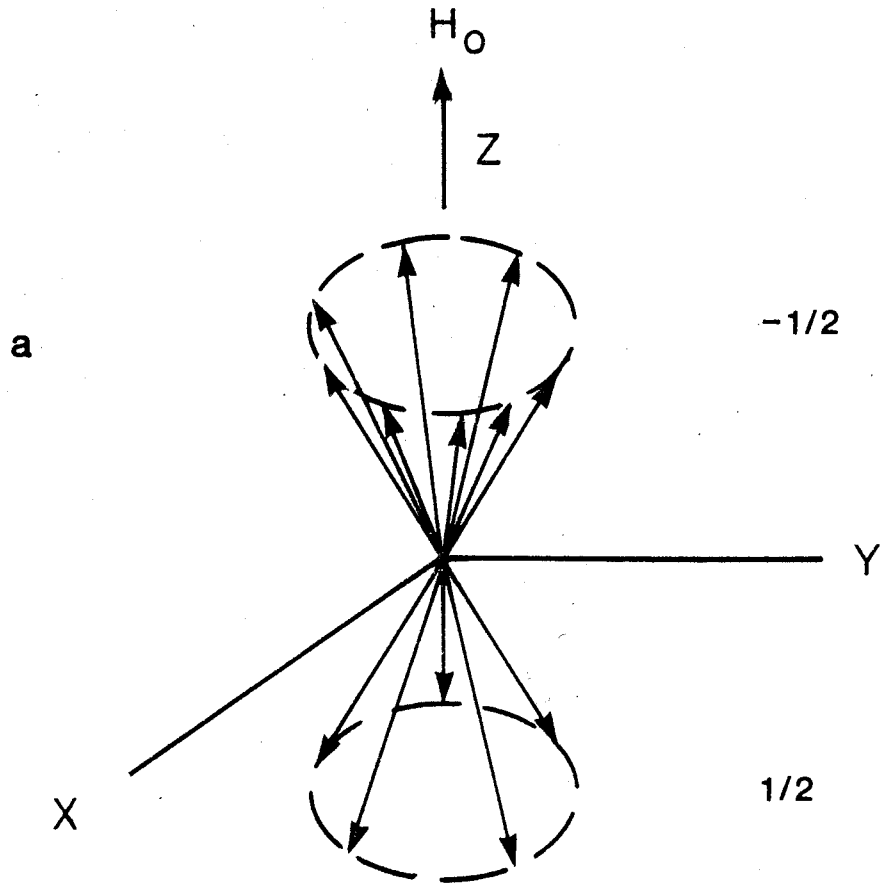
a
H_o
Z
-1/2
Y
X
1/2

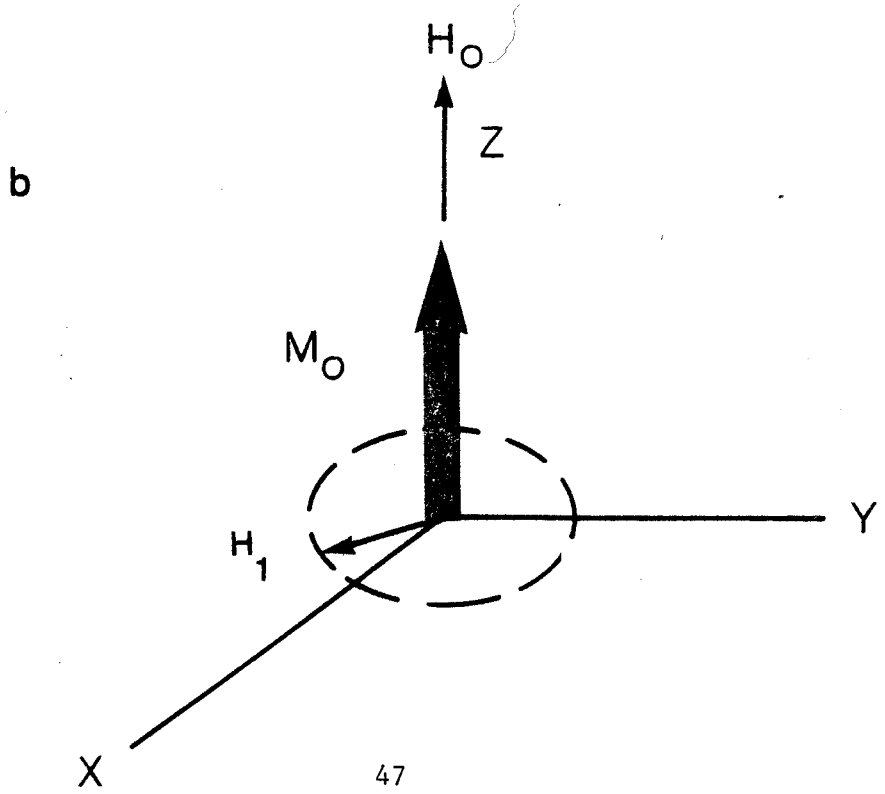
b
H_o
Z
M_o
Y
H_1
X

equal to the Larmor frequency, the macroscopic magnetization vector M_o will experience a torque, and hence be tipped toward the X-Y plane.

The rate of change of M in a magnetic field H is given by the relation (33,57):

$$dM/dt = \gamma [M \times H] \qquad (3.4)$$

Referring again to Figure 4b, it is clear that H is the composite of the applied magnetic field, H_o, and the smaller field, H_1, precessing about H_o at an angular frequency w. The components of H along the three principal axes (57) are:

$$H_x = H_1 \text{ Cos } wt \qquad (3.5a)$$

$$H_y = -H_1 \text{ Sin } wt \qquad (3.5b)$$

$$H_z = H_o \qquad (3.5c)$$

Substituting equations 3.5a-3.5c into the expanded form of equation 3.4, it can be shown (57)

$$dM_x/dt = \gamma (M_y H_o + M_z H_1 \text{ Sin } wt) \qquad (3.6)$$

$$dM_y/dt = \gamma (M_z H_1 \text{ Cos } wt - M_x H_o) \qquad (3.7)$$

$$dM_z/dt = -\gamma(M_x H_1 \text{ Sin } wt + M_y H_1 \text{ Cos } wt) \qquad (3.8)$$

Bloch (12,13) has shown that nuclear spin systems do not possess infinitely long memories, and the components of M relax back to an equilibrium value with a characteristic relaxation time according to the relation:

$$dM_z/dt = -(M_z - M_o)/T_1 \qquad (3.9)$$

$$dM_x/dt = -(M_x)/T_2 \qquad (3.10)$$

$$dM_y/dt = -(M_y)/T_2 \qquad (3.11)$$

The relaxation times, T_1 and T_2, which characterize these relaxation processes are respectively known as the longitudinal and transverse relaxation times. From equations 3.9-3.11 it is clear that M_x and M_y exponentially relax back to equilibrium with a characteristic time T_2, and at equilibrium

$$M_x = M_y = 0 \qquad (3.12)$$

Similarly, M_z approaches equilibrium according to the time constant T_1, and at equilibrium

$$M_z = M_o \qquad (3.13)$$

Taking into account the effect of relaxation (51), the rate of change of each component of M is:

$$dM_x/dt = \gamma(M_y H_o + M_z H_1 \text{ Sin } wt) - M_x/T_2 \qquad (3.14)$$

$$dM_y/dt = \gamma(M_z H_1 \text{ Cos } wt - M_x H_o) - M_y/T_2 \qquad (3.15)$$

$$dM_z/dt = -\gamma(M_x H_1 \text{ Sin } wt + M_y H_1 \text{ Cos } wt) - (M_z - M_o)/T_1 \qquad (3.16)$$

Relaxation is the result of oscillating magnetic fields at the nucleus, caused by random thermal motions occuring within the spin system. Efficient spin lattice relaxation is dependent on one criterion: there must be some time-dependent interaction directly on the spins within the system which is most effective if it occurs at a frequency near the Larmor frequency.

Consider a force F fluctuating randomly about a mean value of zero. If F is measured at time t and again at time $(t+\tau)$ later, then F(t) may be different than $F(t+\tau)$. When τ is small, however, $F(t+\tau)$ is expected to very nearly equal F(t). That is, there will be a high degree of correlation between F(t) and $F(t+\tau)$. This can be expressed by the autocorrelation function of F(t) (33,57):

$$G(\tau) = \langle F^*(t+\tau)F(t) \rangle \qquad (3.17)$$

where the asterisk indicates the complex conjugate, and the angular brackets indicate the time average. Owing to the random nature of thermal motions, the autocorrelation function is assumed to decay exponentially to zero in a characteristic time τ_c, the correlation time. Equation 3.17 can then be rewritten as

$$G(\tau) = \langle F^*(t)F(t) \rangle \exp-(\tau/\tau_c) \qquad (3.18)$$

Random thermal motions span a spectrum of fluctuation frequencies. The intensity of any motion occurring at a given frequency can be evaluated by the spectral density function J(w) (14,33):

$$J(w) = \int_{-\infty}^{+\infty} G(\tau) \exp(iwt)\, d\tau \qquad (3.19)$$

$$= \langle F^*(t)F(t) \rangle [2\tau_c/(1 + w^2 \tau_c^2)] \qquad (3.20)$$

The spectral density function is the Fourier transform of the autocorrelation function. It is a measure of the available energy due to a force F fluctuating at a frequency w, as in the case of fluctuating dipoles or time-dependent oscillations of an electric field gradient. Any process which results in a

modulation of the local magnetic field at a nucleus is a potential relaxation mechanism. The more commonly known relaxation mechanisms are:

(1) Dipole-dipole interactions

(2) Electric quadrupole interactions ($I > 1/2$)

(3) Chemical shift anisotropy

(4) Spin-rotation interactions

(5) Scalar-coupling interactions

The remainder of this chapter will be restricted to a discussion of the first two mechanisms.

Dipole-Dipole Interactions

Dipole-dipole interactions are represented by the Hamiltonian (57):

$$\mathcal{H}_D = -h\ I \cdot D \cdot S \qquad (3.21)$$

where I and S represent nuclear spins, and D is the dipolar coupling tensor. Molecular reorientations result in changes to θ, the angle the internuclear vector between spins I and S subtends with the applied magnetic field H_o. Consequently, the components of D are time-dependent (33,57).

Spin-lattice relaxation is the result of transitions between energy levels of the spin system, and hence related to the probability of a spin transition, W (14). In a system containing two non-equivalent spins, the spin lattice relaxation (197) time is determined by:

$$1/T_1 = W_0 + 2W_1 + W_2 \qquad (3.22)$$

where $W_{(x)}$ is the transition probability per unit time as described by Solomon (197). Selection rules dictate that $|\Delta m| = 1$, therefore the only transition observed is between the $m = +/- 1/2$ spin states. Using the general method of

Bloembergen et al. (14) as extended by Solomon (197), in the case of a proton-decoupled ^{13}C system, the probability of transition, W_I, can be evaluated by the relations:

$$W_0 = \tau_c/8\hbar^2 \overline{F_0^2}\{1/[1 + (w_C - w_H)^2 \tau_c^2]\} \qquad (3.23)$$

$$W_1 = \tau_c/2\hbar^2 \overline{F_1^2}\{1/[1 + w_C^2 \tau_c^2]\} \qquad (3.24)$$

$$W_2 = 2\tau_c/\hbar^2 \overline{F_2^2}\{1/[1 + (w_C + w_H)^2 \tau_c^2]\} \qquad (3.25)$$

where the bar indicates the average over all nuclei, w_C and w_H are the respective Larmor frequencies of ^{13}C and hydrogen, and F_I is a random function of the relative positions of spins I and S (1,197). Assuming, for the moment, that any motion under consideration is isotropic (14,197), the appropiate values of $\overline{F_0^2}$, $\overline{F_1^2}$, and $\overline{F_2^2}$ are:

$$\overline{F_0^2} = 4/5\ K^2 \qquad (3.26)$$

$$\overline{F_1^2} = 3/10\ K^2 \qquad (3.27)$$

$$\overline{F_2^2} = 3/10\ K^2 \qquad (3.28)$$

with

$$K = \hbar^2 \gamma_C \gamma_H r^{-3} \qquad (3.29)$$

where γ_C and γ_H are the magnetogyric ratios of the carbon and hydrogen nuclei respectively, and r is the carbon-hydrogen internuclear distance. Substitution of the calculated transition probabilities into equation 3.22 clearly indicates the ^{13}C spin-lattice relaxation time is related to thermal motion (129,197) by:

$$1/T_1 = \hbar^2 \gamma_C^2 \gamma_H^2 \tau_c / 10r^6 \quad \times \quad [\{1/\langle 1+(\omega_C-\omega_H)^2 \tau_c^2 \rangle\} + \{3/\langle 1+\omega_C^2 \tau_c^2 \rangle\} + \{6/\langle 1+(\omega_C+\omega_H)^2 \tau_c^2 \rangle\}] \qquad (3.30a)$$

In the presence of a paramagnetic ion, relaxation of the ^{13}C nuclei will similarly be via dipole-dipole interactions (197). The magnetic moment of an unpaired electron is 650 times greater than that of a proton (123). As a consequence, in the presence of a paramagnetic centre, the ^{13}C spin-lattice relaxation rate, near the paramagnetic centre, will be dominated by the more efficient electron-nuclear dipolar coupling (123), and equation 3.30a assumes the form:

$$1/T_1 = \hbar^2 \gamma_C^2 g^2 \beta^2 \tau_c / 10r^6 \quad \times \quad [\{1/\langle 1+(\omega_C-\omega_E)^2 \tau_c^2 \rangle\} + \{3/\langle 1+\omega_C^2 \tau_c^2 \rangle\} + \{6/\langle 1+(\omega_C+\omega_E)^2 \tau_c^2 \rangle\}] \qquad (3.30b)$$

where β is the Bohr magneton, g is the electronic g-factor, and ω_E is the Larmor precession frequency of the electron.

The assumption that molecular motions are isotropic may be unjustified. In large molecular aggregates, such as egg PC vesicles or LDL, motion may occur simultaneously about several axes, and display a different correlation time about each axis (4,51,58,205,222). When complex anisotropic motions occur, the relaxation time observed is governed by the correlation time about each axis. Such motions reduce the probability of a spin transition, and therefore are reflected in a decreased spin-lattice relaxation rate (4,58,205). In the presence of anisotropic motion, equation 3.30a can be written (4,205):

$$1/T_1 = \chi N \gamma_C^2 \gamma_H^2 \hbar^2 \tau_c / 10 r^6 \quad \times \quad (3.31)$$
$$[\{1/\langle 1+(\omega_C-\omega_H)^2 \tau_c^2 \rangle\} + \{3/\langle 1+\omega_C^2 \tau_c^2 \rangle\} + \{6/\langle 1+(\omega_C+\omega_H)^2 \tau_c^2 \rangle\}]$$

where, in the limit that internal motions occur much faster than the overall tumbling rate of the molecular aggregate, $\chi = 1/4\ (3\cos^2\theta - 1)^2$ and θ represents the angle between the C-H vector and the axis of internal reorientation (4). In the case of phospholipid membrane systems, ^{13}C spin-lattice relaxation is dominated by intramolecular dipole-dipole interactions between the ^{13}C nucleus and its directly bonded protons (129); therefore N represents the number of protons bonded to the ^{13}C nucleus.

The correlation time, τ_c, may contain contributions from a multiplicity of motions, in addition to contributions arising

from any anisotropy of such motions (20,21,26,27,148-150,154). Therefore, τ_c must be considered an effective correlation time. When internal motion is much faster than the overall tumbling rate of the lipid complex, the observed relaxation rate is dominated by the faster motion, and independent of the tumbling rate of the aggregate (4,26,27,129). The effective correlation time cannot generally be decomposed into components arising from different types of molecular reorientation. Moreover, it is not possible to resolve the correlation time into its isotropic and anisotropic components (171,203). These limitations notwithstanding, spin-lattice relaxation times do reflect overall motion in the system.

Electric Quadrupole Interactions

The deuterium nucleus, with spin I = 1, displays an asymmetric (non-spherical) distribution of nuclear charge, and therefore possesses a nuclear quadrupole moment, Q. At the site of the deuterium nucleus, the surrounding electron cloud and adjacent nuclei produce a non-uniform distribution of charge resulting in an electric field gradient, eq. Electrostatic coupling between the nuclear quadrupole moment and the electric field gradient is responsible for the quadrupole interaction.

The total interaction energy of a nucleus in a homogeneous magnetic field H_o can be represented by the Hamiltonian (1,171):

$$\mathcal{H}_T = \mathcal{H}_z + \mathcal{H}_Q \qquad (3.32)$$

The Zeeman Hamiltonian, $\mathcal{H}_z$, characterizes the interaction between the magnetic field and the magnetic moment, according to the relationship (1,33,40,108,171):

$$\mathcal{H}_z = -g\beta_N H_o m_I \qquad (3.33)$$

where g is the nuclear g-factor and β_N is the nuclear magneton.

The quadrupole interaction is described by the Hamiltonian (40,108):

$$\mathcal{H}_Q = [(e^2qQ/4I(2I-1)][3m_I^2 - I(I+1)] \times 1/2[(3\cos^2\theta-1) + \eta(\sin^2\theta \cos 2\phi)] \quad (3.34)$$

where η is the electric field gradient asymmetry parameter (171) defined as:

$$\eta = (V_{xx} - V_{yy})/V_{zz} \quad (3.35)$$

The quantities V_{xx}, V_{yy}, and V_{zz} indicate the respective axial components of the electrostatic field gradient, θ and ϕ are the polar and azimuthal angles between the electric field gradient, in the principal coordinate system, and the magnetic field (20,58). If the electric field gradient is axially symmetric such that its x- and y- components are equal, the asymmetry parameter, η, ceases to exist, and equation 3.34 assumes the form:

$$\mathcal{H}_Q = [(e^2qQ)/(4I(2I-1)] [3m_I^2 - I(I+1)] \times [(3\cos^2\theta-1)/2] \quad (3.36)$$

In the case of C-^{2}H$_2$ bonds, the electric field gradient generally is axially symmetric about the C-^{2}H$_2$ vector (9,44), and axial symmetry shall be assumed in subsequent discussion.

At high magnetic field strengths the Zeeman interaction is much larger than the energy due to quadrupolar interactions.

For example, in the case of ^2H, at a field strength of 5.9 Tesla, the Zeeman interaction is equivalent to a frequency of 38.8 MHz, whereas the quadrupole interaction energy is on the order of 200 KHz (29). Therefore, the quadrupole interaction may be considered to be a perturbation of the much larger Zeeman energy (171).

By virtue of equations 3.33 and 3.36, the energy levels of the total Hamiltonian (40,171) are determined by:

$$E_T = -gB_N H_o m_I + \qquad (3.37)$$
$$[(e^2qQ)/4I(2I-1)][m_I^2 - I(I+1)][(3\mathrm{Cos}^2\theta-1)/2]$$

Since m_I can assume (2I+1) values, three discrete energy levels exist as shown in Figure 5. Selection rules demand that $|\Delta m| = 1$, therefore only two transitions are observed corresponding to the transitions between the $m_I = -1$ and $m_I = 0$ as well as the $m_I = 0$ and $m_I = +1$ spin states.

Consider for the moment the (hypothetical) case of a single perfect crystal in a homogeneous magnetic field. Furthermore, let the crystal be such that a proton at one site has been replaced by a deuteron. The observed deuterium spectrum will consist of two resonance lines equally spaced about the central frequency V_o where:

Figure 5. Quadrupolar interaction with Zeeman energy levels

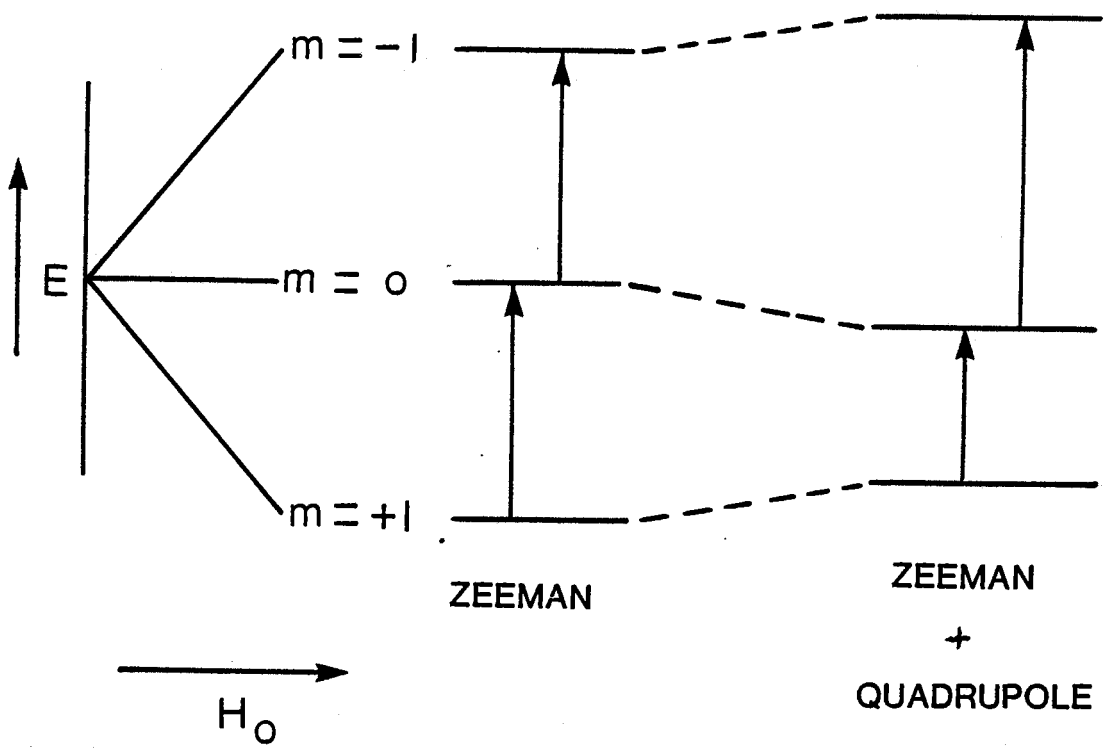
m = -1
E
m = o
m = +1
ZEEMAN
ZEEMAN
+
QUADRUPOLE
H_o

$$V_0 = -g\beta_N H_0/h = \gamma H_0/2\pi \qquad (3.38)$$

Since E = hV, then from equation 3.37, the frequency of each resonance line is:

$$V = V_0 +/- 3/4[e^2qQ/h][(3\cos^2\theta-1)/2] \qquad (3.39)$$

and the two resonance lines are separated by a frequency difference, ΔV_Q, given by (40):

$$V_Q = 3/2[e^2qQ/h][(3\cos^2\theta-1)/2] \qquad (3.40)$$

where ΔV_Q is known as the quadrupolar splitting, and (e^2qQ/h) is the static quadrupolar coupling constant which is typically on the order of 168 kHz for an sp^3 hybridized $C-^2H$ (29). The quadrupolar splitting clearly depends on θ, the angle between the magnetic field and the axis of greatest electric field gradient. Maximum quadrupolar splitting is observed when H_0 is parallel to the major axis of the electric field gradient (θ=0).

In practice, NMR samples consisting of a single perfect crystal seldom exist. More commonly, samples contain a large number of crystallites randomly oriented with respect to each other. As a consequence of random orientation of individual crystals the electric field gradient at each deuterium nucleus can assume any angle θ. The NMR spectrum observed in this case

is a superposition of doublets arising from each orientation and the result is the so-called "powder pattern" shown in Figure 6a. Signal intensity is governed by the number of crystals oriented such that the electric field gradient subtends a given angle θ with H_o, and hence is determined statistically by the probability density, $p(\theta)$, (171) where:

$$p(\theta) = (1/2)\sin\theta \qquad (3.41)$$

Maximum value of $p(\theta)$ occurs at $\theta = 90°$, hence the signal maxima observed in a powder pattern coincide with deuterium nuclei oriented such that the major axis of the electric field gradient is orthogonal to the magnetic field. The separation between the two maxima or quadrupole splitting of the powder pattern is:

$$\Delta\nu_{Powder} = (3/4)(e^2qQ/h) \qquad (3.42)$$

Liquid crystals also exhibit regular organization. Efficient ordered packing is achieved when the long axes of component molecules are aligned in some type of parallel array. Unlike solids, however, molecules in a liquid crystal are not inflexible, and thermal motions both parallel and perpendicular to the long molecular axis do occur. Due to the parallel alignment of the molecules, however, the amplitude of motions perpendicular to the long axis is restricted.

Figure 6. Theoretical powder pattern and Lorentzian spectrum

a

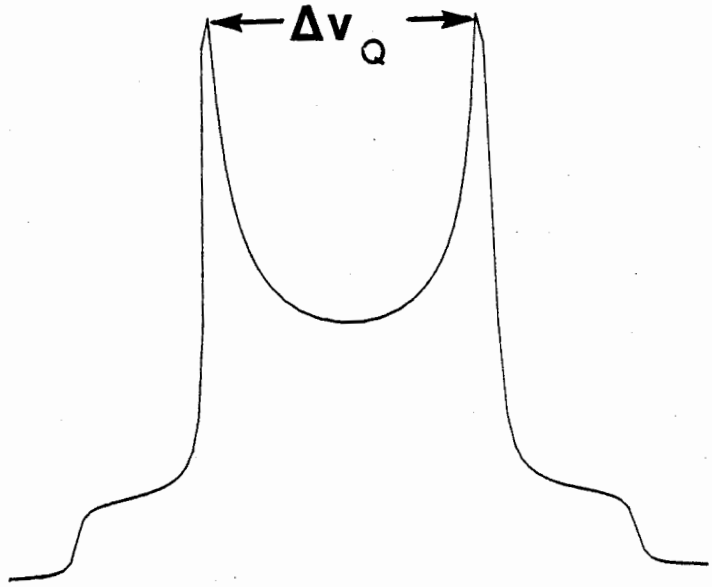

b

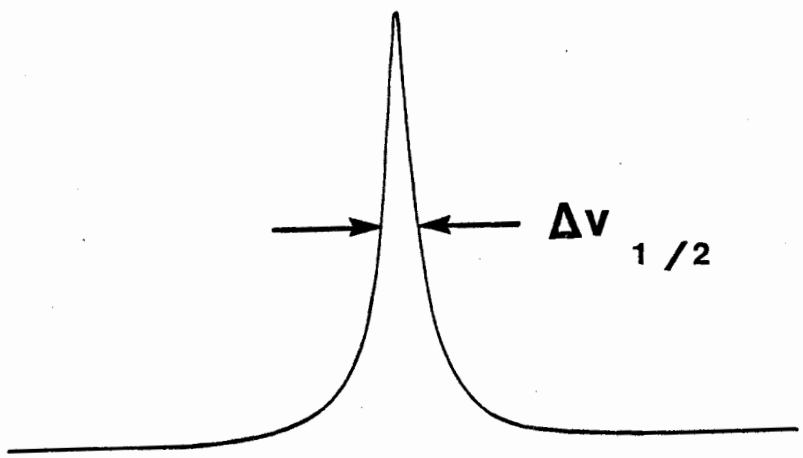

The coordinate system which describes molecular reorientation also defines the electric field gradient. Therefore, as a result of molecular motion, the components of the electric field gradient are time-dependent. In lipid bilayers, mean statistical orientation is defined by a director Z' which, on average, is coincident with the normal to the surface of the bilayer (40,108,171). The effect of motion about the director, then, is to average the electric field gradient at the site of the deuterium nucleus, and the amplitude of these motions determines the extent to which the electric field gradient is averaged.

The amplitude of such motion is reflected by the order parameter, S_{CD}, (40,108,141,171,174-177,202,203) where:

$$S_{CD} = \langle (3\cos^2\beta - 1)/2 \rangle \qquad (3.43)$$

The order parameter is a measure of the time-averaged angular excursion, β, of the C-D bond about the director.

If we consider now a planar (oriented) liquid crystal containing a deuterium nucleus at a unique site, as in the case of the single crystal, the observed spectrum will again consist of a doublet, except at the so-called magic angle, where the two signals coalesce to form a single resonance centered at ν_0 (171). Due to motion within the liquid crystal, however, a time averaged electric field gradient exists at the deuterium nucleus

and the quadrupolar splitting is thus reduced by a factor S_{CD} as shown by:

$$\Delta V_Q = (3/2)(e^2qQ/h)[(3\cos^2\theta - 1)/2]S_{CD} \qquad (3.44)$$

where θ is the angle between the magnetic field and the director.

In non-aligned liquid crystalline samples, consisting of randomly oriented lamellae, the angle θ can assume all possible values, and as with the poly-crystalline sample the resulting spectrum is a powder pattern. The quadrupole splitting, in this case, depends only on the order parameter through the relationship:

$$\Delta V_{powder} = (3/4)(e^2qQ/h)S_{CD} \qquad (3.45)$$

Deuterium NMR spectra of unilamellar phospholipid vesicles and lipoproteins are not characterized by quadrupolar splittings (201,202,217). Small molecular aggregates of ~500 A° or less tumble isotropically in solution. This additional rapid motion further reduces the quadrupole splitting until the maxima of the doublet coalesce to form a single resonance. The NMR spectrum of such small molecular aggregates is characterized by a mid-height linewidth, $\Delta V_{1/2}$, as shown in figure 6b. The linewidth is determined by the transverse relaxation rate by:

$$\Delta\nu_{1/2} = 1/(\pi T_2^*) \qquad (3.46)$$

Equation 3.46 can be expanded to reveal the relative linewidth contributions arising from motions occurring at rates greater than the Larmor frequency, and those occurring more slowly (203) through the relation:

$$1/(\pi T_2^*) = [1/(\pi T_2)_{FAST} + 1/(\pi T_2)_{SLOW}] \qquad (3.47)$$

If one considers fast motions to be those motions characterized by a correlation time, $\omega_0^2 \tau_c^2 << 1$, then the transverse relaxation rate, due to fast motion, is equal to the spin lattice relaxation rate. Neglecting any contributions due to motional anisotropy, the spin lattice relaxation rate is related to the spectral density through the relationship:

$$1/T_1 = (3/80)(e^2qQ/h)[\tilde{J}_{(\omega)} + 4\tilde{J}_{(2\omega)}] \qquad (3.48)$$

where $\tilde{J}_{(\omega)}$ is the Fourier Transform of the "reduced" autocorrelation function (1):

$$\tilde{J}_{(\omega)} = 2\tau_c/(1 + \omega^2 \tau_c^2) \qquad (3.49)$$

Accounting for the effect of the order parameter, S_{OD}, on the

spin-lattice relaxation rate (21,28), in the limit that $\tau_c^2 w_o^2 << 1$, then:

$$1/T_1 = (3/8)(e^2qQ/\hbar)^2(1 - S_{CD}^2)\,\tau_c \qquad (3.50)$$

The transverse relaxation rate, due to slow motions, is readily evaluated (1) by the equation:

$$(1/T_2)_{slow} = (\pi^2/40)(e^2qQ/h)[9\tilde{J}(0) + 15\tilde{J}(\omega) + 6\tilde{J}(2\omega)]S_{CD}^2 \qquad (3.51)$$

Isotropic tumbling of the molecular aggregate is too slow to affect spin latice relaxation (26,27,40,175,176), however it does reduce the transverse relaxation rate. Furthermore, in the case of unilamellar phospholipid vesicles, lateral diffusion is known to further reduce the transverse relaxation rate. These motions can be characterized by an effective correlation time, τ_E, calculated from:

$$1/\tau_E = (3kT/4\pi\eta r^3) + (6D/R^2) \qquad (3.52)$$

where k is Boltzmann's constant, T is the temperature in degrees Kelvin, η is the solvent viscosity, r is the radius of the molecular aggregate, D is the lateral diffusion constant, and R is the radius from the centre of the vesicle to the mid-point of

the vesicle bilayer. For a particle with a diameter of approximately 200 A°, the effective correlation time is on the order of 10^{-6} seconds. Inspection of equation 3.49 demonstrates that only the value of the spectral density at zero frequency need be considered further, and:

$$(1/T_2)_{SLOW} = (9\pi^2/20)(e^2qQ/h)^2 S_{CD}^2 \tau_e \qquad (3.53)$$

After substitution of equation 3.53 into equation 3.47 we obtain (203):

$$\Delta\nu_{1/2} = 1/\pi T_1 + (9\pi/20)(e^2qQ/h)^2 S_{CD}^2 \tau_e \qquad (3.54)$$

It should be emphasized that the observed order parameter may be a product of several order parameters, each reflecting a specific type of motion (20,21,26,27,40,148-150,154). Details concerning the number of statistically independent motions are not known. Nevertheless, the order parameter, S_{CD}, is a reflection of the total order existing at the position of the nucleus. In other words, S_{CD} indicates the time-averaged angular excursions of the C-D bond about the director Z' independent of the number of different types of motions.

Chapter 4

Results and Discussion

I. CHARACTERIZATION OF ISOLATED LDL_2

A. Immunospecificity of isolated LDL_2

Human low density lipoprotein was isolated from fresh plasma as described in Chapter 2. Purity of the LDL_2 was investigated during the intial phase of this investigation using immunoelectrophoresis as detailed by Hatch and Lees (88). A single precipitin line was observed in the presence of human anti-B protein, and no cross reaction was detected in the presence of either human anti-A protein or anti-albumin protein. The results were consistently reproducible; therefore, in later experiments, the isolated LDL_2 was subjected to immunoelectrophoresis at random intervals.

B. Lipid Exchange

Lipid microemulsions containing 27.2% (by wt) egg PC, 11.3% cholesterol, 25.0% cholesteryl linoleate, 13.6% triolein, and 22.7% specifically deuterated cholesteryl oleate were prepared as described in Chapter 2. Preliminary investigations using

cholesteryl [1-^{14}C]oleate indicate that, under the experimental conditions set forth in Chapter 2, ~8% of the cholesteryl oleate was exchanged into the core of LDL_2 during the incubation time. Labelled LDL_2 precipitated in the presence of human anti-B protein but no precipitation was detected in the presence of human anti-A protein.

Lipid analysis of both labelled and native (unlabelled) LDL_2, from the same plasma pool, was conducted using lipid-specific diagnostic kits supplied by Boehringer Mannheim. After incubation with the lipid microemulsions the labelled LDL_2 displayed a 30% increase in triglycerides (Table 1), indicated by the ratio of triglyceride to protein in both lipoprotein samples. At the same time, the cholesteryl ester content decreased 22%. We are unable to conclude (here) that these results are a general feature of the technique used in these experiments for two reasons. Firstly, simultaneous isolation of both labelled and native LDL_2 was only performed once (owing to the practical limitations on having at one's disposal simultaneously two ultracentrifuges with rotors). Secondly, the ratio of triglyceride to protein in the native LDL_2 was 0.39, whereas the expected ratio is 0.52 (162). As a consequence, the triglycerides present in the lipid microemulsions are in excess, and hence, predictably one might expect a net transfer of triglycerides into LDL_2. If the size of the lipoprotein particle remains unaltered by the exchange process, as discussed below,

Table 1

Core Lipid Composition of LDL_m After Incubation With Microemulsions

Lipoprotein Sample	Protein Concentration	Cholesteryl Ester/Protein	Triglyceride/ Protein
Native	1.36 mg/dL	0.94	0.39
Labelled	39 mg/dL	0.74	0.52

net transfer of triglycerides into LDL_2 can only occur if cholesteryl esters are simultaneously removed from the lipoprotein. Moreover, if exchange of triglycerides and cholesteryl esters proceeds in an equimolar ratio, the predicted loss of cholesteryl esters would be 23%, very much in agreement with the data reported here. In support of this hypothesis, it is interesting to note that the ratio of triglyceride to protein in the labelled LDL_2 was 0.52.

The presence of exchangeable proteins such as apo C, apo A-I, and apo A-II, in whole plasma raises the possibility that some protein(s) may transfer to the lipid microemulsions thereby resulting in an increased particle density such that some microemulsion particles may be present as a contaminant in the isolated LDL_2. Observations in this laboratory and others provide evidence against this possibility. Firstly, Sklar et al. (188) have reported that the microemulsion particles are approximately 300 A° in diameter. Particles of this diameter are 50% larger than the LDL_2 particles isolated in these experiments, and therefore will elute from a Sepharose column before LDL_2. As shown in Figure 7 (discussed below) no such particles were detected. Secondly, Craig et al. (35A) have shown that labelled cholesteryl ester not incorporated into the lipoprotein is recovered quantitatively from the plasma by centrifugation at a density of 1.006. Therefore the possibility that protein-containing microemulsion particles are present in

the labelled LDL_2 seems remote.

In a single study, [11,11,12,12-$^2H_4$]dipalmitoyl phosphatidylcholine was exchanged into fresh LDL_2 using the procedure detailed in Chapter 2. Radioactive tracer studies indicate ~2.4% of the phospholipid is exchanged over 37 hours. This procedure is not practical in the case of phospholipid exchange for three reasons. Firstly, the microemulsions prepared with dipalmitoyl phosphatidylcholine are significantly less stable than similar microemulsions prepared using egg PC. Secondly, the microemulsions prepared with dipalmitoyl phosphatidylcholine proved difficult to remove from LDL_2 by ultracentrifugation. Finally, in this experiment, the yield of LDL_2 was reduced to approximately one third compared to the yield of native LDL_2 from the same plasma. Therefore, although the technique used to label LDL_2 with cholesteryl esters appears promising in the case of phospholipid exchange refinements must be made in order to achieve optimum results. It appears likely that all of the difficulties associated with phospholipid exchange are related to the fact that the gel-to-liquid crystalline temperature of dipalmitoyl phosphatidylcholine is approximately 41 °C which is above the temperature presently employed in the exchange reaction. Two potential solutions to this difficulty exist. Firstly, by far the easier solution, is to incubate the plasma-microemulsion mixture at 45 °C, which is above the transition temperature of the phospholipid. The

alternative solution is to synthesize specifically deuterated phospholipids containing one unsaturated acyl chain, such as 1-palmitoyl-2-oleyl phosphatidylcholine. The advantage, in this case, is that the phospholipid will have a transition temperature more closely resembling that of egg PC.

II. DEUTERIUM NMR OF LOW DENSITY LIPOPROTEIN

A. Deuterium NMR of Cholesteryl Esters in Low Density Lipoprotein

(i) Localization of Labelled Esters in LDL_{2}

Cholesteryl oleates, deuterated at selected acyl chain positions, were synthesized as set forth in Chapter 2. Each of the deuterated esters was in turn incorporated into fresh LDL_{2}. The intimate association of deuterium labelled cholesteryl ester with the isolated lipoprotein was demonstrated by column chromatography. Figure 7 presents the elution profile of LDL_{2} labelled with cholesteryl [5,5-$^{2}H_{2}$]oleate plus a trace of cholesteryl [1-^{14}C]oleate. As demonstrated in Figure 7, a single protein peak eluted from the column. Coincident with the maximum in UV absorbance is the maximum in radioactivity. All of the radioactivity was recovered (120%) from the column indicating no protein-free structures were present after

Figure 7. Elution profile of LDL_2 containing cholesteryl [5,5-$^2H_2$]oleate from sepharose 6B at 4 °C

Elution solvent: 0.3 mM EDTA + 0.02% NaN_3 pH 7.0; (●) UV absorbance at 280 nm; (△) ^{14}C activity: 1 = 277 dpm.

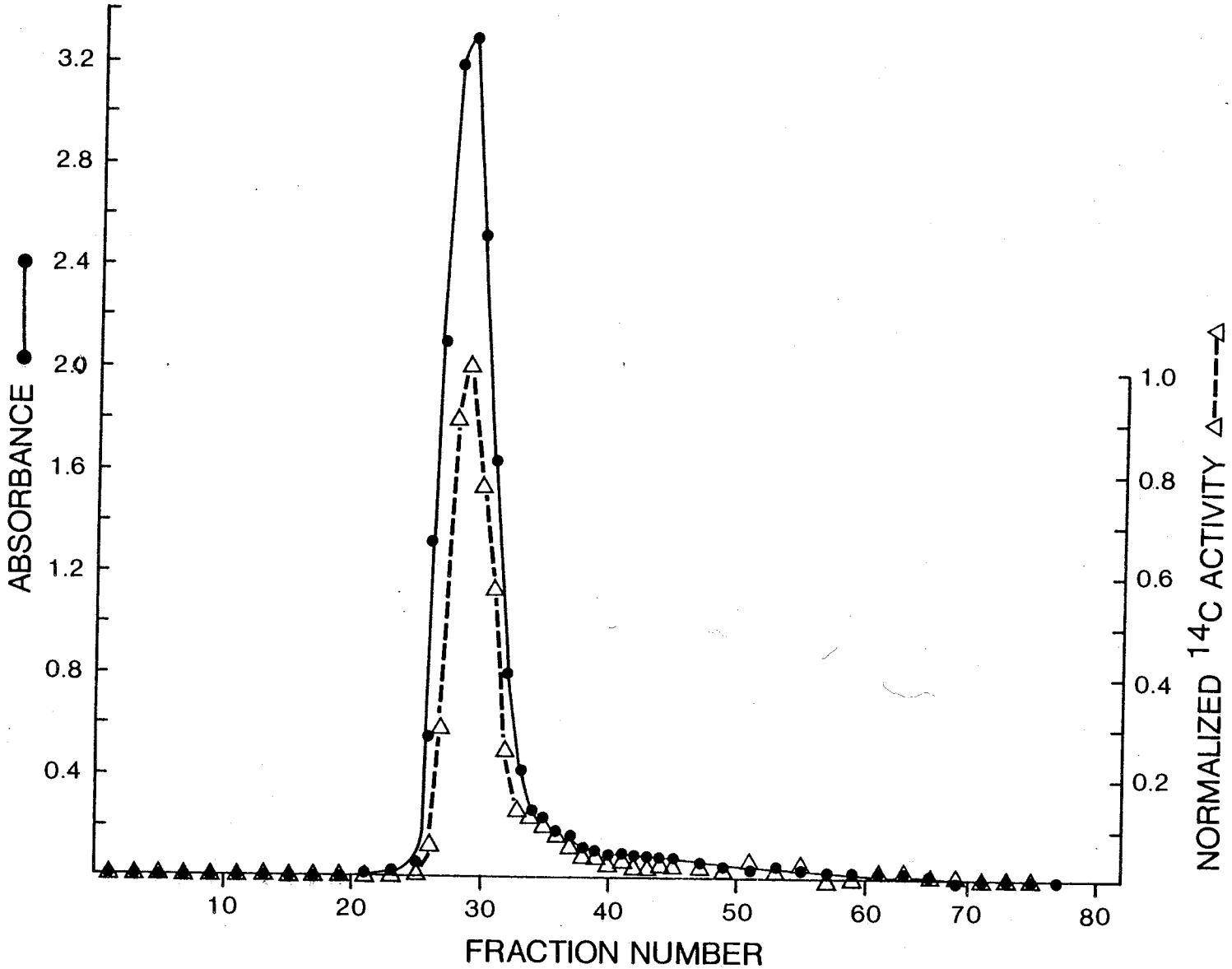
ABSORBANCE
3.2
2.8
2.4
2.0
1.6
1.2
0.8
0.4
NORMALIZED ^{14}C ACTIVITY
1.0
0.8
0.6
0.4
0.2
10
20
30
40
50
60
70
80
FRACTION NUMBER

isolation of the lipoprotein. The fact that the recovered radioactivity exceeds 100% is a reflection of the cumulated uncertainties in both the volume and the ^{14}C-activity of each fraction.

(ii) Electron Microscopy of Labelled LDL_2

The effect of ester exchange on the size of LDL_2 was monitored by electron microscopy. Figure 8 is an electron micrograph of native (unlabelled) LDL_2. An electron micrograph of LDL_2 labelled with cholesteryl [5,5-$^2H_2$]oleate is presented in Figure 9. In these experiments fresh plasma from two donors was pooled and divided into two portions. The first portion was incubated with the lipid microemulsions at 37 °C for 37 hours after which time labelled LDL_2 was isolated as detailed in Chapter 2. From the remaining plasma, native LDL_2 was isolated within the same density range. Approximately 250 particles from each of the samples were measured. In both cases the size was determined to be 200 +/- 10 A°.

(iii) Nuclear Magnetic Resonance of Labelled LDL_2

In order to study the effect of temperature on the organizational order within human LDL_2, ^2H NMR spectra of labelled LDL_2 were collected over the range +15 to +45 °C. The

Figure 8. Electron micrograph of native LDL_2

Magnification: x 198450

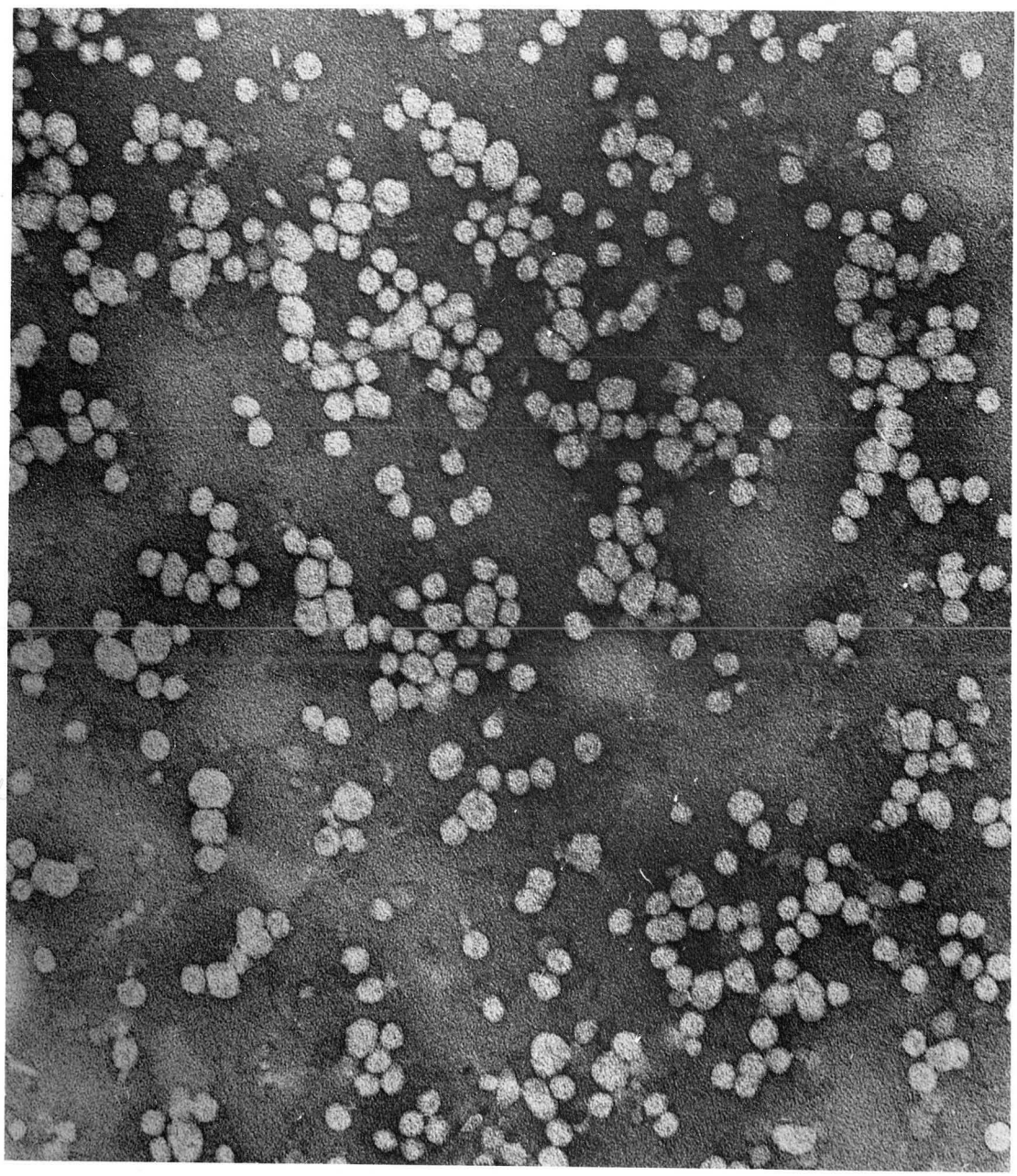

Figure 9. Electron micrograph of LDL_2 containing cholesteryl [5,5-$^2H_2$]oleate

Magnification: x 154440

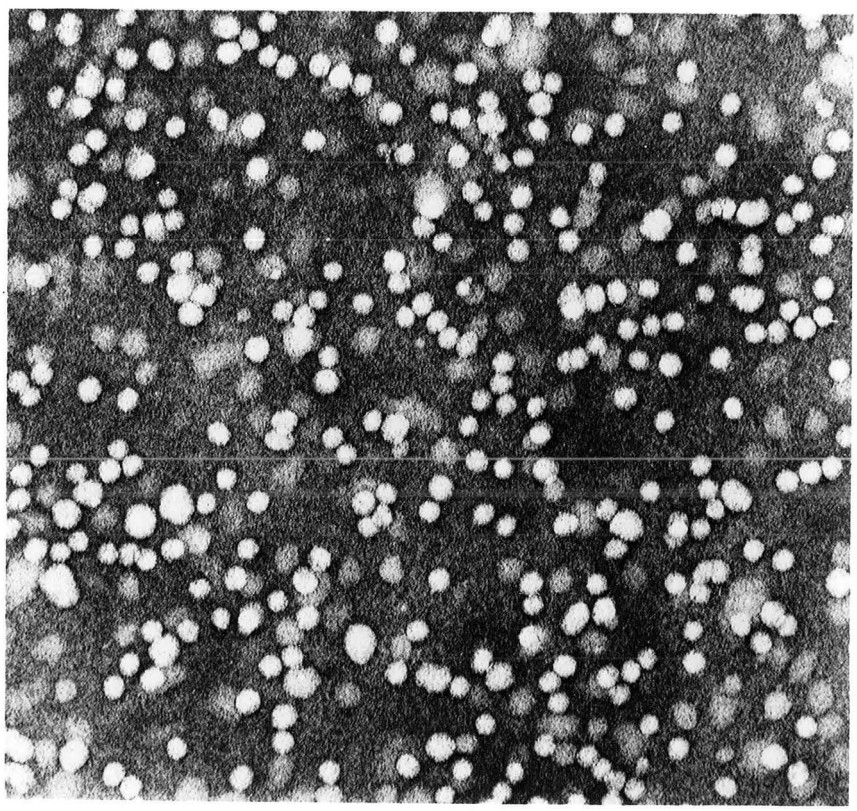

spectra of LDL_2 particles containing cholesteryl [2,2-$^2H_2$]oleate collected at 15 and 45 °C are presented in Figures 10 and 11 respectively. Each spectrum can be simulated by a superposition of two Lorentzian signals whose linewidths at half-height ($\Delta\nu_{1/2}$) differ significantly (Table 2). For example, at 15 °C the linewidth of the broad component is ~2000 Hz while the linewidth of the narrow component is ~210 Hz. The smooth lines indicate the computer calculated fit to the data.

As shown by Figures 12 and 13 these spectra cannot be simulated by a Single Lorentzian. The computer cannot converge and the smooth line represents the "best" fit after 99 iterations.

The inability to fit the recorded spectra by as one Lorentzian function can be demonstrated yet more dramatically. Assume, for the moment, that the observed spectrum is a single Lorentzian function. The mid-height linewidth can then be measured directly from the spectrum. A Lorentzian displaying the measured linewidth and amplitude can be superimposed on the experimental spectrum, as shown in Figures 14 and 15, simply by preventing any computer iteration. Figures 12 through 15 clearly demonstrate that a single Lorentzian function does not represent the recorded spectra.

Similar NMR spectra of LDL_2 labelled with cholesteryl [5,5-$^2H_2$]oleate are presented in Figures 16 to 19. In the temperature range +15 to +35 °C the spectra can only be

Figure 10. ^{2}H NMR spectrum of cholesteryl [2,2-$^{2}H_{2}$]oleate in LDL_{2} at 15 °C.

Spectral Parameters: Sweep width = 20kHz; offset = 10 kHz; number of acquisitions (NA) = 500,000; dataset = 2k zero-filled to 8k; line broadening (LB) = 20 Hz; pulse width = 8 us (80° flip angle); repetition time = 0.09 s. Spectral width simulated = 16 kHz; spectral width displayed = 2.44 kHz. The smooth line indicates the computer calculated spectrum representing the sum of two Lorentzians. The crosses indicate experimental data points.

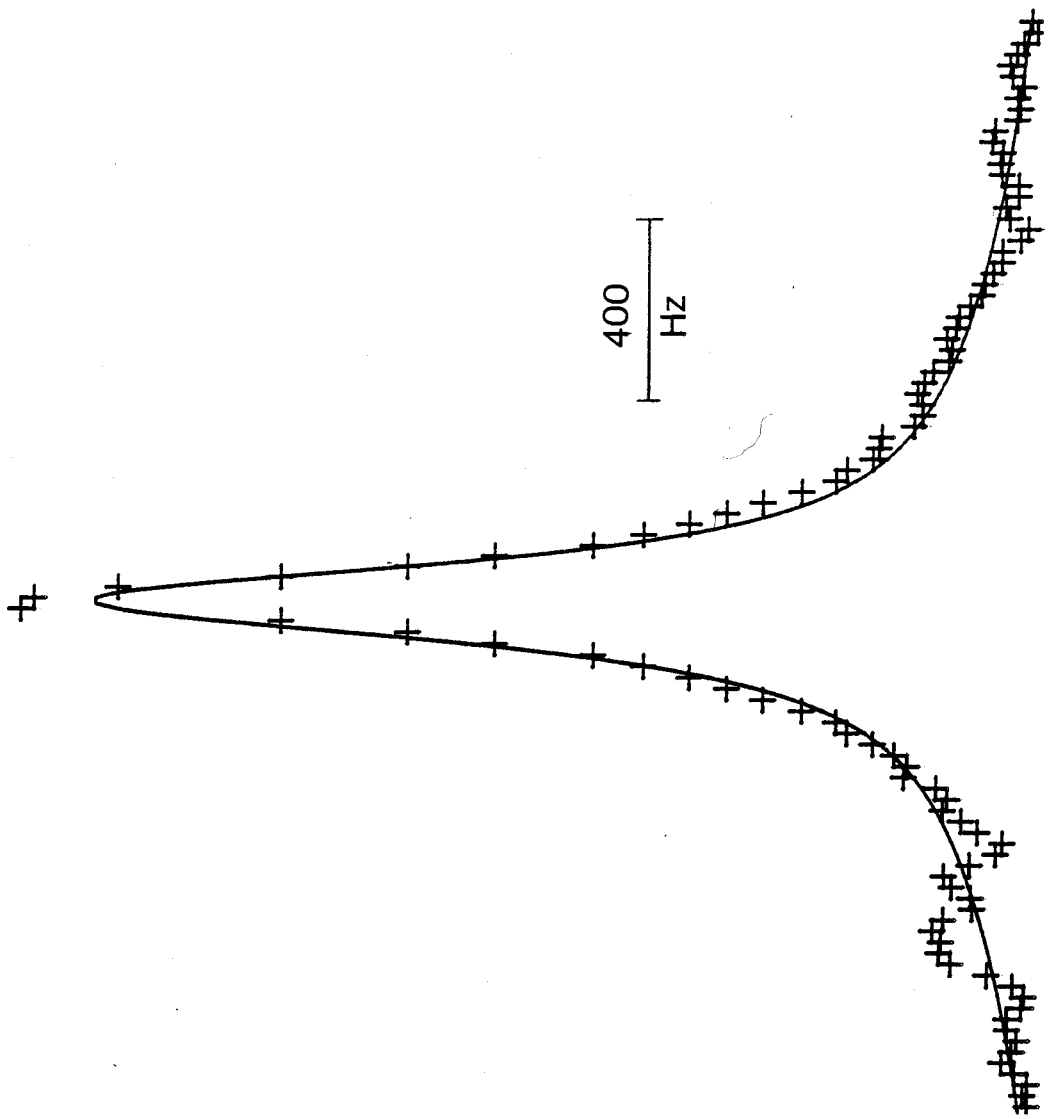
400
Hz

Figure 11. ^{2}H NMR spectrum of cholesteryl [2,2-$^{2}H_{2}$]oleate in LDL_{2} at 45 °C.

Spectral Parameters: Sweep width = 20kHz; offset = 10 kHz; number of acquisitions (NA) = 400,000; dataset = 2k zero-filled to 8k; line broadening (LB) = 10 Hz; pulse width = 8 us (80° flip angle); repetition time = 0.071 s. Spectral width simulated = 7.7 KHz; spectral width displayed = 1.95 kHz. The smooth line indicates the computer calculated sum of two Lorentzians. The crosses indicate experimental data points.

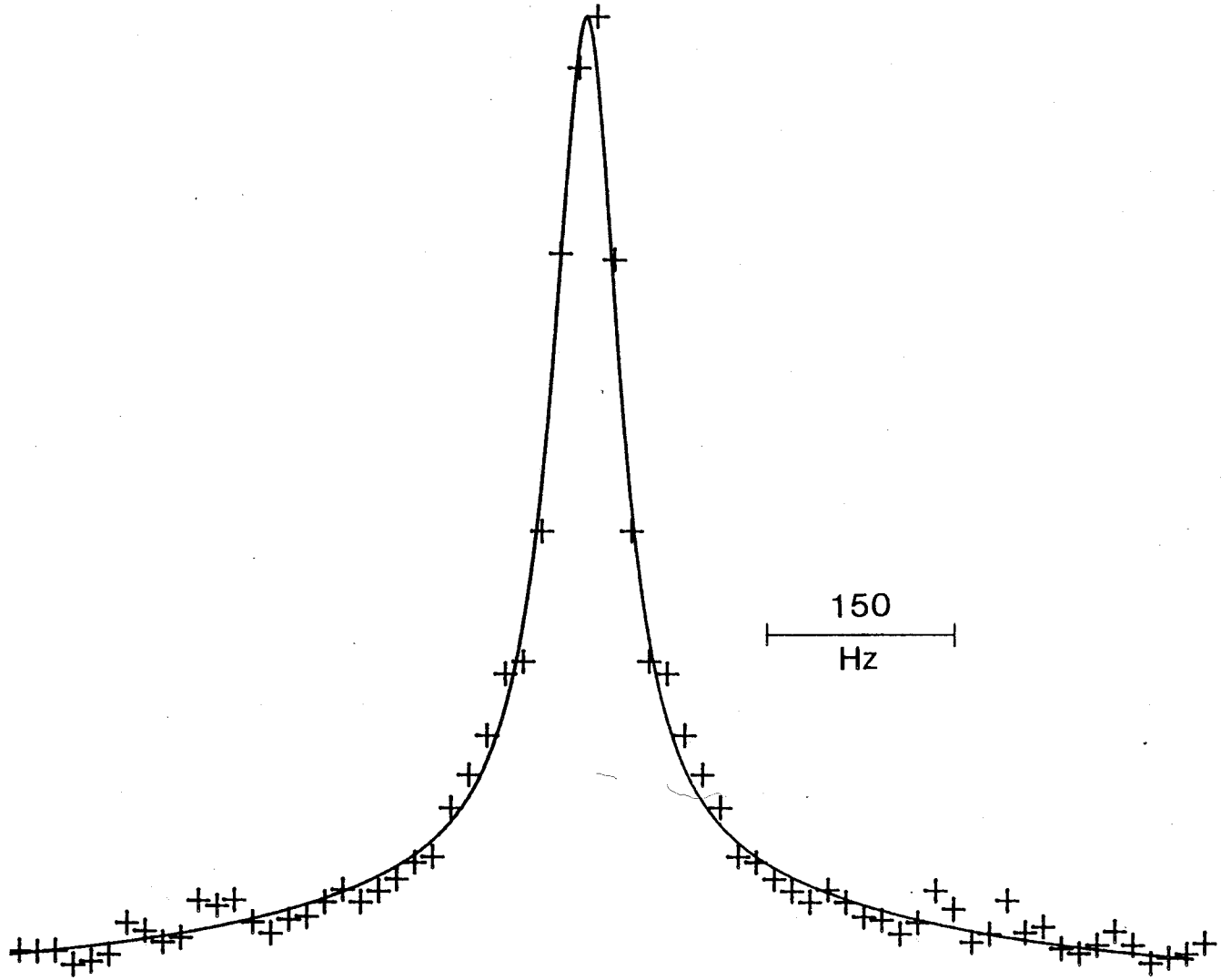
150
Hz

Figure 12. ^{2}H NMR spectrum of cholesteryl [2,2-$^{2}H_{2}$]oleate in LDL_{2} at 15 °C.

Spectral Parameters: Sweep width = 20kHz; offset = 10 kHz; number of acquisitions (NA) = 500,000; dataset = 2k zero-filled to 8k; line broadening (LB) = 20 Hz; pulse width = 8 us (80° flip angle); repetition time = 0.09 s. The dotted line indicates computer calculated "best" single Lorentzian after 99 iterations.

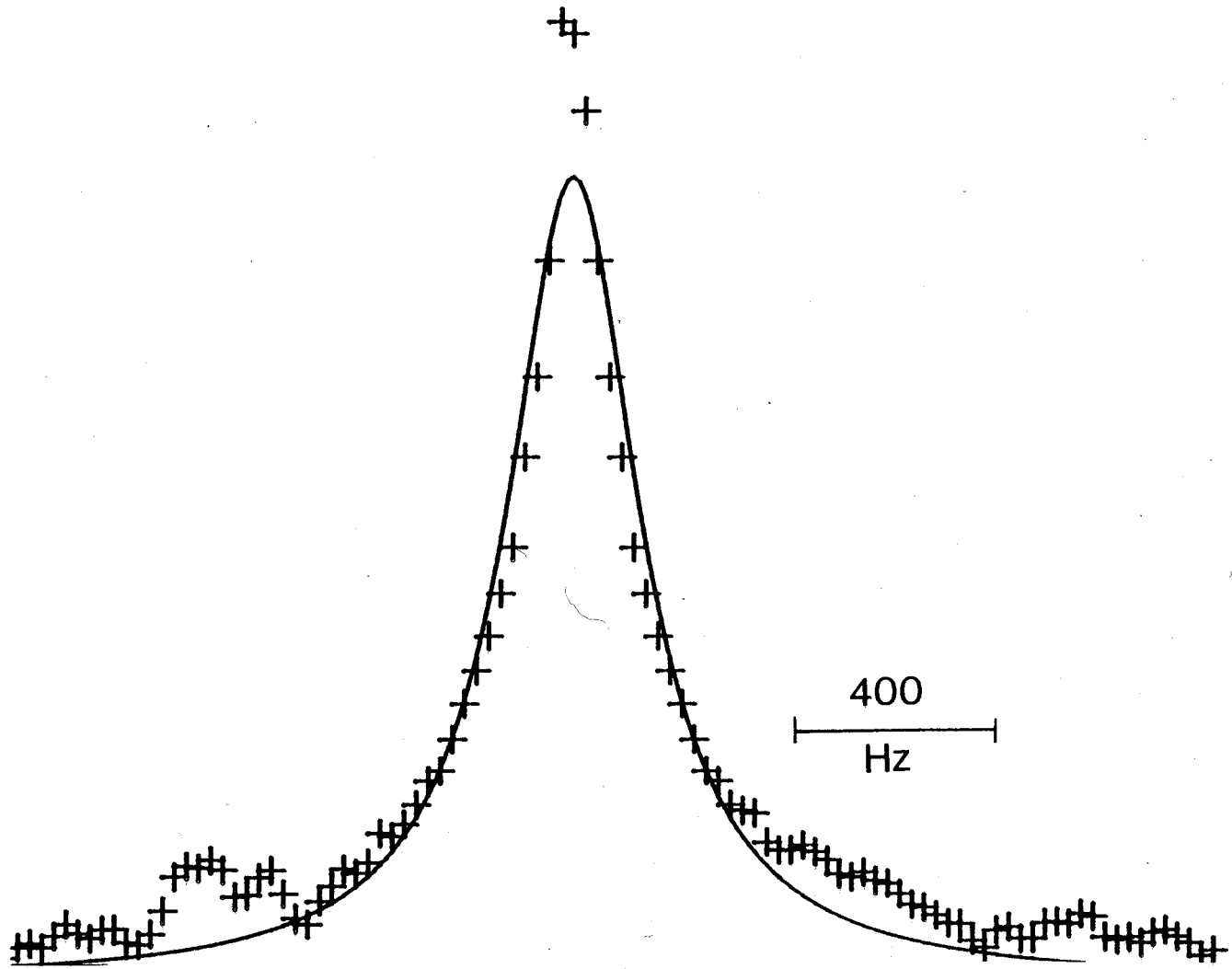
400
Hz

Figure 13. ^{2}H NMR spectrum of cholesteryl [2,2-$^{2}H_{2}$]oleate in LDL_{2} at 45 °C.

Spectral Parameters: Sweep width = 20kHz; offset = 10 kHz; number of acquisitions (NA) = 400,000; dataset = 2k zero-filled to 8k; line broadening (LB) = 10 Hz; pulse width = 8 us (80° flip angle); repetition time = 0.071 s. The smooth line indicates the computer calculated "best" single Lorentzian function after 99 iterations.

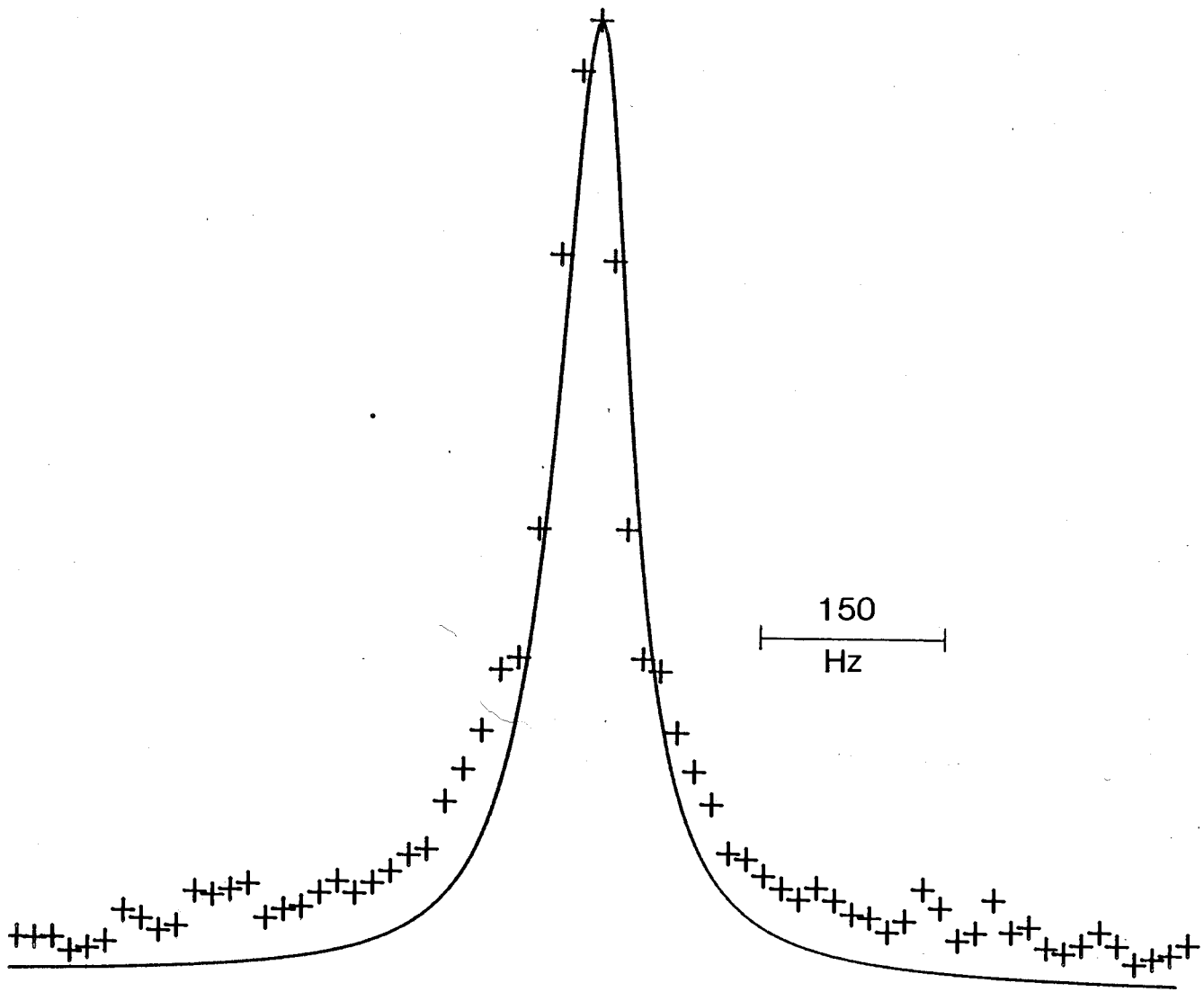
150
Hz

Figure 14. ^{2}H NMR spectrum of cholesteryl [2,2-$^{2}H_{2}$]oleate in LDL_{2} at 15 °C.

Spectral Parameters: Sweep width = 20kHz; offset = 10 kHz; number of acquisitions (NA) = 500,000; dataset = 2k zero-filled to 8k; line broadening (LB) = 20 Hz; pulse width = 8 us (80° flip angle); repetition time = 0.09 s. The smooth lines indicates a single Lorentzian function as described in the text. The crosses indicated experimental data points.

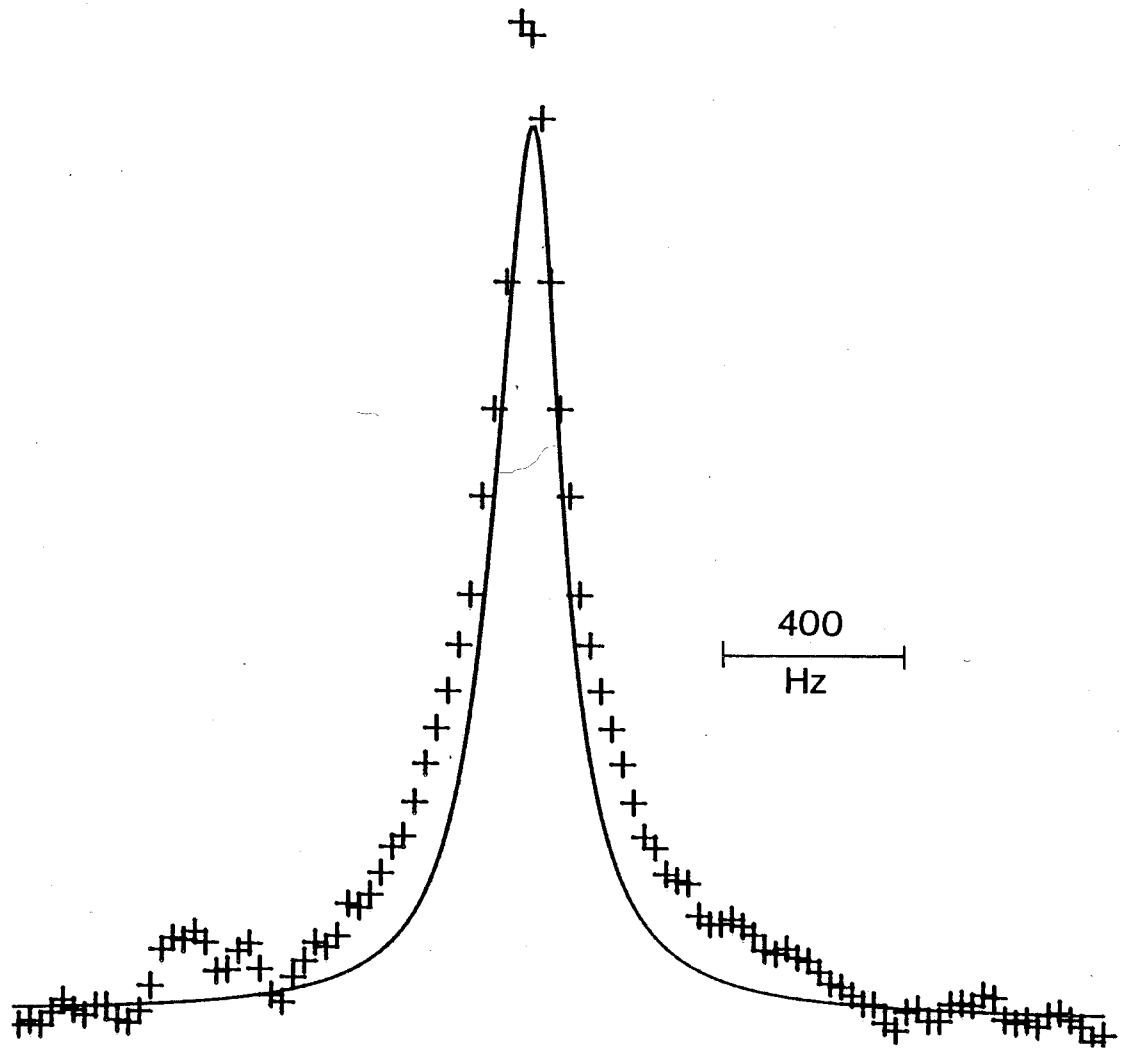
400
Hz

Figure 15. ^{2}H NMR spectrum of cholesteryl [2,2-$^{2}H_{2}$]oleate in LDL_{2} at 45 °C.

Spectral Parameters: Sweep width = 20kHz; offset = 10 kHz; number of acquisitions (NA) = 400,000; dataset = 2k zero filled to 8k; line broadening (LB) = 10 Hz; pulse width = 8 us (80° flip angle); repetition time = 0.071 s. The smooth line indicates the computer generated single Lorentzian function as described in the text. The crosses indicate experimental data points.

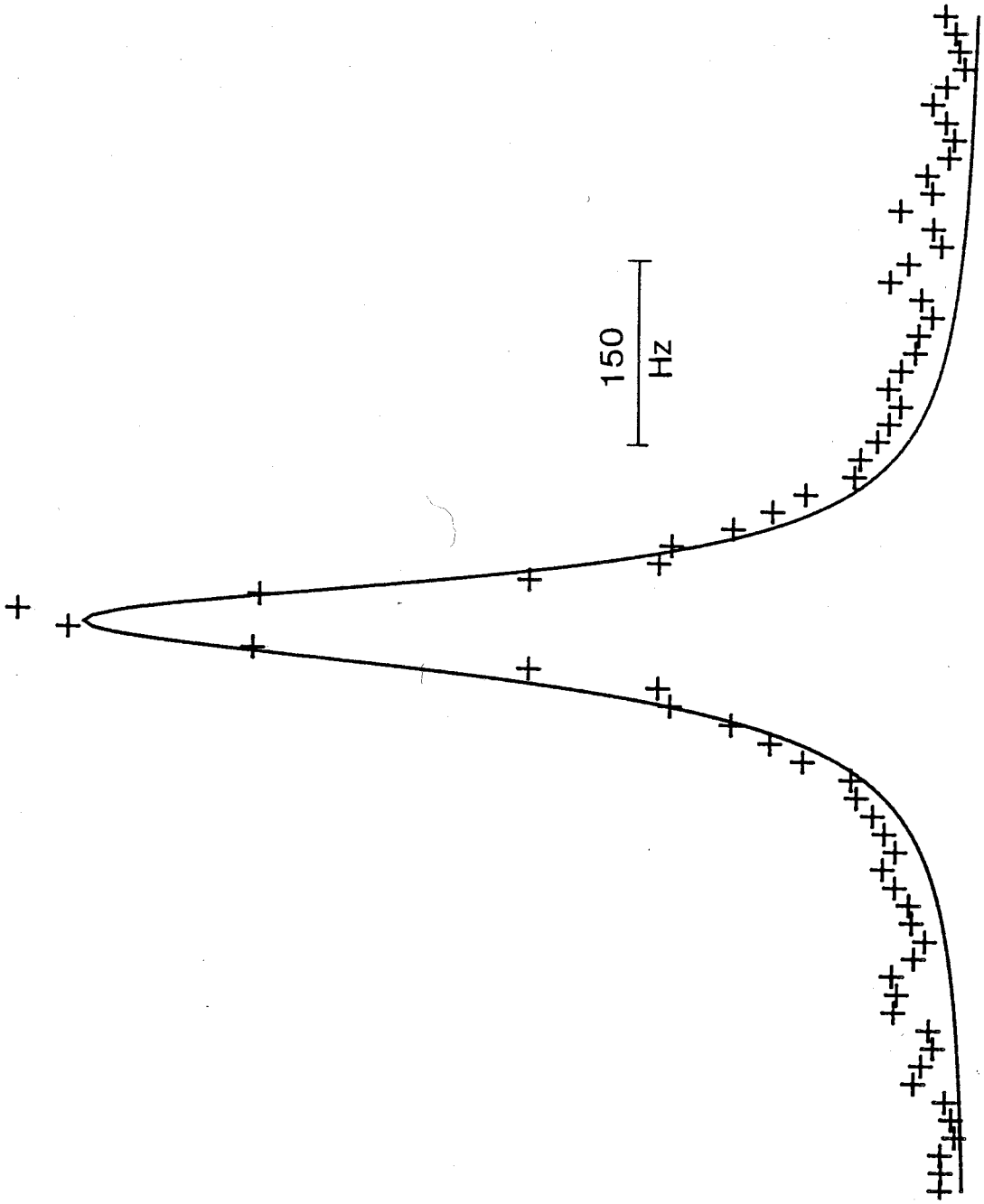
150
Hz

simulated by a superposition of a broad and a narrow Lorentzian function. At 45 °C, however, the broad and narrow components cannot be resolved. Indeed, as demonstrated in Figure 20, the spectrum recorded at 45 °C could be fit to a single Lorentzian with very good accuracy.

Figures 21 and 22 present the ^2H NMR spectra of LDL_2 containing cholesteryl oleate, selectively deuterated at various acyl chain positions at 25 and 45 °C, respectively. At chain positions beyond the 5-position, a broad spectral component may be present as well, but it is not detectable. However, these spectra can be adequately simulated by a single Lorentzian signal. The linewidths determined from Figures 21 and 22 are presented in Table 2.

The ability to unmistakably resolve two superimposed spectral components clearly depends, to a large degree, on the magnitude of the difference in linewidths between the two components. Computer simulations of theoretical spectra reveal that when two Lorentzian functions differ in linewidth by a factor of three of more, they can be resolved, without question. On the other hand, if the difference in linewidths between the broad and narrow components is a factor of two or less, they may be difficult if not impossible to resolve. To illustrate, Figure 23A presents the sum of a broad Lorentzian and a narrow Lorentzian of 200 and 100 Hz. respectively. As shown in Figure 23B, this composite spectrum can also be accurately simulated by

Figure 16. ^{2}H NMR spectrum of cholesteryl [5,5-$^{2}H_{2}$]oleate in LDL_{2} at 15 °C.

Spectral Parameters: Sweep width = 50 kHz; offset = 25 kHz; number of acquisitions (NA) = 250,000; dataset = 4k zero-filled to 8k; line broadening (LB) = 5 Hz; pulse width = 9.5 us (90° flip angle); repetition time = 0.091 s. Spectral width simulated = 28 kHz; spectral width displayed = 3.66 kHz. The smooth line indicates the computer calculated sum of two Lorentzian functions. The crosses indicate experimental data points.

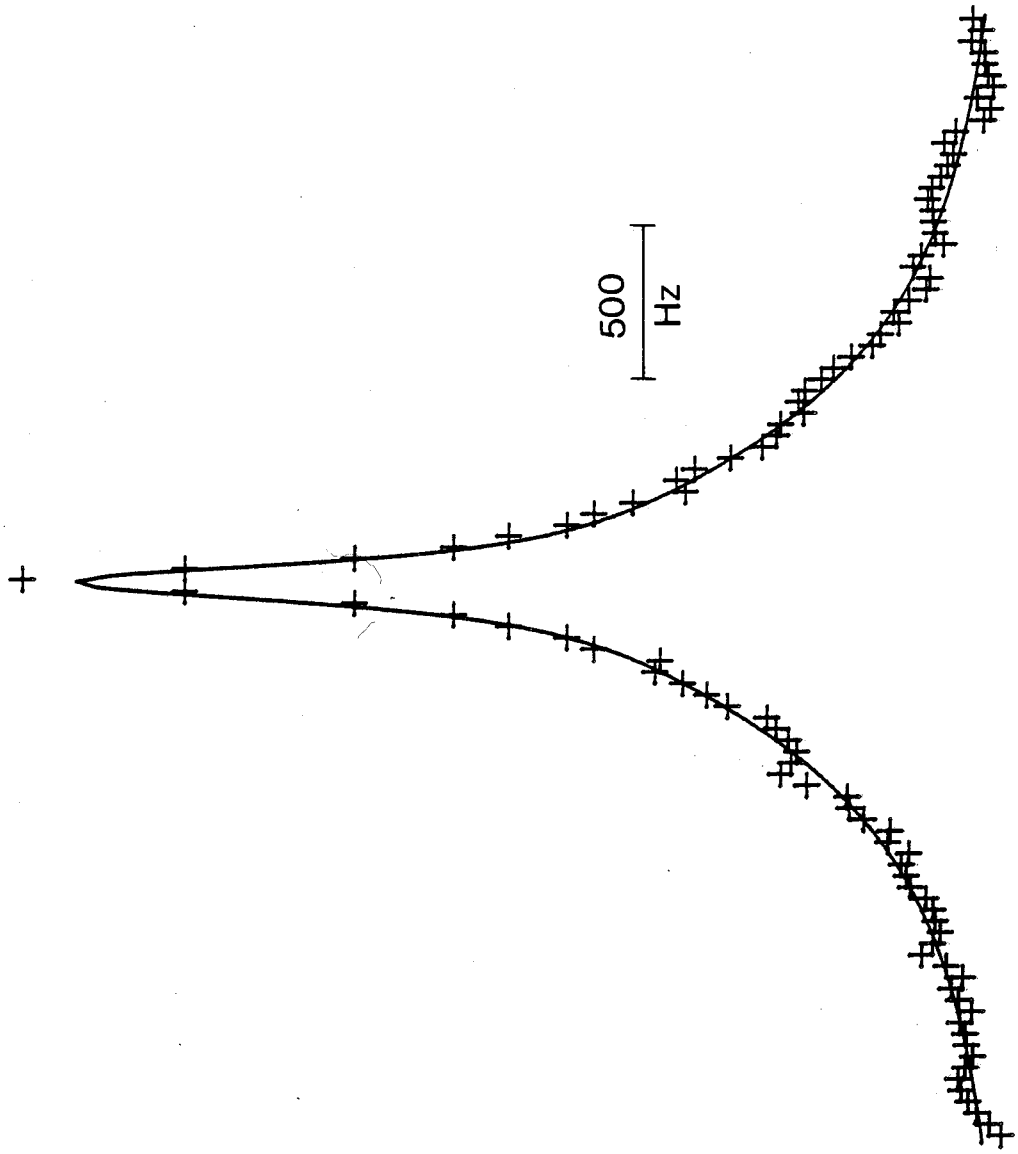
500
Hz

Figure 17. ^{2}H NMR spectrum of cholesteryl [5,5-$^{2}H_{2}$]oleate in LDL_{2} at 15 °C.

Spectral Parameters: Sweep width = 50 kHz; offset = 25 kHz; number of acquisitions (NA) = 250,000; dataset = 4k zero-filled to 8k; line broadening (LB) = 20 Hz; pulse width = 9.5 us (90° flip angle); repetition time = 0.091 s. Spectral width simulated = 28 kHz; spectral width displayed = 3.66 kHz. The smooth line indicates the computer calculated "best" single Lorentzian function after 99 iterations. The crosses indicate experimental data points.

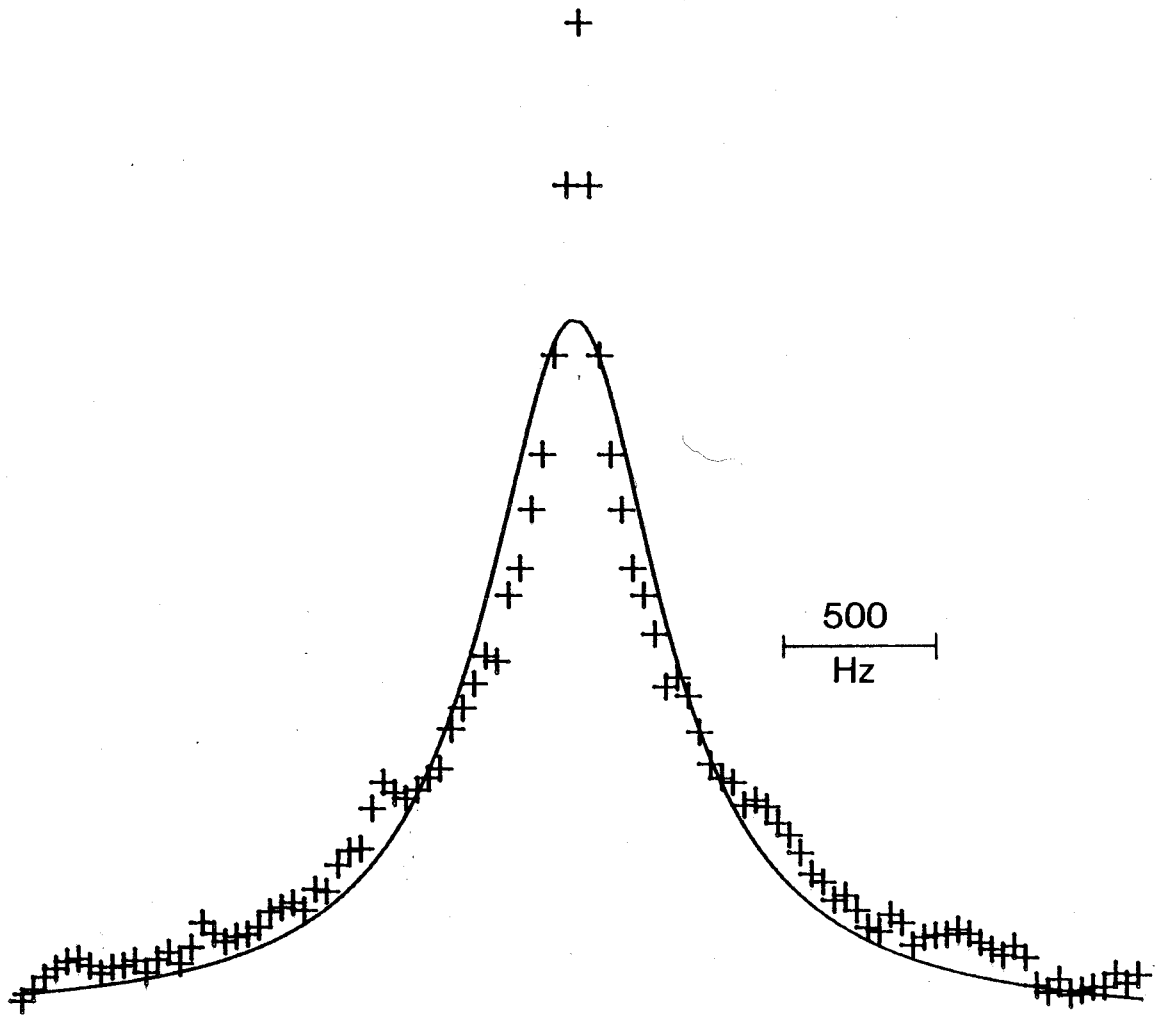
500
Hz

Figure 18. ^{2}H NMR spectrum of cholesteryl [5,5-$^{2}H_{2}$]oleate in LDL_{2} at 35 °C.

Spectral Parameters: Sweep width = 50 kHz; offset = 25 kHz; number of acquisitions (NA) = 250,000; dataset = 4k zero-filled to 8k; line broadening (LB) = 5 Hz; pulse width = 9.5 us (90° flip angle); repetition time = 0.091 s. Spectral width simulated = 4.88 kHz; spectral width displayed = 976 Hz. The smooth line indicates the computer calculated sum of two Lorentzian functions. The crosses indicate experimental data points.

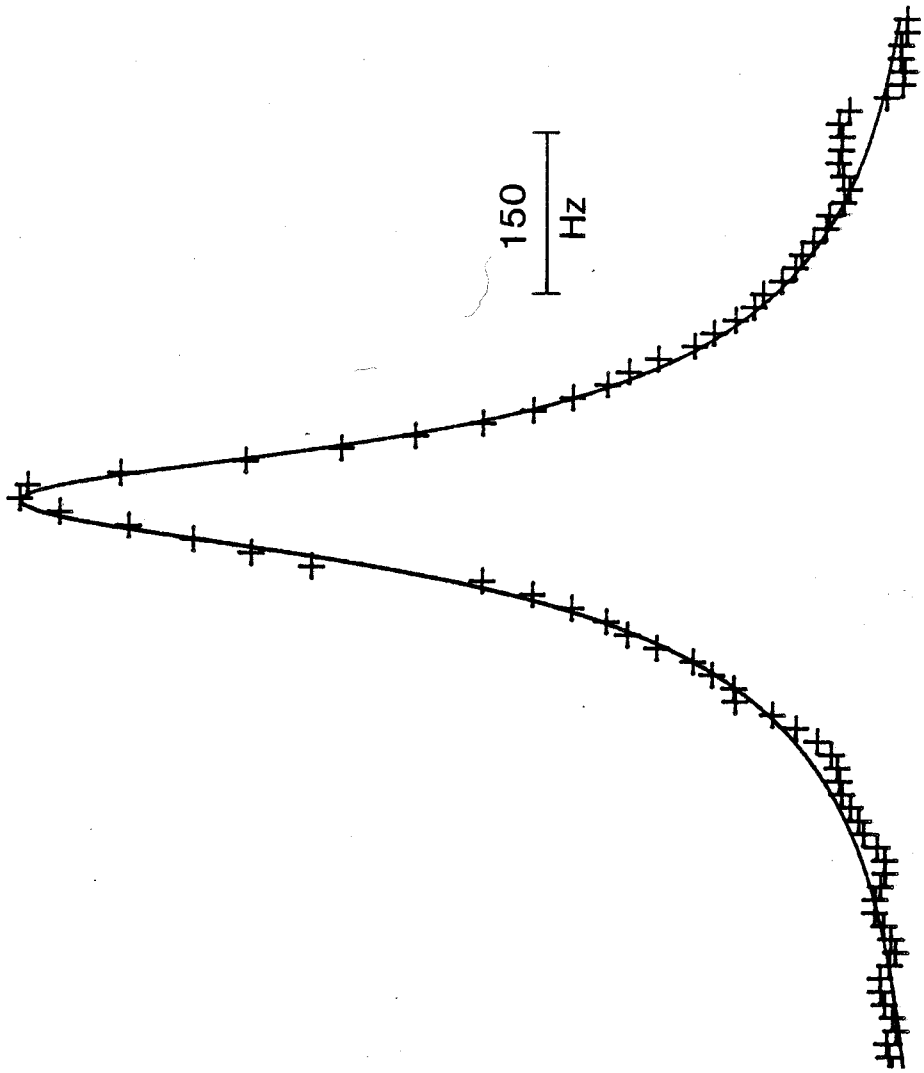
150
Hz

Figure 19. ^{2}H NMR spectrum of cholesteryl [5,5-$^{2}H_{2}$]oleate in LDL_{2} at 35 °C.

Spectral Parameters: Sweep width = 50 kHz; offset = 25 kHz; number of acquisitions (NA) = 250,000; dataset = 4k zero-filled to 8k; line broadening (LB) = 20 Hz; pulse width = 9.5 us (90° flip angle); repetition time = 0.091 s. Spectral width simulated = 4.88 kHz; spectral width displayed = 976 Hz. The smooth line indicates the computer calculated "best" single Lorentzian function.

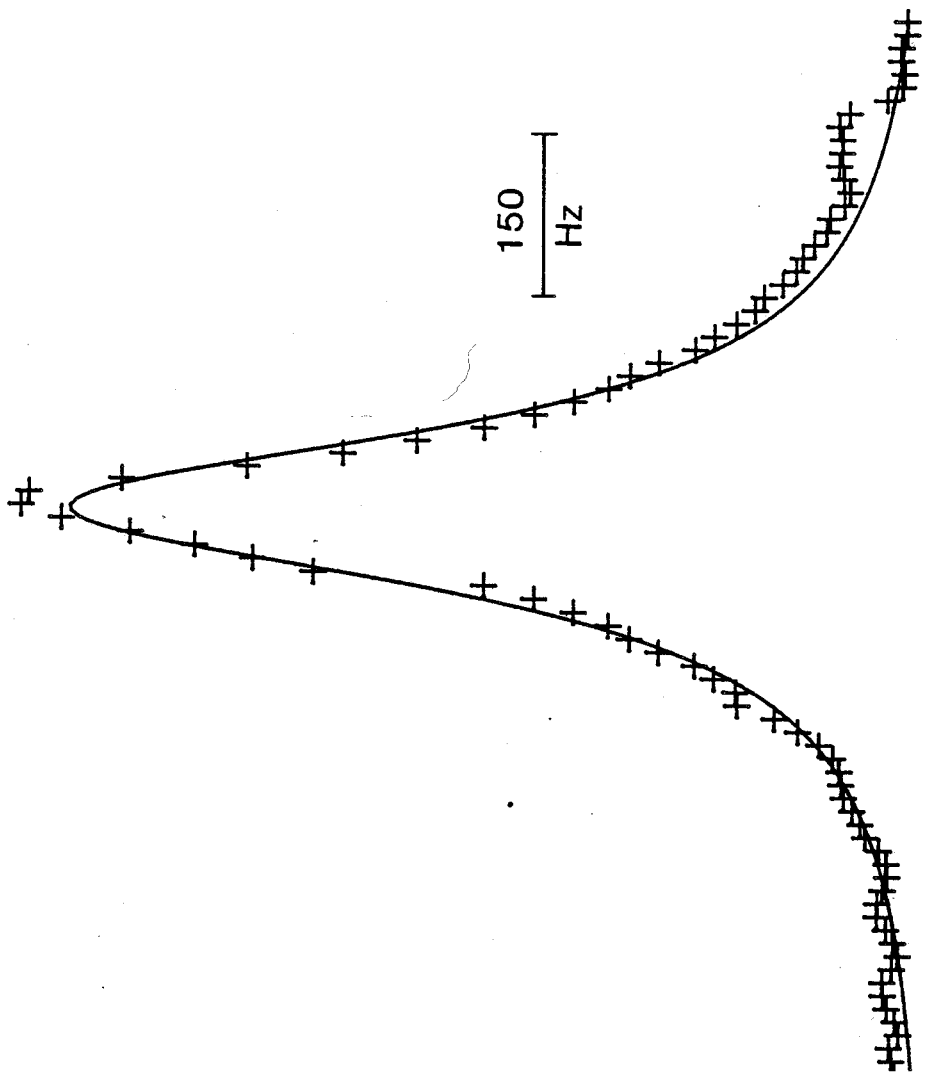
150
Hz

Figure 20. ^{2}H NMR spectrum of cholesteryl [5,5-$^{2}H_{2}$]oleate in LDL_{2} at 45 °C.

Spectral Parameters: Sweep width = 50 kHz; offset = 25 kHz; number of acquisitions (NA) = 250,000; dataset = 4k zero-filled to 8k; line broadening (LB) = 5 Hz; pulse width = 9.5 us (90° flip angle); repetition time = 0.091 s. Spectral width simulated = 1.75 kHz; spectral width displayed = 1.7 kHz. The smooth line indicates the computer calculated sinlge Lorentzian function. The crosses indicate experimental data points.

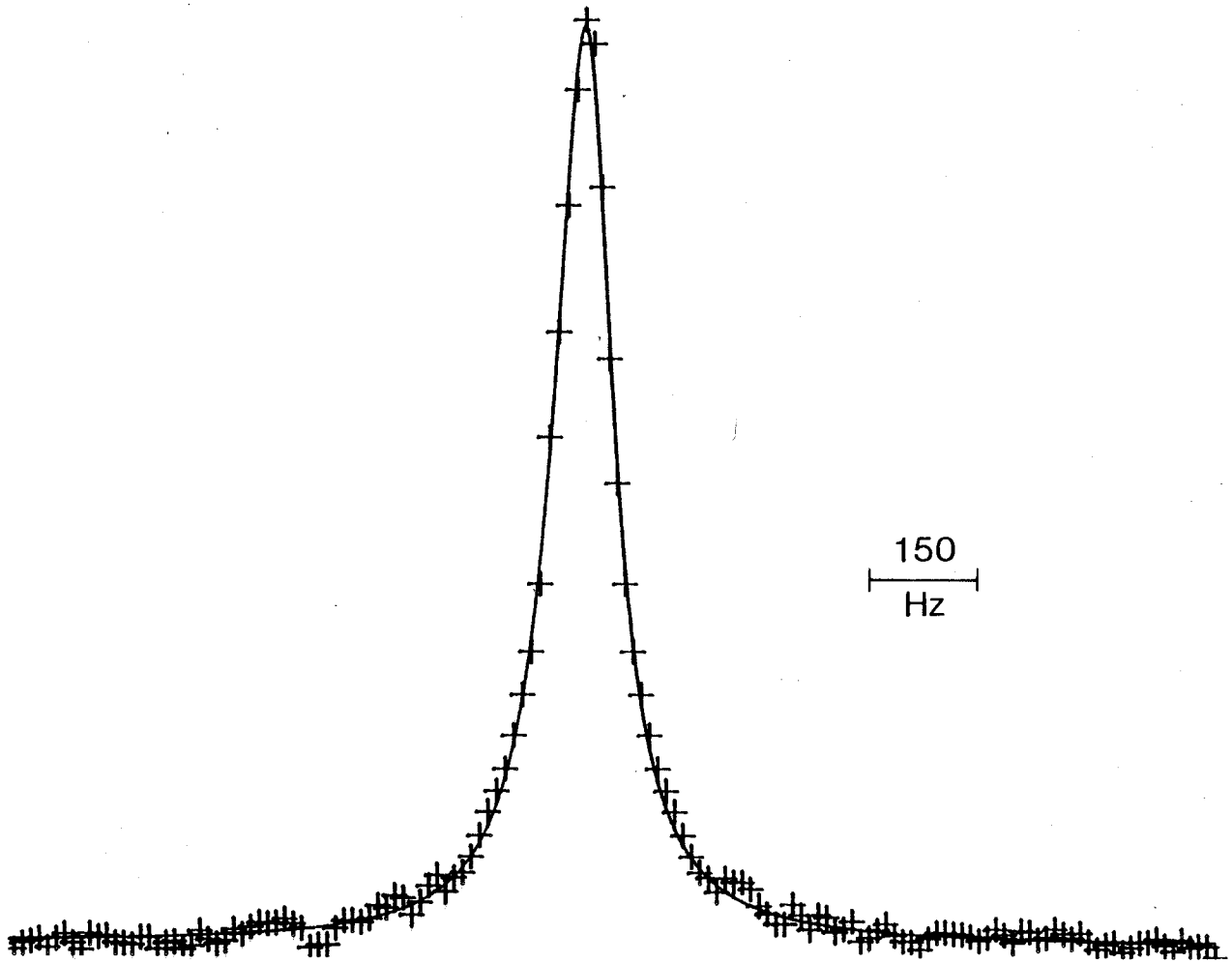
150
Hz

Figure 21. ^2H NMR spectra of selectively deuterated cholesteryl oleate in LDL_2 at 25 °C

Spectral parameters: Unless indicated otherwise, the free induction decays were collected in 2k datasets and zero-filled to 8k; 5,5-: Sweep width = 50 kHz; number of acquisitions (NA) = 250,000; dataset = 4k zero-filled to 8k; line broadening (LB) = 10 Hz; pulse width = 9.5 us (90° flip angle); repetition time = 0.091 s.

8,8-: Sweep width = 50 kHz; NA = 300,000; dataset = 8k; LB = 10 Hz; pulse width = 7.5 us (83 ° flip angle); repetition time = 0.091 s.

14,14-: Sweep width = 25 kHz; NA = 250,000; LB = 5 Hz; pulse width = 5 us (56° flip angle); repetition time = 0.051 s.

16,16-: Sweep width = 41.666 kHz; NA = 200,000; LB = 5 Hz; pulse width = 5 us (56° flip angle); repetition time = 0.035 s.

18,18,18-: Sweep width = 5 kHz with quadrature detection; NA = 10,000; LB = 1 Hz; pulse width = 40 us (90° flip angle); repetition time = 0.255 s.

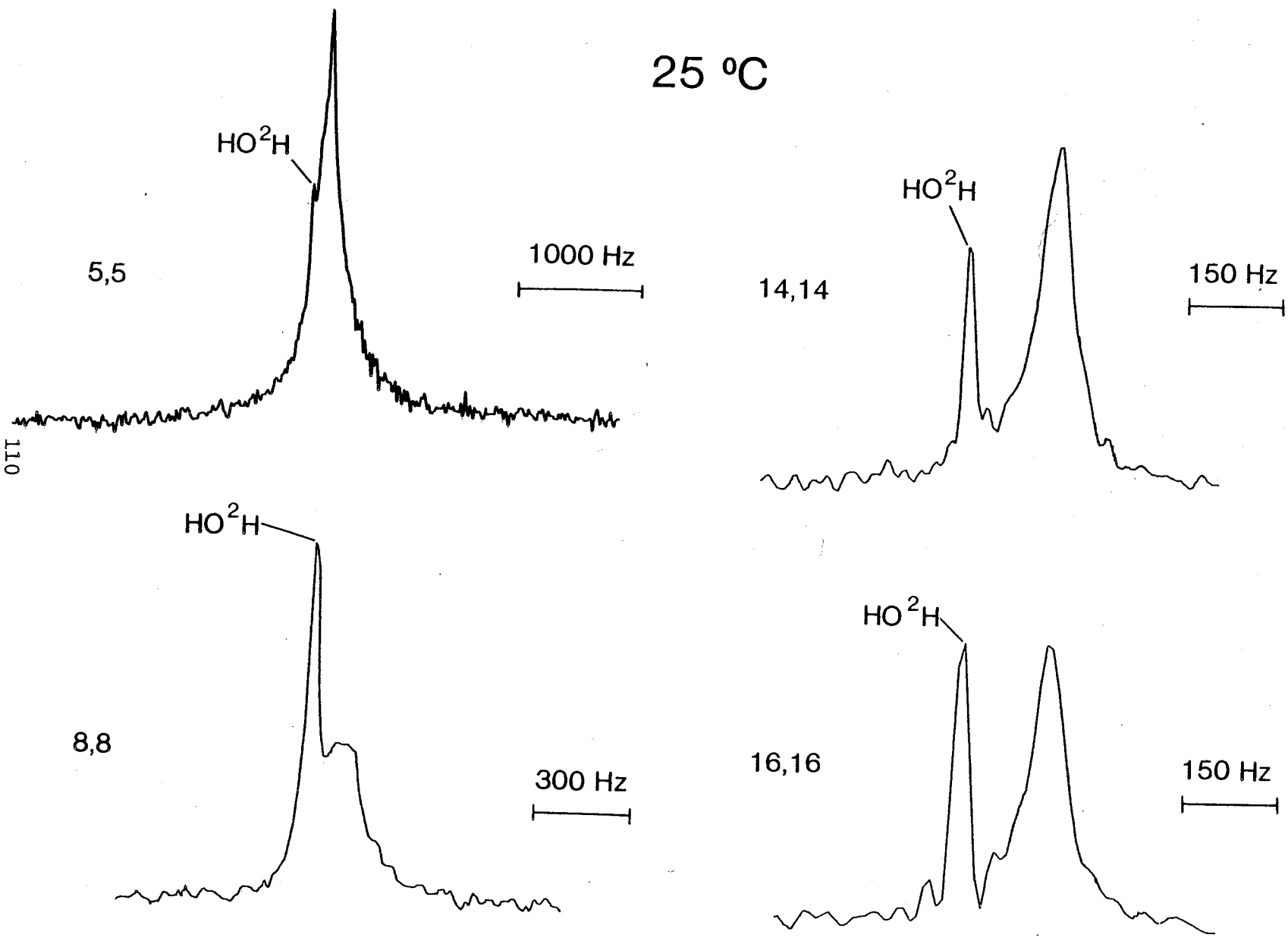
25 °C
HO²H
5,5
1000 Hz
110
HO²H
14,14
150 Hz
HO²H
8,8
300 Hz
HO²H
16,16
150 Hz

Figure 22. ^{2}H NMR spectra of selectively deuterated cholesteryl oleate in LDL_{2} at 45 °C Spectral parameters: Unless indicated otherwise, the free induction decays were collected in 2k datasets and zero-filled to 8k; 5,5-: Sweep width = 50 kHz; number of acquisitions (NA) = 750,000; dataset = 4k zero-filled to 8k; line broadening (LB) = 5 Hz; pulse width = 9.5 us (90° flip angle); repetition time = 0.091 s. 8,8-: Sweep width = 50 kHz; NA = 500,000; dataset = 4k zero-filled to 8k; LB = 5 Hz; pulse width = 7.5 us (83 ° flip angle); repetition time = 0.051 s. 14,14-: Sweep width = 25 kHz; NA = 250,000; LB = 5 Hz; pulse width = 5 us (56° flip angle); repetition time = 0.051 s. 16,16-: Sweep width = 41.666 kHz; NA = 100,000; LB = 5 Hz; pulse width = 5 us (56° flip angle); repetition time = 0.035 s.

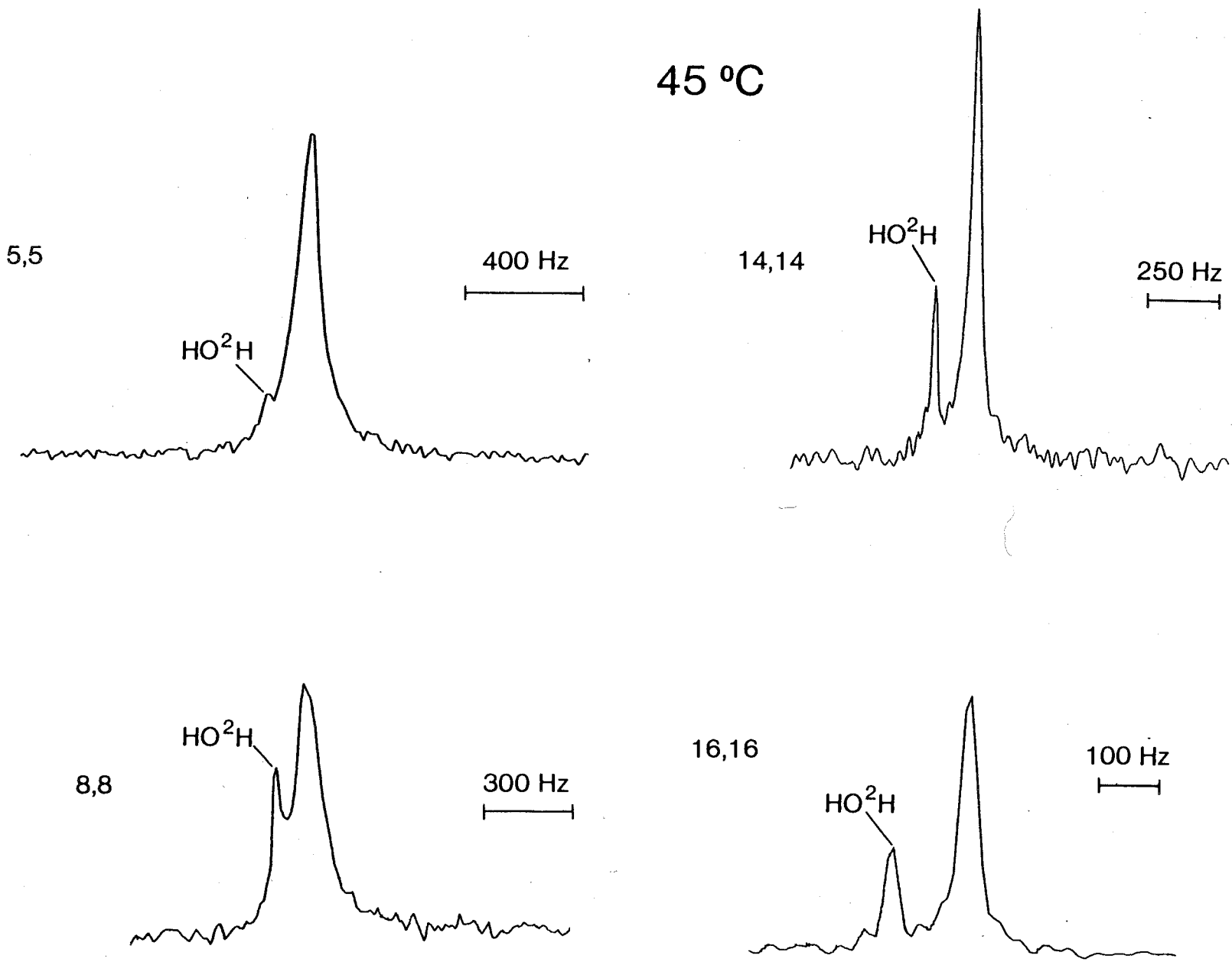
45 °C
5,5
400 Hz
HO²H
14,14
HO²H
250 Hz
8,8
HO²H
300 Hz
16,16
100 Hz
HO²H

Figure 23. Simulated Lorentzian spectra

a) Narrow component = 100 Hz.

Broad component = 200 Hz.

b): Linewidth = 136 Hz.

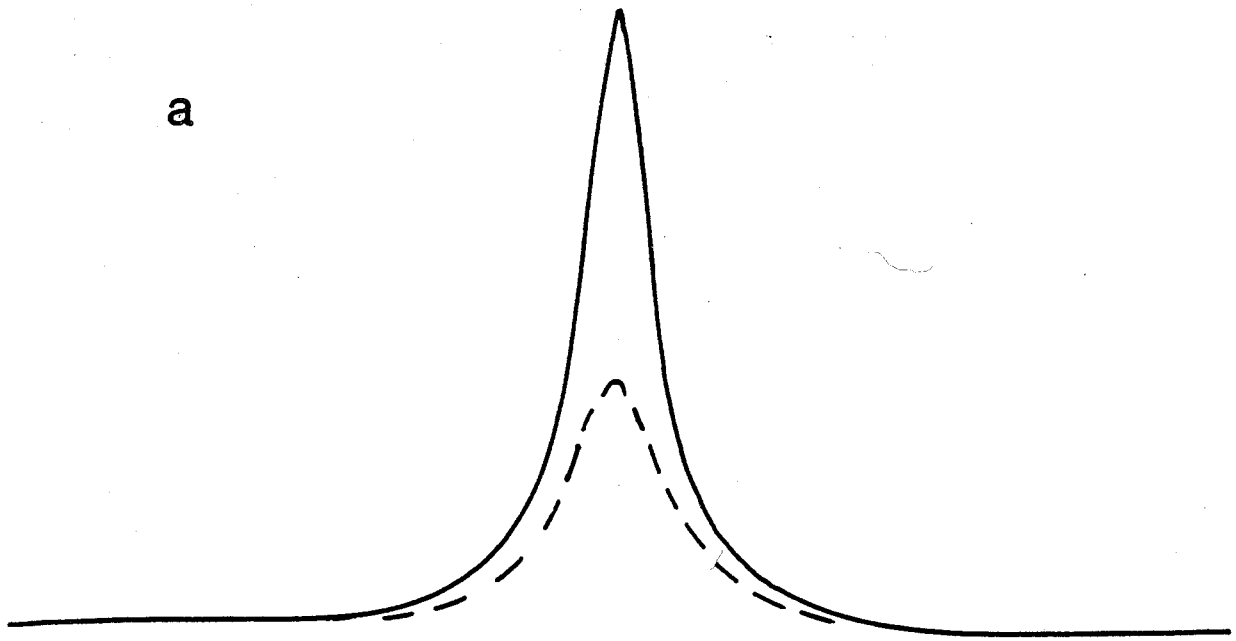
a

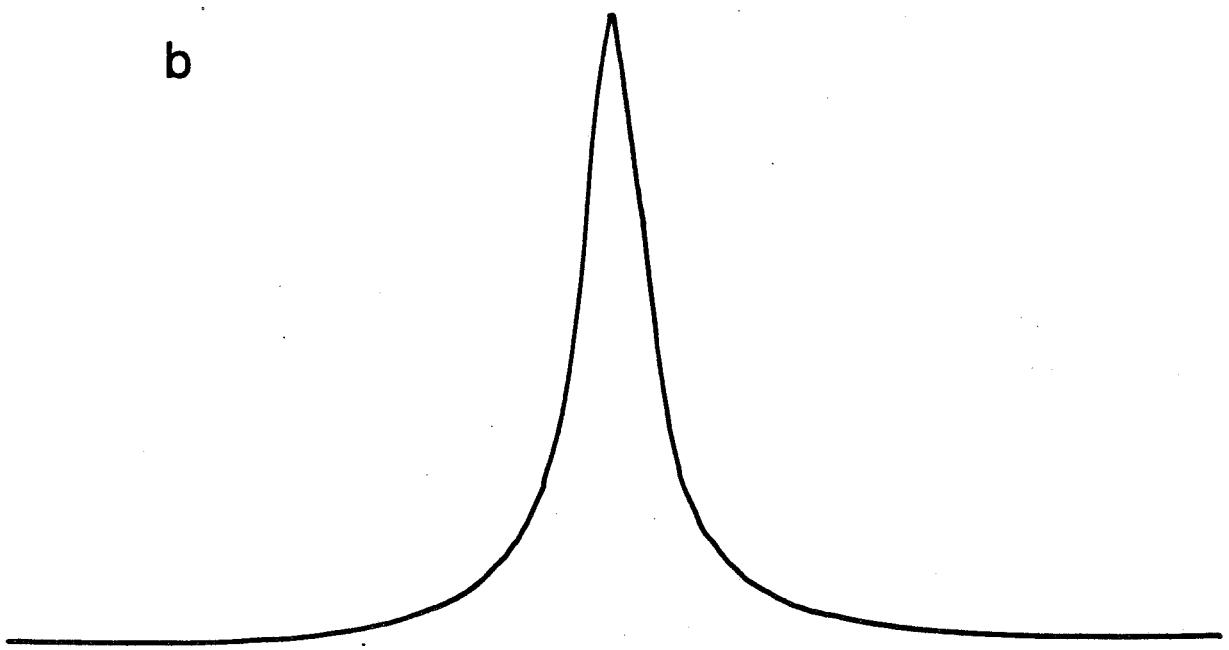
b

by a single Lorentzian function with a linewidth of 136 Hz. In this regard, the spectrum of LDL_2 containing cholesteryl [5,5-$^2H_2$]oleate, at 45 °C, may be a composite of two spectra, and therefore the linewidth observed may be a mean value. This has been indicated in Table 2.

In general the linewidths measured at selected positions at various temperatures over the range +15 to +45 °C (Table 2) tend to decrease as one proceeds from the ester linkage toward the methyl end of the acyl chain. The very narrow linewidth at the methyl position is due, in part, to rapid rotation of the methyl group in addition to the low order at that position. At each acyl chain position the linewidth decreases with increasing temperature. This trend of decreasing linewidth as temperature is raised is reversible upon reducing the temperature. The linewidths reported in Table 2 decrease with the age of the sample. Upon storage of LDL_2 labelled with cholesteryl [8,8-$^2H_2$]oleate, at 4 °C under nitrogen for 7 to 8 weeks, the observed linewidths decrease 25% to 35% as shown in Table 3. This indicates decreasing order within the lipoprotein core, and suggests structural modifications of LDL_2 occurring over time. Previously reported fluorescence energy transfer experiments (50) indicate that as LDL_2 ages, the apoprotein (apoprotein-B) migrates away from the geometric centre of the lipoprotein particle. The precise nature of the interrelationship between the apolar lipid core and the components in the polar outer

Table 2

Mid-Height Linewidth (Hz) for Selectively Deuterated Cholesteryl Oleate in LDL_2 at Various Temperatures

Chain Position	Temperature (°C)						
	15	20	25	30	35	40	45
2(NARROW)[1]	210(4)[2]	--	124(4)	--	60(2)	--	66(2)
2(BROAD)	1964(122)	--	1494(44)	--	611(44)	--	593(34)
5(NARROW)	154(5)	--	131(5)	--	119(7)	--	103(1)[3]
5(BROAD)	1230(18)	--	542(18)	--	350(36)	--	
8	172(3)	165(4)	153(4)	132(3)	117(2)	--	115(3)
14[4]	95	82	69	60	56	47	43
16	130	105	85	75	65	48	45
18	--	17	13	11	10	--	--

1 Narrow and Broad indicate respective spectral components.

2 The linewidths for the 2-, 5-, and 8-positions were determined by a 6 parameter iterative least squares lineshape analysis. The numbers parentheses indicate the uncertainty in the measurement determined from the computer calculated standard deviation.

3 Only one Lorentzian was detected.

4 Linewidths for the 14-, 16-, and 18-positions were measured directly from the spectra and are accurate to +/-10%

TABLE 3

The Effect of Ageing on Linewidths of Cholesteryl [8,8-$^2H_2$]Oleate in LDL

Sample Age	Temperature (°C)						
	15	20	25	30	35	40	45
Fresh	172(3)[1]	165(4)	153(4)	132(3)	117(2)	--	115(3)
7 weeks	---	---	108	---	86	--	75
8 weeks	---	127	103	---	94	82	77

1 Numbers in parentheses indicate uncertainty in linewidths determined from the computer calculated standard deviation. All other linewidths are accurate to +/- 10%

monolayer is unknown. However, it is possible that the apoprotein may impose packing constraints on the LDL core. The observations reported here are consistent with the reported effect of the apoprotein on the LDL core (109). At present, the physiological significance of these observations is not understood, since it has been reported by Goldstein and Brown (71) that isolated LDL_2 still exhibits complete biological activity after three months storage.

The temperature dependence of the NMR linewidths provides new insight into the molecular organization within human LDL_2. In particular, the superposition of resonances at the 2- and 5-positions of the cholesteryl ester acyl chain demonstrates the existence of two distinct regions or domains within the lipoprotein particle. Fluorescence energy transfer experiments (188) indicate that when fluorescent cholesteryl esters are exchanged into LDL_2, the esters are localized within the lipoprotein core. Futhermore, it has been amply demonstrated that cholesteryl esters display low solubility in phospholipid bilayers (76,77,86,215). Therefore it is the conclusion of this author that both cholesteryl ester regions are within the apolar core of the lipoprotein. The observation, by ^2H NMR, of two domains of cholesteryl ester within the core of LDL_2 is in accord with recent fluorescence experiments by Sklar et al. (189) which present evidence of a heterogeneous core within the lipoprotein particle.

From an intuitive point of view, one might speculate on the presence of some esterified cholesterol in the outer monolayer of LDL_2 since it is known that cholesteryl esters exchange between LDL_2 and other serum proteins as well as peripheral tissue. It must be emphasized that the conclusion reported here does not preclude the existence of cholesteryl oleate in the outer shell of the lipoprotein. Furthermore, it is interesting to note here a study on the partitioning of spin labelled lipids into different lipid domains of LDL_2 reported by Keith et al. (114). The EPR spectrum of LDL_2 containing spin labelled 2,2,5-trimethyl-5-dodecane-N-oxyl oxazolidine contained three overlapping spectral components, one of which was assigned to a region near the aqueous interface. Upon addition of ascorbic acid, the spectral component assigned to a polar environment was quickly abolished while the two remaining signals remained unaltered indicating these signals originate from lipid domains inaccessible to ascorbic acid. Unfortunately these authors did not estimate the relative magnitude of any of the components.

Our inability to observe cholesteryl oleate in the monolayer, using ^2H NMR, can be readily explained. Consider, for a moment, a sample of LDL_2 containing 25 mg of phospholipid. This is approximately the size of a typical NMR sample employed during these experiments. Hamilton and Small (86) have reported the maximum solubility of cholesteryl oleate in egg PC vesicles

is 1.6 wt%. In the case of LDL_2, however, this figure may represent the upper limit to be expected in the outer shell since it has been demonstrated that the solubility of cholesteryl oleate in egg PC vesicles decreases by approximately 50% in the presence of 20 mol% cholesterol (76). If cholesteryl linoleate and cholesteryl oleate are present in the LDL_2 phospholipid monolayer in the same weight ratio (cholesteryl linoleate:cholesteryl oleate = 52:20) as in the lipoprotein core (162) then the maximum weight of cholesteryl oleate in the monolayer cannot exceed 0.15 mg. However, based on radiolabel studies reported here, only 8%, or 0.012 mg, of this ester will be deuterium labelled. This small amount is below the limit of detection of our instruments.

The deuterium spin-lattice relaxation times, T_1, of deuterated cholesteryl oleate in LDL_2 at 25 °C are shown in Table 4. For the deuterated methylene segments the T_1 values range from 0.015-0.04 seconds, and for the methyl position T_1 is 0.19 seconds. This indicates molecular motion increases toward the methyl end of the chain.

From the linewidths presented in Table 2 and the spin-lattice relaxation times in Table 4 the orientational order at a given chain position can be quantified through the order parameter, S_{CD}, by application of equation 3.54. For the convinience of the reader, the assumptions underlying equation 3.54 are briefly recounted here. Firstly, it is

Table 4

Spin-Lattice Relaxation Times of Selectively Deuterated Cholesteryl Oleate in LDL_2 at 25 °C

Acyl Chain Position	Relaxation Time (msec.)
2 (Broad Component)	----
2 (Narrow Component)	----
5 (Broad Component)	15 (+/-1.5)
5 (Narrow Component)	15 (+/-1.5)
8	15 (+/-1.5)
14	25 (+/-2.5)
16	40 (+/-4.0)
18	191 (+/-19)

assumed that the linewidths reported in Table 2 are the result of two classes of motion, one fast and the other 2-3 orders of magnitude slower (203). Then, as shown in equation 3.47:

$$\Delta\nu_{1/2} = (1/\pi T_2^*) = [1/(\pi T_{2(FAST)}) + (1/(\pi T_{2(SLOW)})]$$

Secondly, fast local (segmental) motions characterized by the correlation time t_c are assumed to be in the extreme narrowing limit such that $\omega_0^2 t_c^2 << 1$. Therefore

$$(1/\pi T_{2(FAST)} = (1/\pi T_1)$$

One final assumption implied by the discussion in Chapter 3 is that there are no other slow fluctuations of the C-^{2}H bond, such as rigid-stick type motions, contributing to the linewidth (175). It must be emphasized, however, that should this last assumption not be strictly true, the conclusions drawn from the data presented here are not negated, since motions of this type will uniformly reduce S_{CD} at all acyl chain positions by the same factor (175). In this regard, the order parameters determined by equation 3.54 represent the lower limit of S_{CD}.

In phospholipid vesicles, the effective correlation time t_c of equation 3.54 contains contributions from isotropic rotation of the vesicle as well as lateral diffusion. The lateral diffusion coefficient, D, can be evaluated through

the relationship:

$$D = kT/6\pi n_m r_m$$

where k is the Boltzmann constant, T is the temperature in degrees Kelvin, n_m is the viscosity at the site of the molecule, and r_m is the radius of the diffusing molecule. In LDL_2 the effect of lateral diffusion is difficult to assess. According to the currently popular model of LDL structure, extended cholesteryl esters are thought to be arranged radially in concentric layers (42,43). From X-ray crystallographic experiments it is known that the radius of cholesteryl oleate in the extended form is 21 A° (36), but the viscosity within the core of LDL_2 can only be estimated. Fluorescence depolarization studies of 1,6 diphenyl-1,3,5-hexatriene in human LDL_2 (109) indicate the viscosity within LDL_2 is 6.1 poise at 25 °C in contrast to a viscosity of only 0.86 poise in egg PC vesicles at the same temperature. However, the exact location of the fluorescent probe in the lipoprotein could not be ascertained since fluorescence energy transfer experiments revealed that the probe was 23-60 A° away from tryptophan residues of the apoprotein. More recent experiments (50) indicate the tryptophan residues of the apoprotein rest 10-20 A° from the surface of fresh LDL_2, therefore it may be inferred that at least some of the fluorescent probe partitions into the core of

the lipoprotein. Within the limits of the accuracy of the core viscosity, the effect of diffusion can be calculated.

Assuming an average distance of 40 A° from the geometric centre of LDL_2 particles to the site of the deuterium nucleus, it can be shown that lateral diffusion reduces the value of t_e by ~5% relative to the value calculated considering only the isotropic rotation of the particle. Therefore, to a first approximation, lateral diffusion can be neglected. Considering only the isotropic rotation of the lipoprotein, the correlation time can be calculated from the Stokes-Einstein equation:

$$t = (4\pi nR^3/3kT)$$

where, in this case, n refers to the solvent viscosity. At 298 °K solvent viscosity is 0.8904 cp and the radius of labelled LDL_2, determined by electron microscopy, is 100 +/- 10 A°. The rotational correlation time has a value of 9×10^{-7} s. The order parameters for selected cholesteryl ester acyl chain positions are shown in Table 5. Since the effect of lateral diffusion has been neglected, these order parameters represent the lower limit to S_{CD}. Order parameters have not been calculated at the high temperature extreme of the temperature range of the experiments since electron microscopy was not performed at 45 °C, and there is no reason to assume <u>a priori</u> that particle size remains constant over this temperature range.

Table 5

Order Parameters for Selectively Deuterated Cholesteryl Oleate in LDL_2 at 25 °C

Acyl Chain Position	Order Parameter S_{CD}
2 (Broad Component)	0.20*
2 (Narrow Component)	0.05*
5 (Broad Component)	0.12
5 (Narrow Component)	0.05
8	0.06
14	0.04
16	0.05
18	0.018

* Spin-Lattice Relaxation time is assumed to be 15 msec.

As shown in Table 5 some of the cholesteryl oleate exists in a relatively more ordered domain, S_{CD} = 0.12 - 0.20, while, as indicated by the narrow component, some of the ester exists in a region of approximately 3 times less order. The S_{CD} values for cholesteryl oleate in the disordered domain are in excellent agreement with the order parameter one can determine from the EPR spectrum of cholesteryl 12-doxyl stearate in LDL at 37 °C presented in a study by Keith et al. (114). A value of S_{EPR} ($\sim 2S_{CD}$) of 0.13-0.14 was calculated. The order parameters reported here are considerably lower than those determined by fluorescence experiments using cholesteryl cis-parinarate in (Figure 24) LDL_2 at 25 °C (189). The order parameter reported by Sklar et al. (189) is 0.74, indicating a very high degree of order. Two factors may contribute to this discrepancy. Firstly, deuterium order parameters are sensitive to motions substantially slower than the order parameters determined by fluorescence spectroscopy (101). Therefore, motions that appear slow on the fluorescence time scale may still appear fast when measured by ^2H NMR. Secondly, a conjugated polyene such as the acyl chain of cholesteryl cis-parinarate (Figure 24) is less flexible than the acyl chain of cholesteryl oleate and may actually induce order into the lipoprotein core. The fluorescence order parameter would then reflect the mean orientation of a rigid octatetraene. The level of perturbation introduced into the lipoprotein core by cholesteryl cis-parinarate is evidenced

Figure 24. Cholesteryl cis-Parinarate

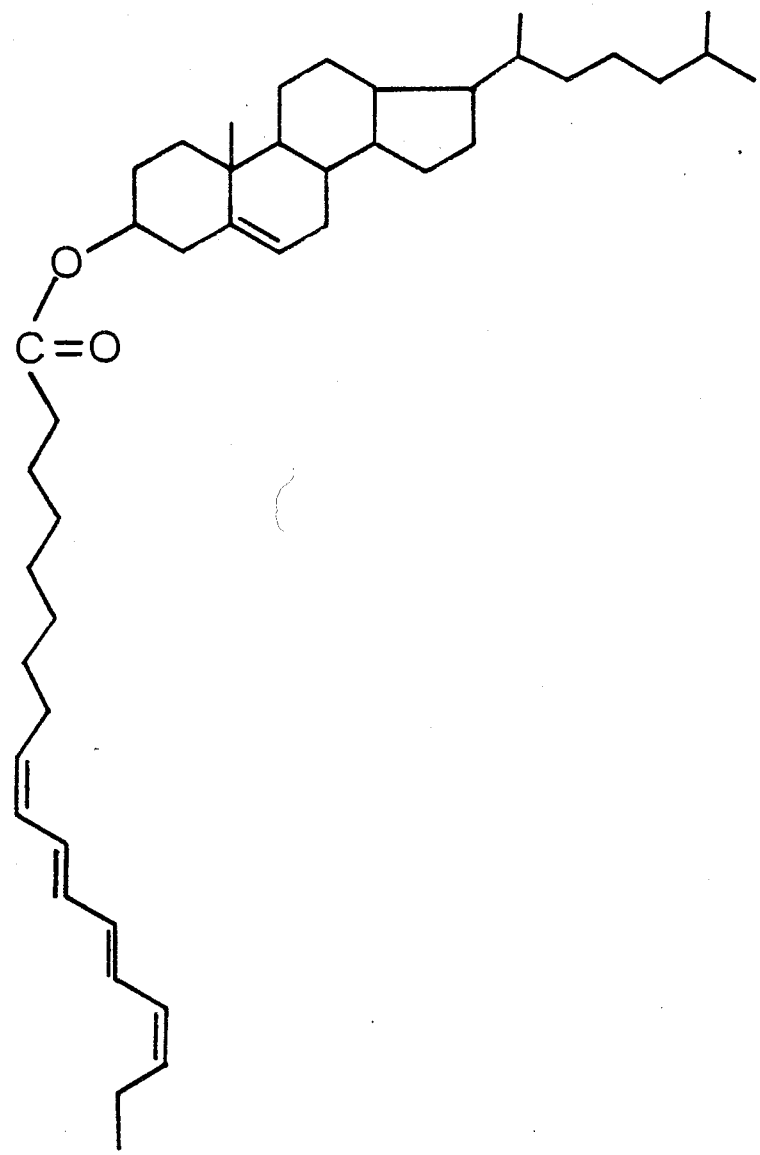
O
C=O

by the fact that the thermal transition temperature (T_M), measured by differential scanning calorimetry, is depressed by 10-15 °C upon incorporation of 5 wt% of the ester (189).

The order parameters in the less ordered domain are considerably lower than those reported by Parmar et al. (151) in reconstituted high density lipoprotein (HDL) containing selectively deuterated cholesteryl palmitate at 25 °C. In reconstituted HDL the values reported are S_{CD} ~0.35 for positions 2 through 6, S_{CD} ~0.20 at the 11- and 12-positions, and S_{CD} ~0.06 for the methyl terminus of the acyl chain. Moreover, even the more highly ordered ester region of LDL_2, where S_{CD} = 0.20, is significantly less ordered than in HDL. The low values of the order parameter determined for cholesteryl oleate in LDL_2 may be due to two factors. Firstly, in contrast to LDL_2, no triglycerdes were present in the reconstituted HDL. Moreover, if an elevated LDL_2 triglyceride content (discussed earlier) is a general feature of this technique, orientational order in the LDL_2 core will be reduced (43). Secondly, there might exist an orientational effect due to the presence of the cis-double bond in the oleic acyl chain (178) such that anisotropic motions of the C-^{2}H bond may not be axially symmetric about the normal to the lipoprotein surface. The decreased linewidths observed at the 14-position relative to the 16-position may also be a consequence of such an orientation effect.

The phase behaviour of the LDL_2 core can be demonstrated by

plotting the data in Table 2 as illustrated in Figure 25. At chain positions between the steroid moiety and the olefinic region the linewidths decrease sharply, as the temperature is increased from 15 to 35 °C. This dramatic decrease in linewidth cannot be completely accounted for by lower solvent viscosity at higher temperature, and therefore signals a significant decrease in order within the lipoprotein core. As shown by the insert to Figure 25, the broad spectral component observed at the 2- and 5-positions displays similar linewidth behaviour. Above 35 °C, the decrease in linewidth is less dramatic thus indicating the phase transition is complete. Therefore, as indicated by the linewidths, the core of LDL_{2} is significantly less ordered at physiological temperature than at lower temperatures. It is important to note, however, that although the orientational order is reduced at physiological temperature, a finite amount of order remains in both cholesteryl ester domains. In support of the observations reported here, ^{13}C NMR experiments of Sears et al. (168) indicate that cholesteryl esters in native LDL_{2}, at 50 °C, are more ordered than in isotropic esters at the same temperature.

Linewidths at the 14-, 16-, and 18-positions display a monotonic decrease with increasing temperature between 15 and 45 °C, with no inflection near 35 °C. This indicates that acyl chain positions near the methyl terminus are less sensitive to the phase behaviour of the lipoprotein core. These observations

Figure 25. Plot of ^2H NMR linewidths *versus* temperature for selectively deuterated cholesteryl oleate in LDL_2

(□) 2,2-$^2H_2$

(○) 5,5-$^2H_2$

(△) 8,8-$^2H_2$

(●) 14,14-$^2H_2$

(■) 16,16-$^2H_2$

(▲) 18,18,18-$^2H_3$

Inset indicates the temperature dependence of the broad component:

(□) 2,2-$^2H_2$

(○) 5,5-$^2H_2$

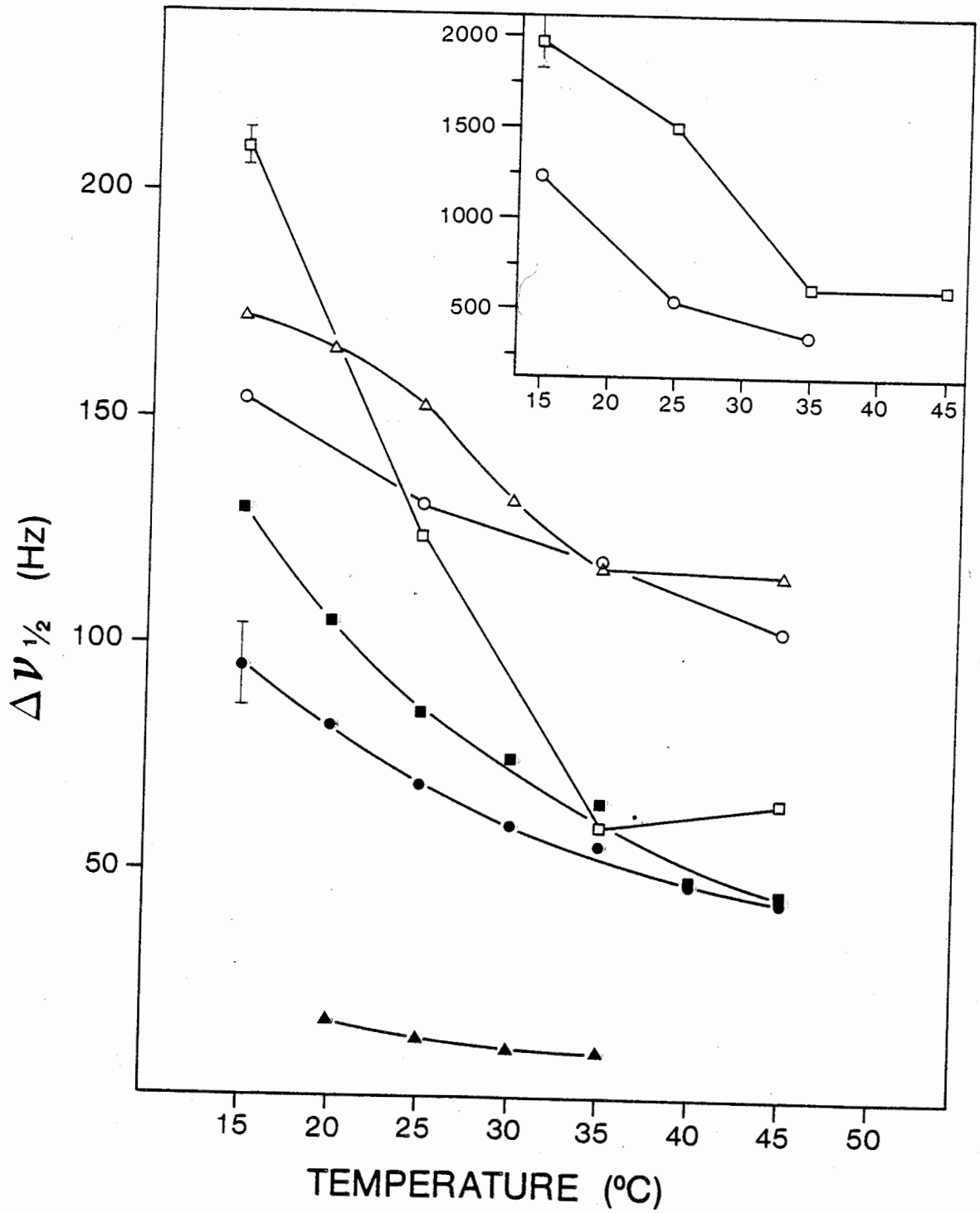
2000
1500
1000
500
15
20
25
30
35
40
45
200
150
100
50
$\Delta \nu_{1/2}$ (Hz)
15
20
25
30
35
40
45
50
TEMPERATURE (°C)

are in accord with the calorimetric studies reported by Barrall and Johnston (10) which indicate that chain positions between the beginning of the olefinic region and the methyl terminus contribute little to the phase behaviour of the cholesteryl esters.

Previous literature has reported a broad phase transition extending from ~20 °C to ~40 °C which has been attributed to a phase change of the cholesteryl esters within the core of LDL_{∞} (43,188). Table 2 and Figure 25 demonstrate that even at 15 °C, which is below the onset of the phase transition observed by DSC, some of the esters exist in a disordered state. Moreover, from Table 2 and Figure 25 it is clear that the more highly ordered domain persists even at 45 °C.

At the 2-position the more highly ordered domain, represented by the broad component, constituted 60 +/- 7% of the cholesteryl oleate signal throughout the temperature range of these experiments. By way of contrast, at the 5-position the more highly ordered domain constituted 85% of the signal at 15 °C. As the temperature was increased the broad component decreased steadily until at 45 °C in constituted 53% of the spectrum. As a consequence of these contracictory data, it is not possible to determine if the relative population of each region is temperature dependent.

Above the thermal transition the core of LDL_{∞} has been described as "liquid-like" (43,168). However, in view of the

fact that orientational order persists even after the thermal transition is completed, such a description is not completely accurate. More recent investigators have used the term "nematic-like" to describe the organization within the lipoprotein core above T_M. This description appears more accurate, but as the data presented here demonstrate this "nematic-like" state is heterogeneous.

B. Selectively Deuterated Palmitic Acid in Low Density Lipoprotein

(i) Association of Palmitic Acid with LDL_2

Trace amounts of free fatty acids are present in human low density lipoprotein. Recent studies of phospholipid bilayers (153,204) and membranes (41) have shown deuterated fatty acids to be reliable non-perturbing probes which accurately reflect the orientational order surrounding them. Therefore incorporation of exogenous deuterated fatty acids into LDL_2 represents an excellent method of studying the polar lipid environment in LDL_2.

Deuterium labelled fatty acids were incorporated into LDL_2 as detailed in Chapter 2. The degree of incorporation was monitored using a trace of [1-^{14}C]palmitic acid. The association of labelled palmitic acid and the lipoprotein was

demonstrated by gel chromatography. Figure 26 presents the elution profile of LDL_2 containing 7 mol% [$^2H_{31}$]palmitic acid plus a ^{14}C-tracer. A single protein peak eluted from the column, and coincident with this peak was the maximum in radioactivity. All of the radioactivity was recovered (109%) indicating no protein-free structures were formed spontaneously during the incorporation of the fatty acid into LDL_2.

(ii) Effect of Fatty Acid Incorporation on Particle Size

To assess the feasibility of ^2H NMR experiments using selectively deuterated fatty acids, preliminary investigations were conducted using perdeuterated palmitic acid. The effect of exogenous fatty acid incorporation into LDL_2 on particle size was monitored by ^{31}P NMR. If fatty acid incorporation increased the diameter of the lipoprotein particle, the isotropic tumbling rate of the particle would be reduced. As a consequence, the ^{31}P spectrum would be broader than that observed in the absence of exogenous fatty acid. Figure 27 presents the ^1H noise-decoupled spectra of LDL_2 both in the presence and in the absence of 7 mol% [$^2H_{31}$]palmitic acid. The upfield resonance appearing at -0.8 +/- 0.1 ppm is assigned to phosphatidylcholine, and the resonance at -0.2 +/- 0.1 ppm is assigned to sphingomyelin. Similar spectral assignments have been reported previously (225,227). The absence of yet a third

Figure 26. Elution profile of LDL_2 containing 7 Mol% [$^2H_{31}$]palmitic acid from Sepharose 6B at 4 °C

Elution solvent: 0.3mM EDTA + 0.02% NaN_3 pH 7.0; (●) UV absorbance at 280 nm; (△) ^{14}C activity; 1.0 = 1572 dpm.

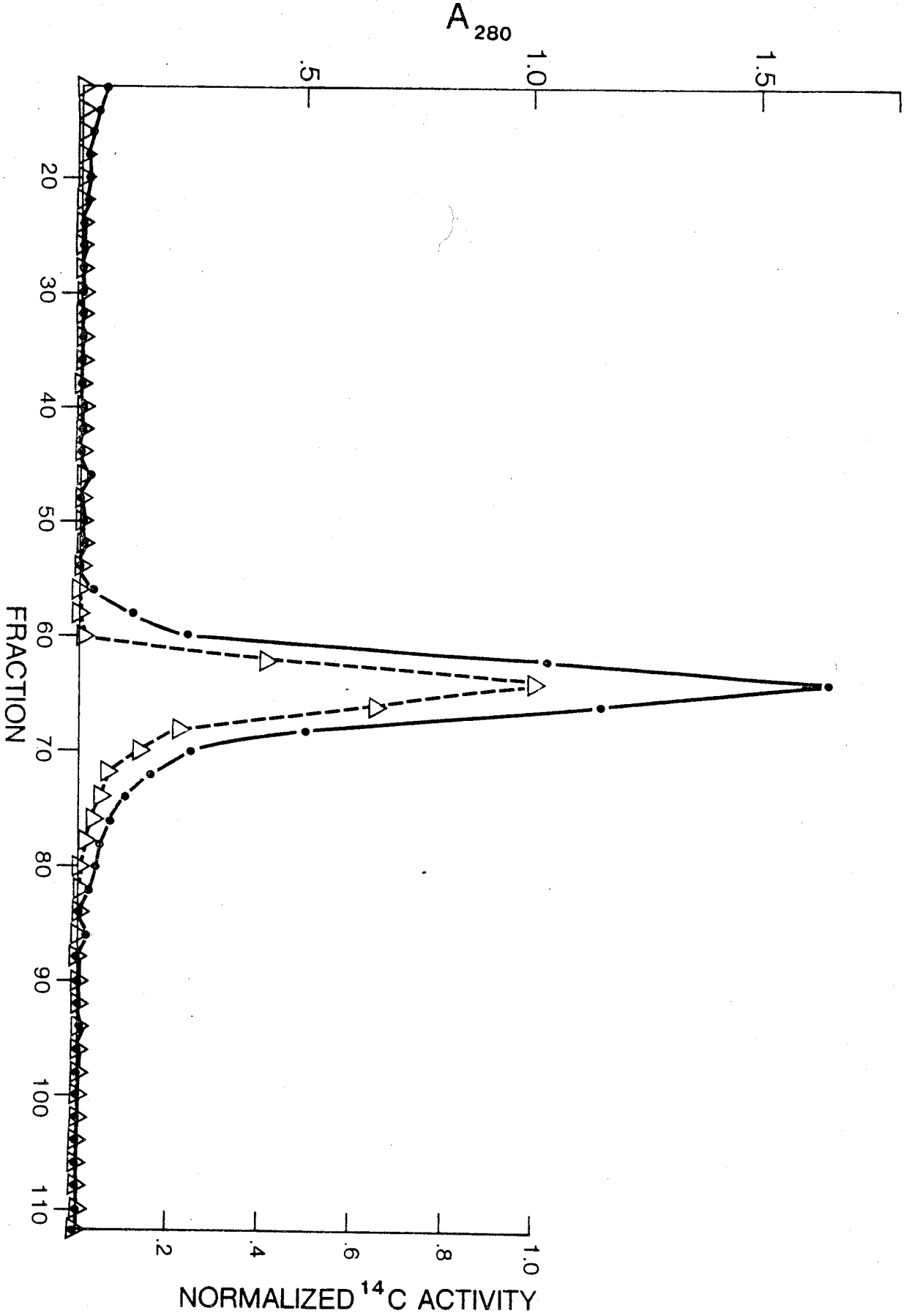
A 280
.5
1.0
1.5
20
30
40
50
60
70
80
90
100
110
FRACTION
.2
.4
.6
.8
1.0
NORMALIZED 14C ACTIVITY

Figure 27. ^{1}H decoupled ^{31}P NMR spectra of LDL_{2}:

a) native LDL_{2}, 20 mg protein per mL

b) LDL_{2} + 7mol% [$^{2}H_{31}$]palmitic acid

Spectral parameters: Sweep width = 2 kHz; dataset = 2k zero filled to 4k; number of acquisitions = 1024; line broadening = 1 Hz. Chemical shifts are with respect to external $H_{3}PO_{4}$.

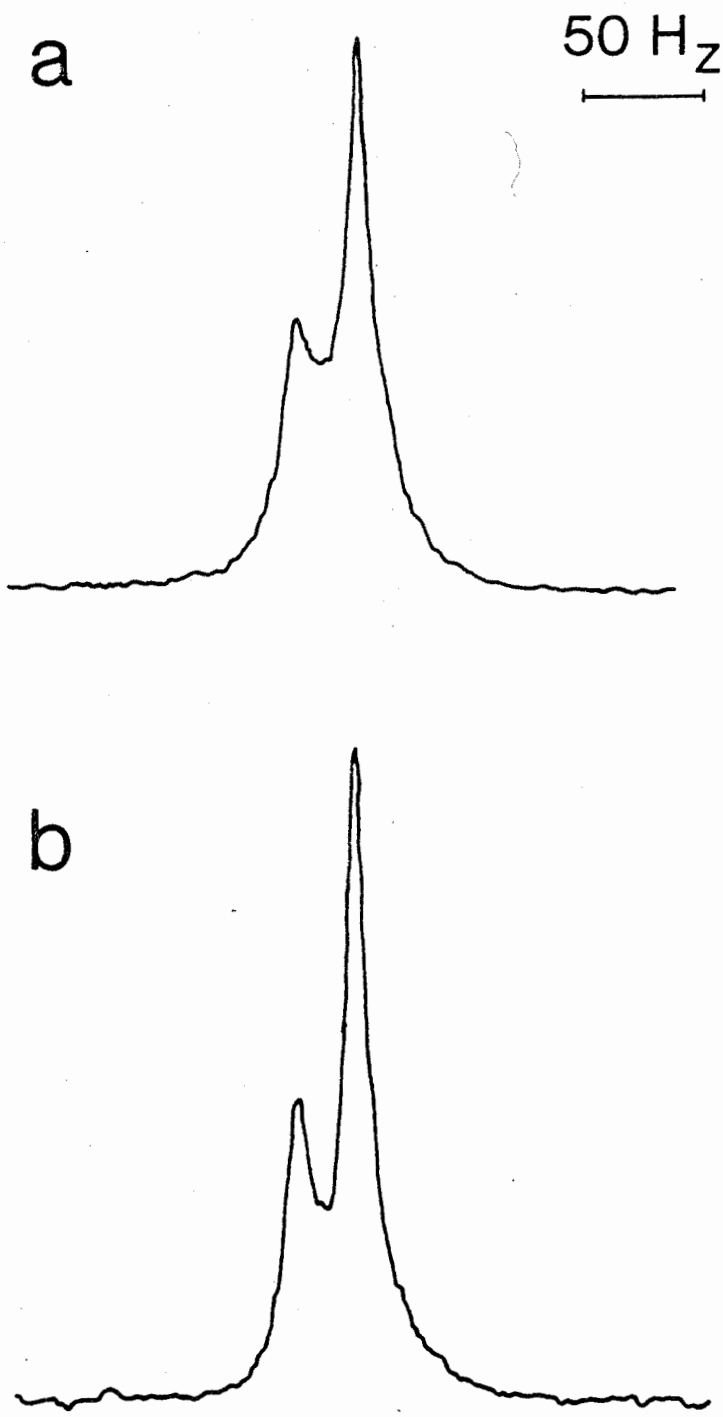
a
50 Hz
b
1 0 −1 −2
ppm

^{31}P signal occuring between these resonances clearly indicates no lysophosphatidylcholine is present in either sample. Lysophosphatidylcholine would be expected to be present in aged or partially degraded LDL_a (90). The ^{31}P linewidth of both sphingomyelin and phosphatidylcholine is 12 +/- 1 Hz in both native and labelled LDL_a. This indicates, firstly, that motion of the headgroup is similar in both classes of phospholipid. More importantly, this demonstrates that the conformation of the respective headgroups and the size of the lipoprotein particle remain unaltered by the incorporation of deuterated fatty acid.

The ^2H NMR spectrum of LDL_a containing 7 mol% [$^2H_{31}$]palmitic acid is presented in Figure 28. As indicated in the figure, the spectrum can be resolved into a relatively narrow Lorentzian signal, assigned to the terminal methyl group, superimposed on and shifted ~15 Hz upfield from a much broader composite resonance assigned to the methylene chain positions. As previously discussed, the linewidths of the spectral components reflect the molecular order at the site of the deuterium nucleus. On the basis of the amphiphilic character of palmitic acid, one might predict that fatty acid is located in the outer shell of LDL_a. This prediction is supported by ascorbic acid reduction of nitroxide labelled stearic acid (114) as well as fluorescence energy transfer experiments using cis-parinaric acid (188). Therefore, it is assumed that the palmitic acid probe is anchored at or near the aqueous interface

by the carboxyl function while the long molecular axis of the fatty acid is aligned parallel to the phospholipid acyl chains. Owing to the composite nature of the spectrum shown in Figure 28, order parameters were not calculated. This can be accomplished more accurately using specifically deuterated palmitic acids.

Figure 28. ^2H NMR spectrum of LDL_2 containing 7 mol% [$^2H_{31}$]palmitic acid. Spectral parameters: Sweep width = 10 kHz; dataset = 8k; line broadening = 2 Hz.

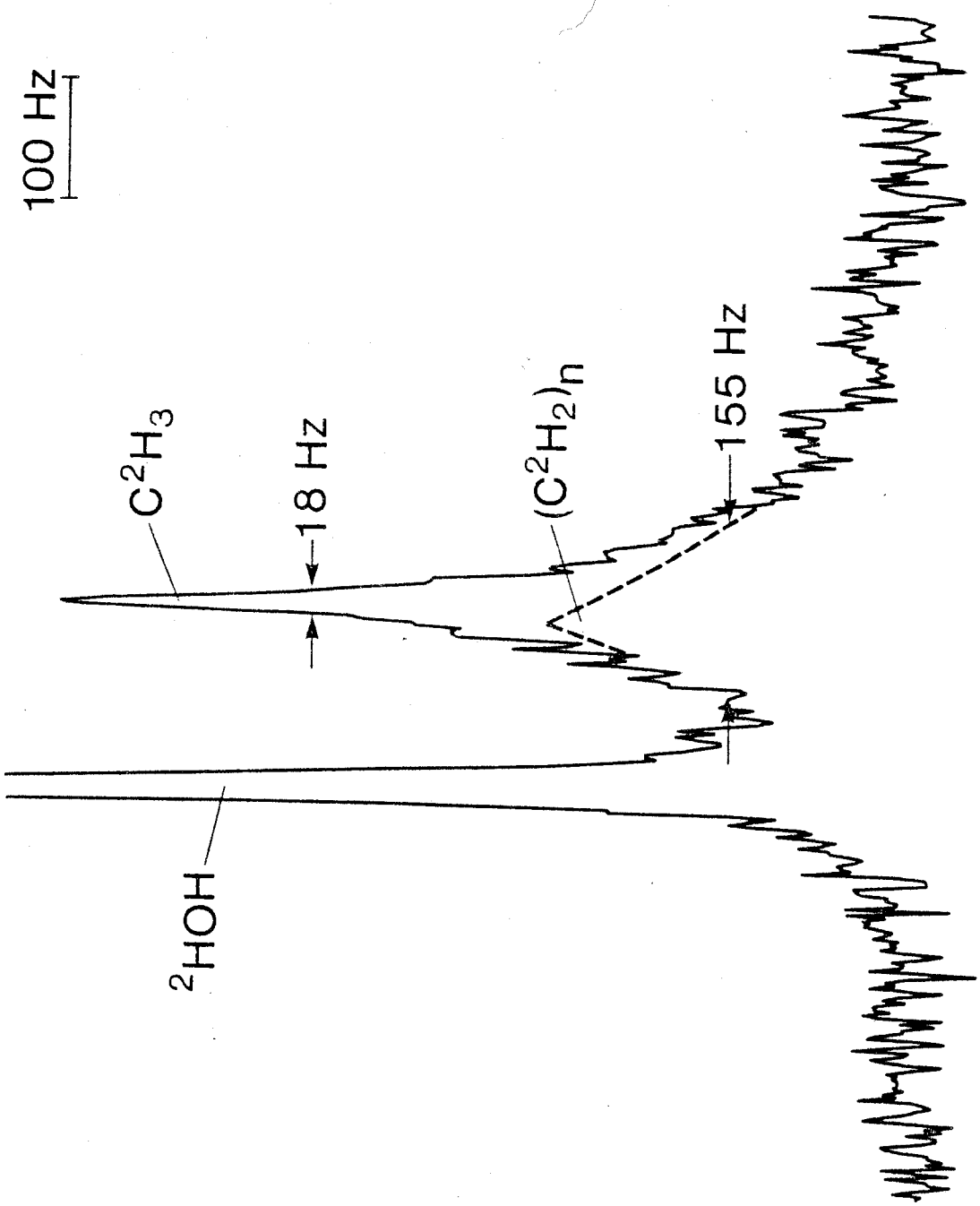
100 Hz
C^2H_3
18 Hz
$(C^2H_2)_n$
155 Hz
^2HOH

(iii) Specifically Deuterated Palmitic Acid in Low Density Lipoprotein

Pauls et al. (153) issue the caveat that high degrees of fatty acid incorporation (20 mol%) in phospholipid bilayers artificially increase the order parameter, S_{CD}, at a given acyl chain position by approximately 10%. This was investigated in preliminary experiments using LDL_{∞} labelled with [4,4-$^2H_2$]-palmitic acid, over the range of 2.5 to 20 mol% incorporation. No increase in linewidth, and therefore S_{CD}, was observed at increased levels of incorporation. Figure 29 displays the ^2H spectra of LDL_{∞} containing 5 mol% and 20 mol% [4,4-$^2H_2$]palmitic acid. The spectra in both cases are very similar and, in particular, the linewidths are the same within experimental error. One notable difference between these spectra is the better signal-to-noise ratio observed at 20 mol% incorporation. Owing to the characteristically better spectra recorded at 20 mol% incorporation, and in light of the fact that S_{CD} appears to be the same over a 10-fold range of fatty acid concentration, experiments using selectively deuterated palmitic acids containing only two deuterium nuclei were performed at 20 mol% incorporation.

Figure 30 presents the NMR spectra of LDL_{∞} containing palmitic acid deuterated at the indicated positions. At

Figure 29. ^2H NMR spectra of [4,4-$^2H_2$]palmitic acid in LDL_2. a) 5 mol% [4,4-$^2H_2$]palmitic acid. b) 20 mol% [4,4-$^2H_2$]palmitic acid. Spectral parameters: Sweep width = 50 kHz; offset = 25 kHz; number of acquisitions: (a) 1,000,000 (b) 375,000; dataset = 4k zero-filled to 8k; line broadening = 20 Hz; pulse width 5 us (56° flip angle).

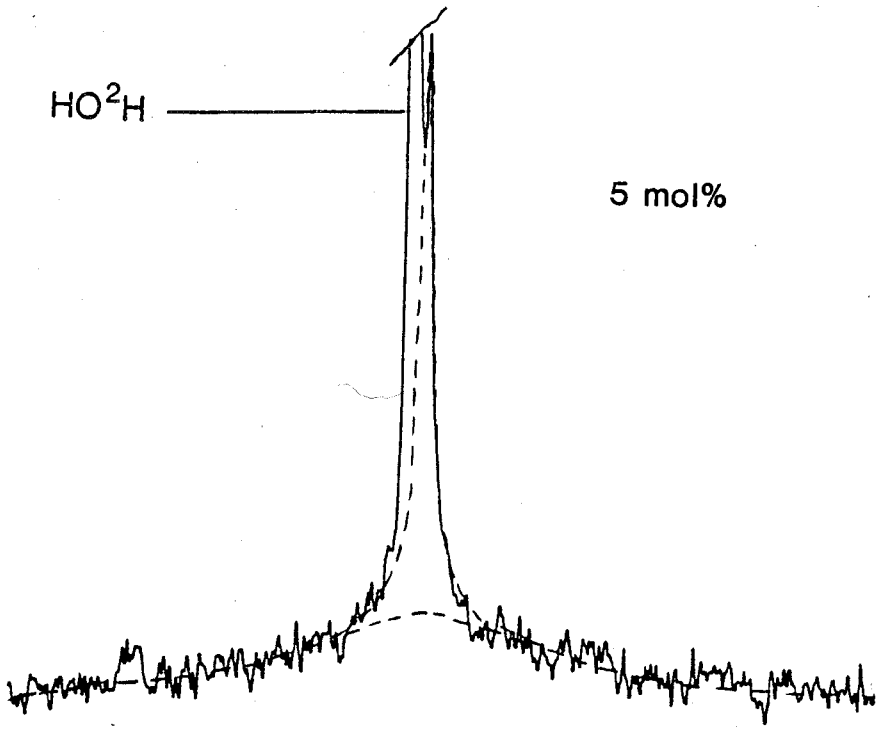
HO²H
5 mol%

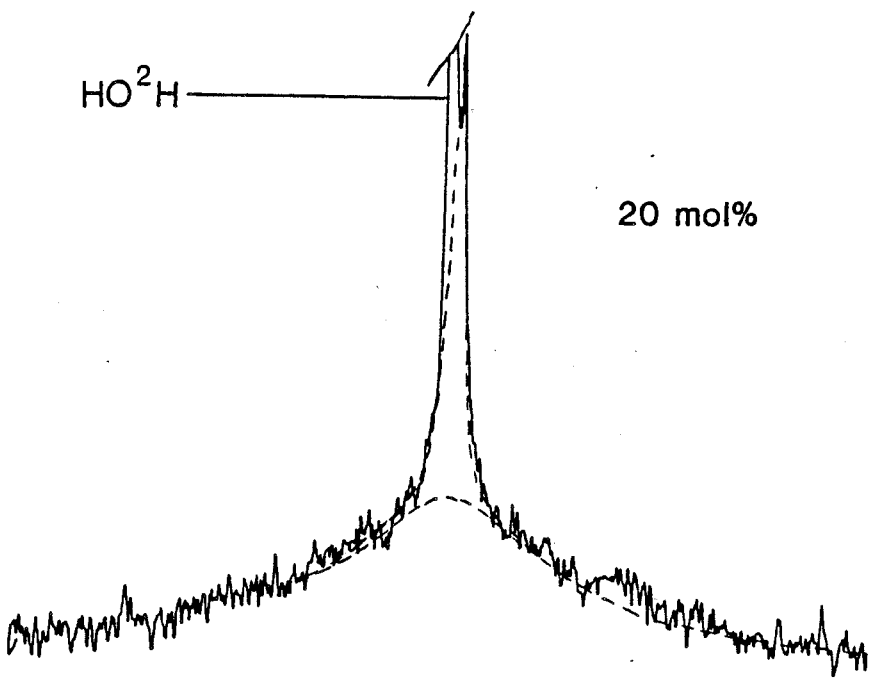
HO²H
20 mol%

positions 2 through 12, the spectra can be simulated by a superposition of two Lorentzian signals. None of the spectra can be simulated by a single Lorentzian function. The dotted lines in the figure indicate the two spectral components. These spectra clearly indicate the coexistence of two regions of significantly different order within the outer shell of LDL_{α}. Furthermore, if exchange occurs between these two sites it must be slow since, if the exchange rate was fast, a single, broad resonance representing the average order in both regions would be observed. The less ordered lipid domain, characterized by the narrow component, represented 8% of the total signal at each position except at the 5,6 position where it was 35% of the signal. The linewidths at each chain position are recorded in Table 6.

Evidence of separate, non-equivalent phospholipid domains in LDL_{α} has been reported by earlier investigators. After correcting for Nuclear Overhauser Enhancement (NOE) effects Yeagle et al. (225) estimated that ~20% of the headgroup phosphorus in their LDL_{α} was not detectable by ^{31}P NMR. Similarly, Finer et al. (61) reported that 20-30% of the trimethylammmonium resonance was not detected by ^{1}H NMR of porcine LDL. Moreover, they estimated that approximately half of the linewidth observed at 220 MHz is due to a distribution of chemical shifts indicating a range of magnetically non-equivalent environments. Yeagle et al. (225) suggested that

Figure 30. ^2H NMR spectra of selectively deuterated palmitic acid in LDL. Spectral parameters: unless otherwise indicated offset = 25 kHz and pulse width = 5 usec (55 ° flip angle). 2,2-: Incorporation = 20 mol%; sweep width = 50 kHz; number of acquisitions (NA) = 500,000; dataset = 4k zero-filled to 8k; line broadening = 20 Hz. 4,4-: Incorporation = 20 mol%; sweep width = 50 kHz; NA = 375,000; dataset = 4k zero-filled to 8k; line broadening = 20 Hz. 5,6-: Incorporation = 6 mol%; sweep width = 50 kHz; NA = 300,000; dataset = 4k zero-filled to 8k; line broadening = 30 Hz. 11,12-: Incorporation = 6 mol%; sweep width = 50 kHz; NA = 100,000; dataset = 4k zero-filled to 8k; line broadening = 10 Hz. 16,16,16-: Incorporation = 5 mol%; sweep width = 10 kHz; offset = 5 kHz; NA = 20,000; dataset = 8k; line broadening = 2 Hz.

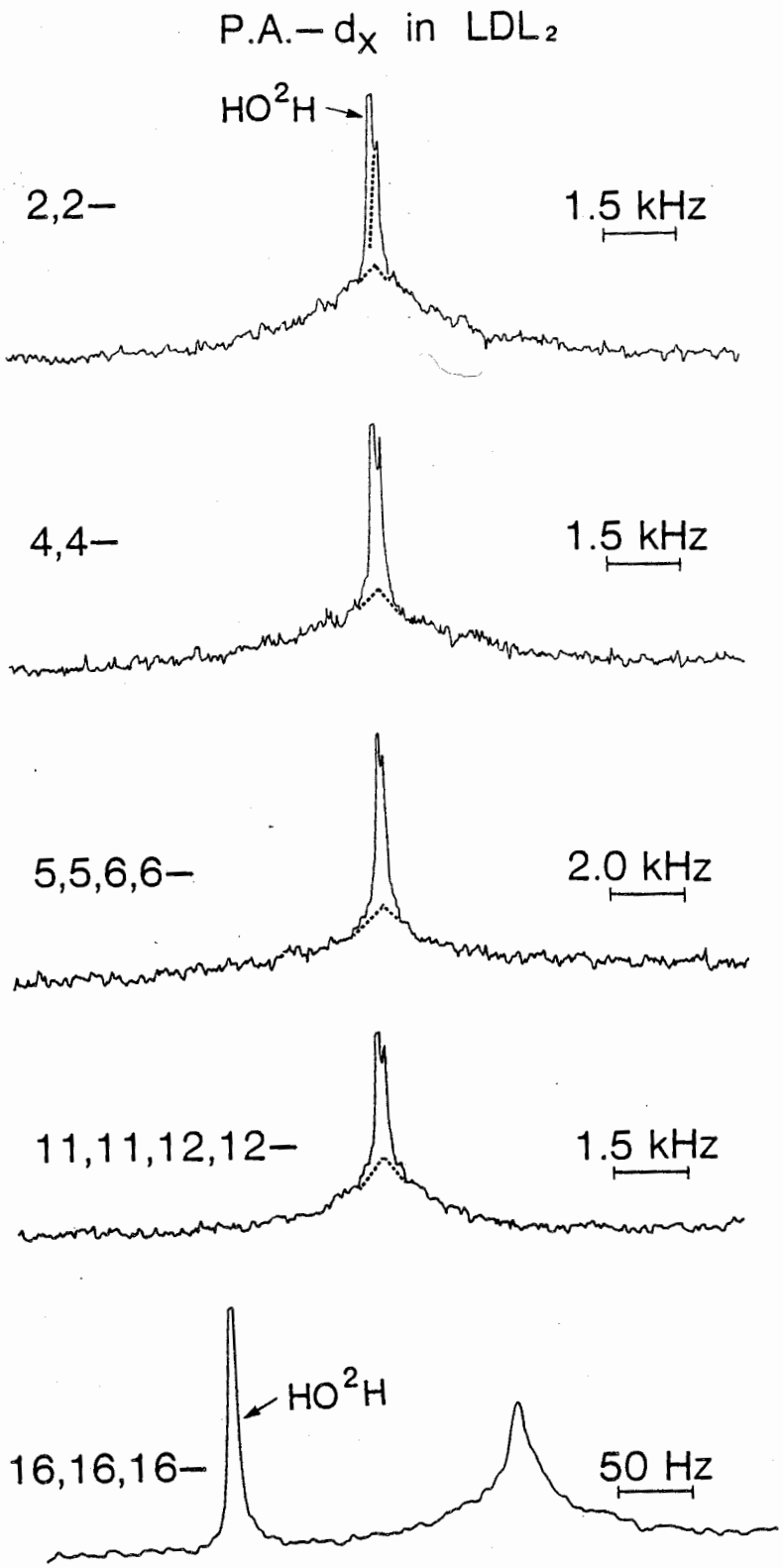
P.A.– d_X in LDL_2
HO^2H
2,2–
1.5 kHz
4,4–
1.5 kHz
5,5,6,6–
2.0 kHz
11,11,12,12–
1.5 kHz
HO^2H
16,16,16–
50 Hz

Table 6

Linewidths (Hz) and Spin-Lattice Rexation Times (msec) of Selectively Deuterated Palmitic Acid in LDL_{25} at 25 °C

Acyl Chain Position	Narrow Component $\Delta\nu_{1/2}$	Narrow Component T_1	Broad Component $\Delta\nu_{1/2}$	Broad Component T_1
2	140 (+/-6)	---	3432 (+/-57)	---
4	142 (+/-4)	---	4200 (+/-65)	---
5,6	203 (+/-4)	20 (+/-4.0)	2920 (+/-130)	20 (+/-4.0)
11,12	90 (+/-4)	25 (+/-4.0)	2140 (+/-40)	25 (+/-4.0)
16	17 (+/-1)	184 (+/-15)	---	---

1 Linewidths were determined from a 6 parameter iterative least squares analysis of the NMR spectrum.

2 Numbers in parentheses indicate the linewidth uncertainty determined from the computer calculated standard deviation.

the unobservable phosphorus signal is a result of immobilization of the phospholipid headgroups through protein-lipid interactions. Support for this hypothesis stems from the observation that after partial trypsin digestion of the LDL_{∞} apoprotein, as much as 99% of the headgroup phosphorus signal can be detected from the still intact particle.

In the presence of Pr^{3+} ions all of the detectable ^{31}P signal is shifted downfield (227). In like manner, addition of Mn^{2+} ions to LDL_{∞} quickly broadens all of the ^{31}P signal to the point of non-detection (90). These observations indicate that either all of the phospholipid headgroups are located at the surface of the lipoprotein particle or at least are readily accessible to these ions. However, if Mn^{2+} ions are first complexed with ethylenediaminetetraacetic acid (EDTA) (Mn^{2+}:EDTA = 1:2.2) only half of the phosphorus signal is quenched indicating that the remaining signal arises from phospholipids inaccessible to the large manganese-EDTA complex.

Spin-lattice relaxation times measured at selected acyl chain positions are presented in Table 6. In general, the relaxation times increase toward the methyl terminus of the fatty acid indicating increased motion away from the aqueous interface. The relatively long T_1 value measured at the methyl position reflects the additional rotation of the methyl group.

Through application of equation 3.54 and using the data presented in Table 6 the order parameters can be evaluated.

Table 7 presents the order parameters at each chain position of palmitic acid in LDL_2 at 25°C. The order parameters of the less ordered phospholipid region, represented by the narrow component, are in accord with the S_{CD} values measured by Parmar et al. (152) in unilamellar egg PC/sphingomyelin vesicles. On the other hand, in the more highly ordered domain S_{CD} values are on the order of 5 times higher. Indeed, in this region, S_{CD} values are approximately 50% higher than values measured in phospholipid multilamellar liposomes (153,175,204). The order parameters of the more highly ordered environment are in excellent agreement with EPR order parameters determined by Laggner and Kostner (125) using 5-doxyl and 12-doxyl stearic acid in LDL_2 at 25 °C. These authors reported values of S_{EPR} ($\sim 2S_{CD}$) of 0.6-0.7.

The fact that S_{CD} values for the more highly ordered LDL_2 phospholipid domain are significantly greater than in vesicles or liposomes may be the consequence of two factors. Firstly, the presence of free cholesterol in the outer shell of LDL_2 may increase S_{CD} in a manner similar to that reported previously in egg PC bilayers (204). Secondly, apoprotein-B may increase S_{CD} through lipid-protein interactions. However, a recent review of lipid-protein interactions, by Bloom and Smith (15), finds no evidence of immobilized phospholipid acyl chains in the presence of protein. Therefore, this explanation appears unlikely.

TABLE 7

Order Parameters of Selectively Deuterated Palmitic Acid in LDL_2 at 25 °C

Chain Position	Narrow Component	Broad Component
2	0.06 *	0.31 *
4	0.06 *	0.34 *
5,6	0.07	0.28
11,12	0.05	0.24
16	0.02	---

* A spin-lattice relaxation time of 20 msec was assumed. This assumption is justified since Parmer et al. (152) have demonstrated that the deterium spin-lattice relaxation times of palmitic acid in egg PC/beef brain sphingomyelin vesicles are essintially constant over the first 6 acyl chain positions.

The order parameter profiles of both phospholipid domains are presented in Figure 31. It must be recognized that the lines shown in the figure serve only to indicate the trend in the data and do not imply any mathematical function, nor do they imply the existence of fractional chain positions. In the more highly ordered environment S_{CD} remains essentially constant over at least the first six acyl chain positions, and then declines gradually. A similar profile has been reported in multilamelar liposomes both in the presence and in the absence of cholesterol (153,175,204). In the less ordered region, on the other hand, S_{CD} remains essentially constant from the C2 position to the methyl terminus of the acyl chain.

There are two possible explanations for the coexistence of two phospholipid regions of vastly different orientational order within the outer shell of LDL_2. Firstly, apoprotein-B may influence the order of the phospholipid molecules immediately surrounding the protein through lipid-protein interactions. The interactions between phospholipid and apoprotein-B are not fully understood. However, from measurements of optical rotary dispersion (ORD) it is known that the helical structure of apoprotein-B decreases by 27% upon removal of phospholipid from the lipoprotein particle (163,164). Moreover, both ^{31}P NMR (225) and ^{1}H NMR (61) indicate that some of the phospholipid headgroups are rigidly immobilized. There is no justification to assume a priori that any lipid-protein interactions which result

Figure 31. Order parameter profile of palmitic acid in LDL_{ox}

(▲) indicates the broad spectral component

(●) indicates the narrow spectral component

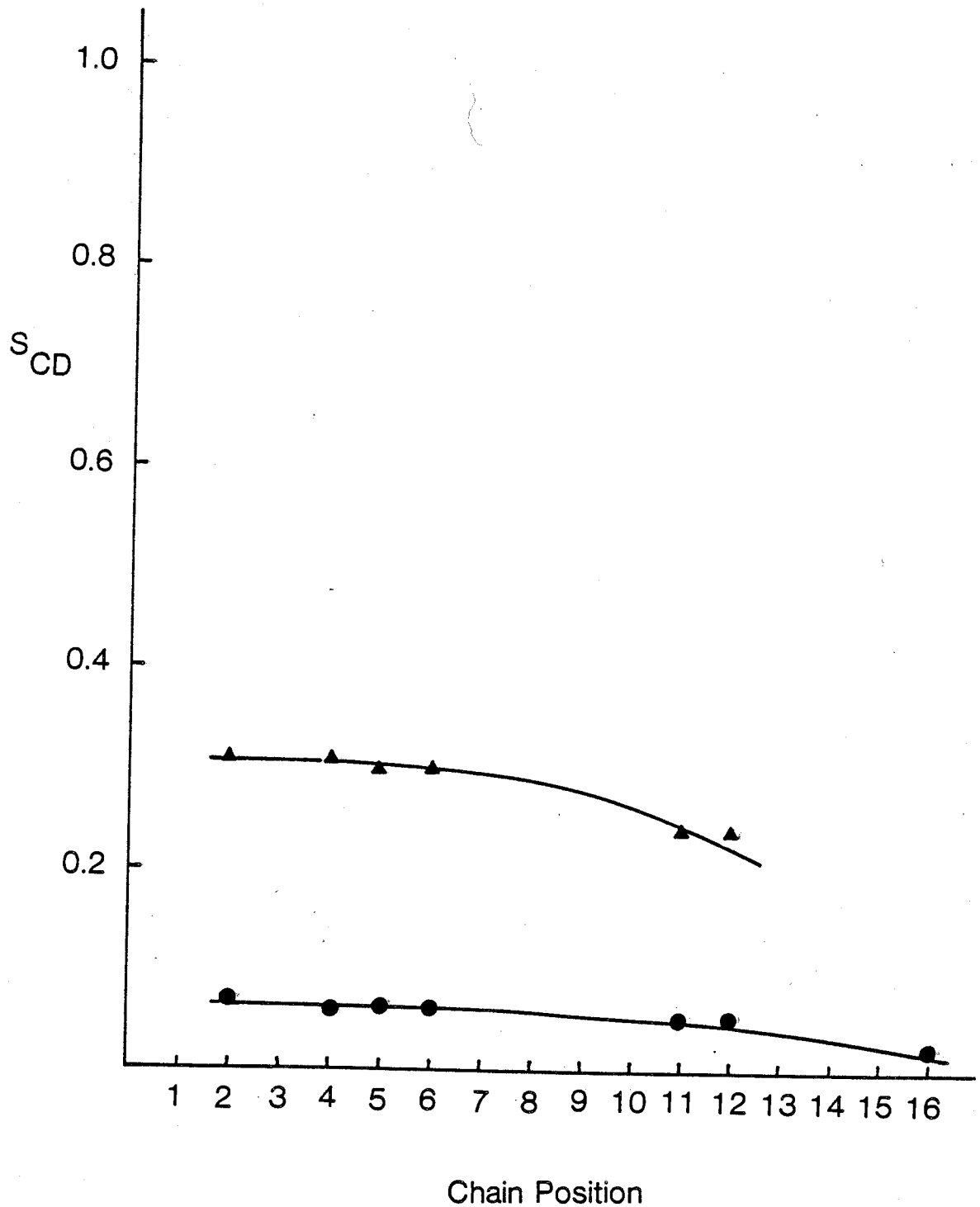
1.0
0.8
S_{CD}
0.6
0.4
0.2
1 2 3 4 5 6 7 8 9 10 11 12 13 14 15 16
Chain Position

in restricted motion of the phospholipid headgroup, as evidenced by broadening of the ^{31}P spectrum, will similarly lead to restricted motion of the phospholipid acyl chains. Indeed, spectral parameters from phospholipid headgroups and fatty acyl chains may display opposing trends in the presence of protein. To illustrate, Yeagle et al. reported increased phosphorus linewidths of vesicles after incorporation of cytochrome c (225). By way of contrast, Oldfield and coworkers investigated a wide range of different proteins in selectively deuterated phospholipid bilayers (111,147,158) and reported that lipid immediately adjacent to proteins (boundary lipid) is not immobilized by the protein. To the contrary, boundary lipid is disordered by the presence of the protein. Similar results have been observed in membrane vesicles derived from Escherichia coli (110). Additional support for the conclusions of Oldfield et al. can be found in the laser Raman experiments reported by Curatolo et al. (37). In the presence of proteolipid apoprotein, a protein found in myelin, and also studied by Oldfield, dimyristoyl phosphatidylcholine acyl chains display an increased number of gauche conformers below the transition temperature. In view of the evidence presented above, it is entirely possible that the less ordered phospholipid domain of LDL_2 represents lipid intimately associated with apoprotein-B.

Alternatively, the coexistence of two phospholipid domains may be the consequence of a non-uniform distribution of lipids

in the LDL_2 monolayer. Aggerbeck et al. (2) reported that following digestion of human LDL_2 with phospholipise A_2 all of the phosphatidylcholine is hydrolyzed by the phospholipase. Careful study of the kinetics of the reaction revealed that ~15% of the phosphatidylcholine was hydrolyzed at a rate substantially greater than the remaining phospholipid. In studies on mouse cells, it has been demonstrated that phospholipase A_2 is very sensitive to the sterol content of the plasma membranes (62). In particular, membranes classified as 70% sterol depleted were susceptible to phospholipase hydrolysis at a rate 4 times greater than membranes with normal sterol content. From the data presented here, one cannot distinguish between possible phospholipid-apoprotein-B interactions, and irregular lipid distribution in the LDL_2 monolayer. However, when taken together with the phospholipase studies of Aggerbeck et al.(2) and Fisher et al. (62) plus the NMR studies of Parmar et al. (152), they infer the less ordered phospholipid domain in LDL_2 represents a cholesterol deficient region. Further, the possibility must be considered that such sterol deficient regions are in close proximity to apoprotein-B.

III. SPIN LABEL-INDUCED ^{13}C RELAXATION in PHOSPHATIDYLCHOLINE MODEL MEMBRANES

A. Spin-Lattice Relaxation in Phosphatidylcholine Unilamellar Vesicles

Carbon-13 spin-lattice relaxation times, T_1, of approximately 20% (w/v) unilamellar egg PC vesicles in $^{2}H_2O$ have been measured at 25.15 MHz and 30 °C as well as 100.6 MHz and 46 °C. A representative ^{13}C spectrum at each frequency is presented in Figures 32A and 33A. Each spectrum exhibits several well resolved resonances originating from the fatty acid chains. Resonances were assigned according to Batchelor et al. (11). The spin-lattice relaxation times are presented in Table 8 and are accurate to +/- 10%. In general, specific carbon nuclei on each of the acyl chains cannot be uniquely resolved from each other. Therefore, the T_1 values reported here represent the average spin-lattice relaxation times of both chains. An example of data collected during a T_1 experiment is displayed in Figure 34. The relaxation time is calculated from absolute value of the reciprocal of the slope of the line.

The data shown in Table 8 demonstrate a general increase in T_1 toward the methyl terminus of the fatty acyl chains thus reflecting a progressive increase in motional freedom. This

Figure 32. Proton decoupled ^{13}C NMR spectra of 20% W/V egg phosphatidylcholine vesicles in $^{2}H_{2}O$ at 25.15 MHz and 30 °C
a) Egg PC only b) Egg PC + ~1.7 mol% 5-doxyl cholesteryl palmitate

Spectral Parameters: Sweep width = 5 kHz; pulse width = 24 us (90° flip angle); dataset = 8k; line broadening = 2 Hz; number of acquisitions = 1500; decoupling bandwidth = 2 kHz.

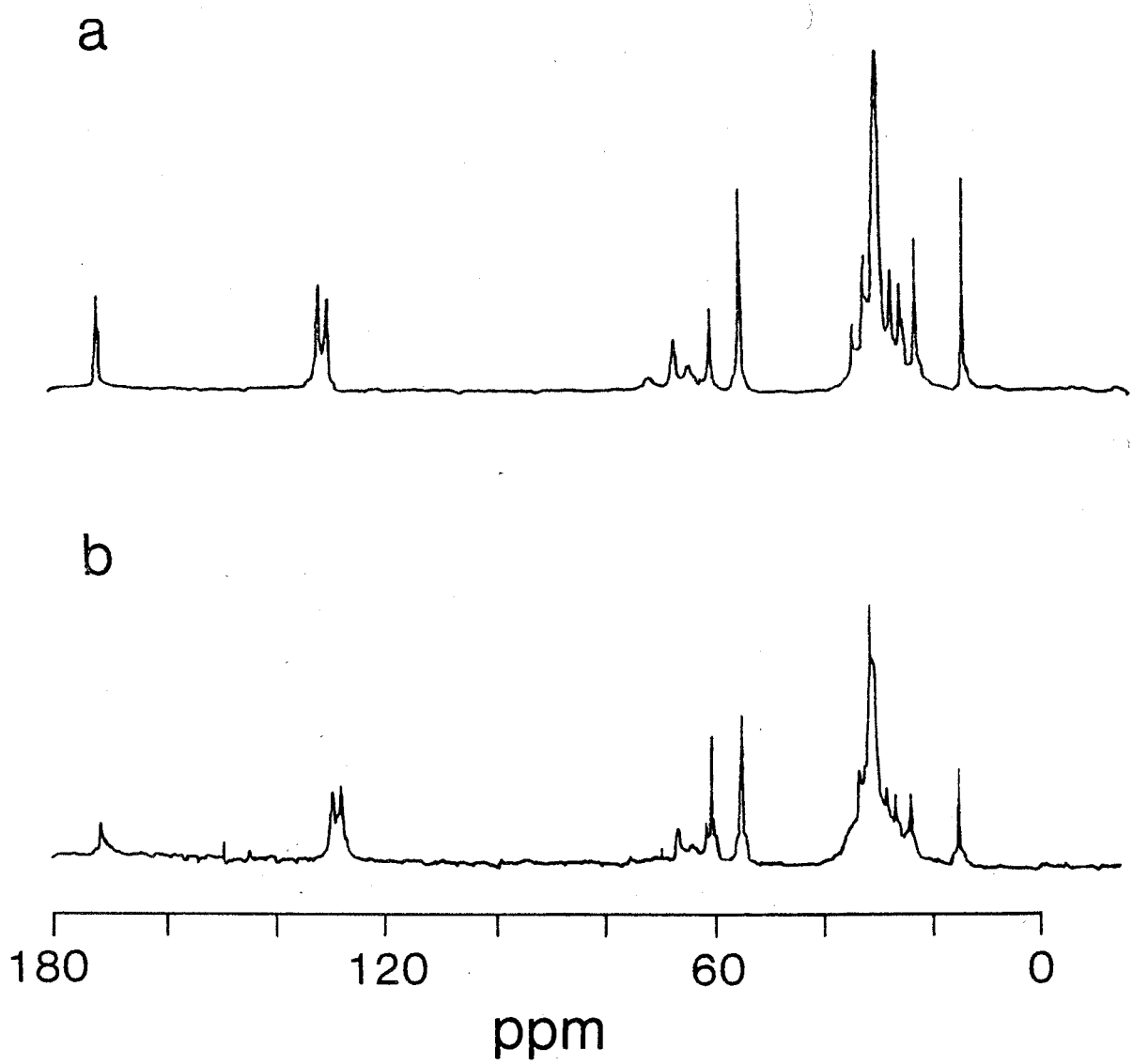
a
b
180
120
60
0
ppm

Figure 33. Proton decoupled ^{13}C NMR spectra of 20% W/V egg phosphatidylcholine vesicles in $^{2}H_{2}O$ at 100.6 MHz and 46 °C (a) egg PC only (b) egg PC + ~ 1.7 mol% 5-doxyl cholesteryl palmitate. Inset indicates expansion of carbonyl region. Spectral parameters: Sweep width = 20 kHz; number of acquisitions = 1024; dataset = 32k; line broadening = 1.5 Hz; pulse width = 25 us (90° flip angle).

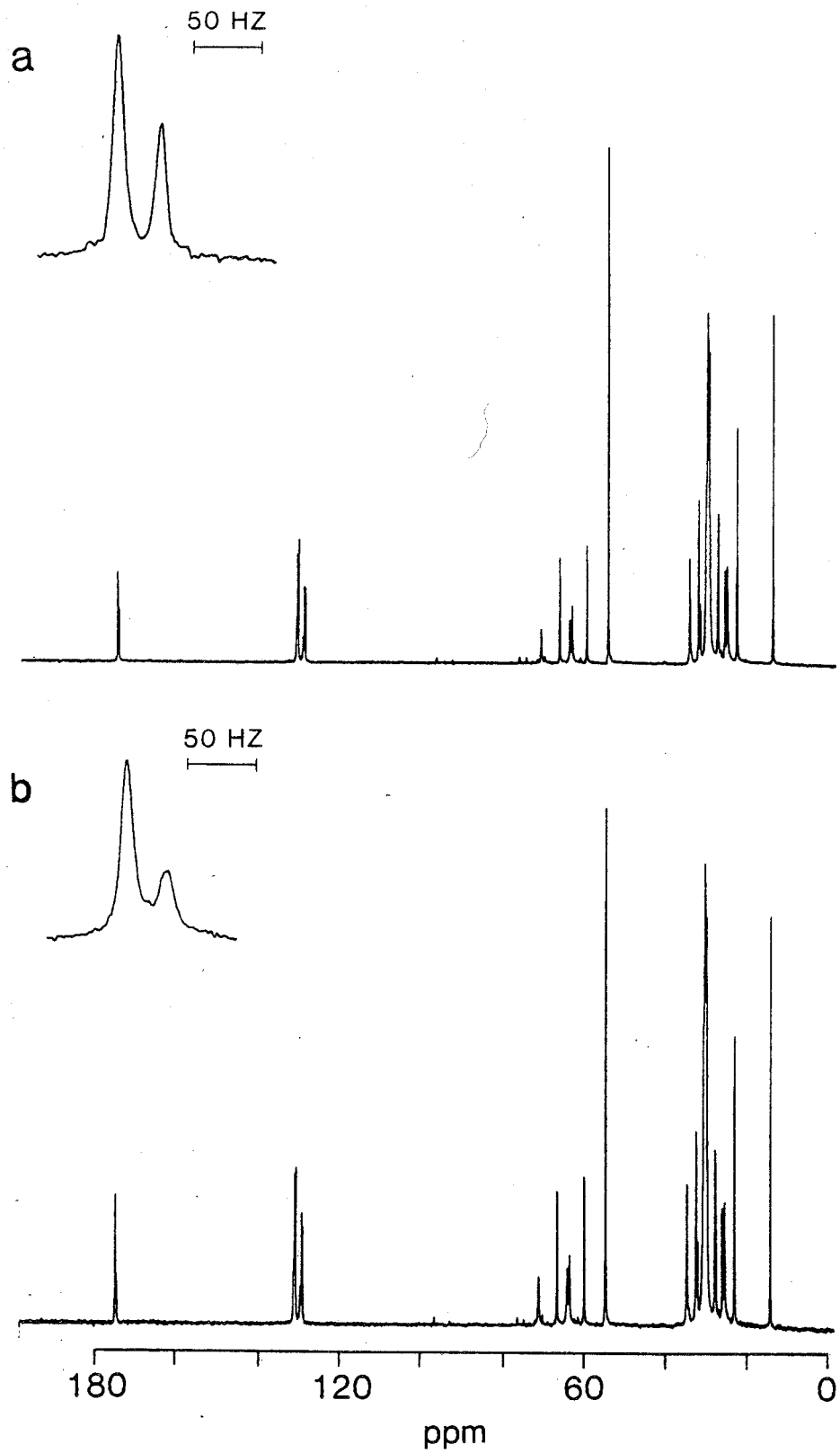
50 HZ
a
50 HZ
b
180
120
60
0
ppm

Figure 34. Plot of A_t versus t for the C3 position of Phosphatidylcholine at 100.6 MHz. and 46 °C in the absence of spin-labelled cholesteryl ester.

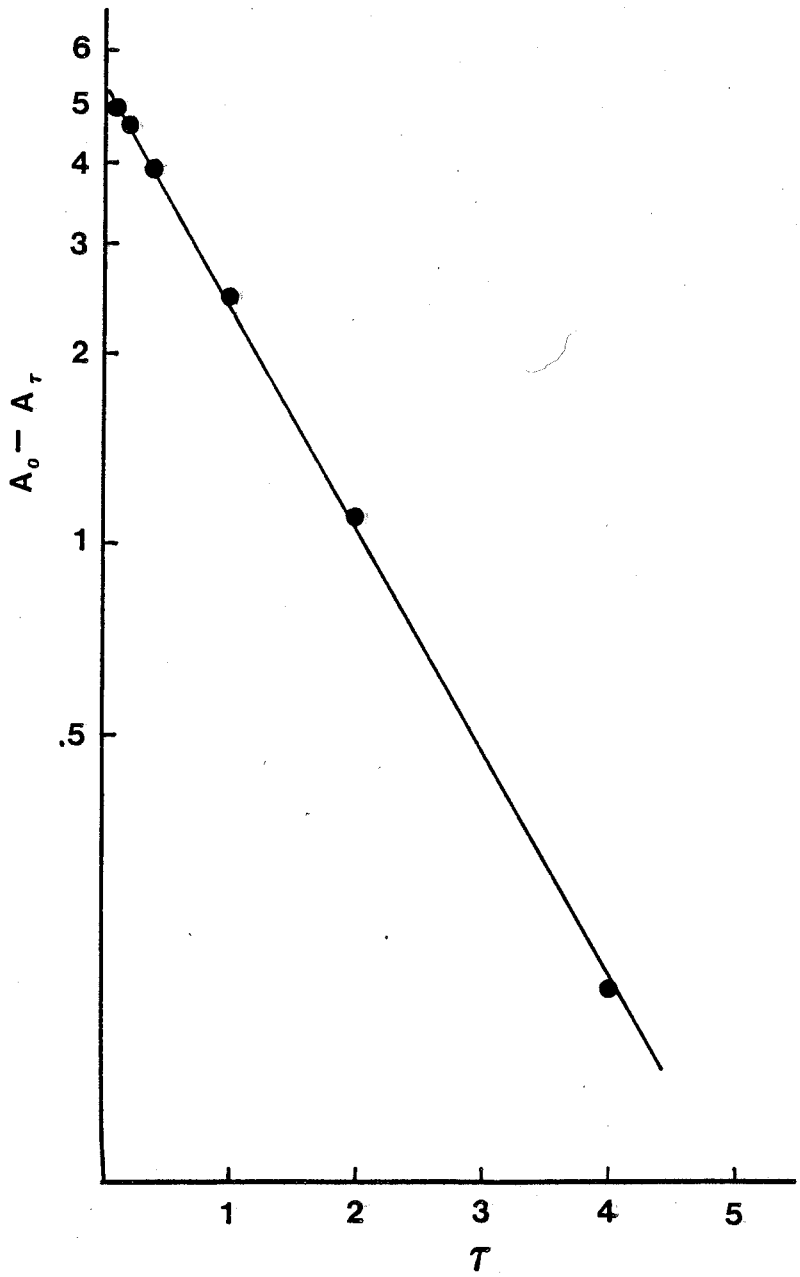
6
5
4
3
2
1
.5
$A_0 - A_\tau$
1
2
3
4
5
τ

trend can be represented graphically as shown in Figure 35, by plotting NT_1 against relative chain position, where N is the number of bonded protons at each position. A very similar profile is observed at 100.6 MHz. It should be emphasized that chain positions indicated in Figure 35, particularly toward the methyl terminus, are approximate. This is a consequence of the distribution of fatty acids of differing lengths in egg PC. The trend shown in Figure 35 is in accord with similar observations reported by Lee et al. (129).

B. Spin-Lattice Relaxation in the Presence of 5-Doxyl Cholesteryl Palmitate.

For the convinience of the reader, Figure 3 is again displayed here. The spin-lattice relaxation times of the fatty acid chains at both 25.15 and 100.6 MHz, in the presence of 1.7 mol% 5-doxyl cholesteryl palmitate, are presented in Table 9. The induced relaxation rates due to the presence of the spin labelled ester have been calculated from the data of Tables 8 and 9 using the relationship:

$$1/T_{1,SL} = 1/T_1^{+} - 1/T_1^{o}$$

where $1/T_1^{+}$ and $1/T_1^{o}$, respectively, indicate the spin-lattice

Table 8

Spin-Lattice Relaxation Times (sec) for 20 wt%

Egg Phosphatidylcholine Vesicles

Chain Position	25.15 MHz and 30 °C	100.6 MHz and 46 °C
C1	2.34 (+/-0.23)	5.16, 5.04[1] (+/-0.51)
C2	0.19 (+/-0.02)	1.03 (+/-0.10)
C3	0.27 (+/-0.03	1.32 (+/-0.13)
$(CH_2)_n$	0.36 (+/-0.04)	1.91 (+/-0.19)
C8 Oleic[2]	0.38 (+/-0.04)	1.78 (+/-0.18)
C9 Oleic	0.50 (+/-0.05)	2.01 (+/-0.20)
C10 Lino[3]	0.75 (+/-0.08)	3.44 (+/-0.34)
C11 Lino	0.46 (+/-0.05)	2.88 (+/-0.29)
w-2[4]	0.65 (+/-0.07)	4.28 (+/-0.43)
w-1[5]	1.18 (+/-0.12)	6.25 (+/-0.63)
w[6]	2.83 (+/-0.28)	11.25 (+/-1.10)

1. Two carbonyls were resolved (see Text)
2. Denotes oleic acid
3. Denotes linoleic acid
4. w-2 indicates the anti-penultimate chain position
5. w-1 indicates the penultimate chain position
6. w indicates the terminal methyl position

Figure 35. NT_1 *versus* phospholipid acyl chain position at 25.25 MHz and 30 °C

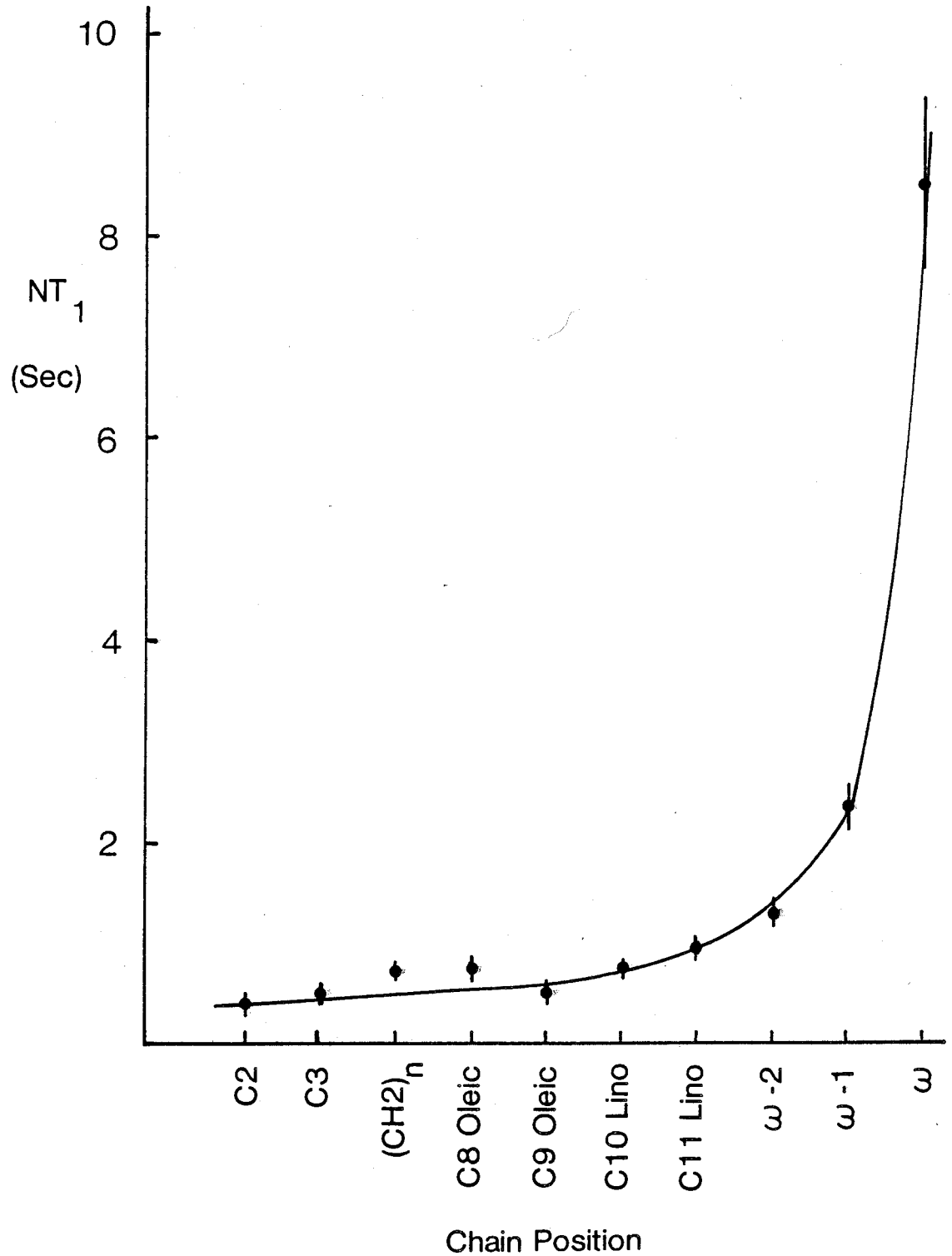
10
8
6
4
2
NT 1
(Sec)
C2
C3
(CH2)n
C8 Oleic
C9 Oleic
C10 Lino
C11 Lino
ω -2
ω -1
ω
Chain Position

Figure 3. Spin labelled esters

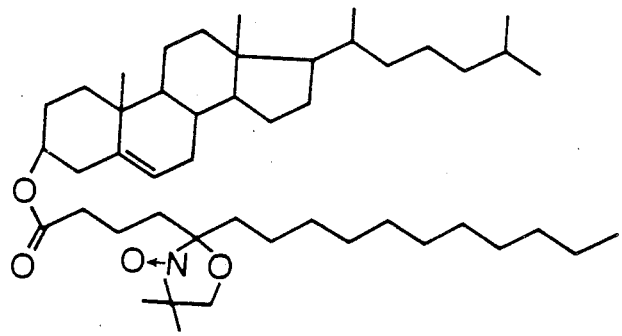

I

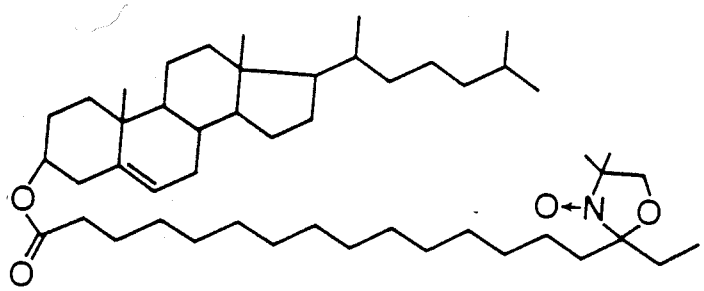

II

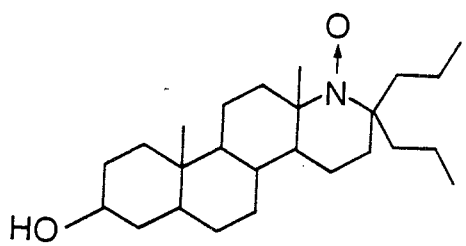

III

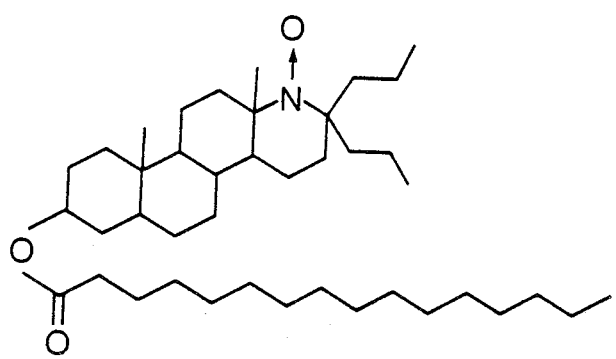

IV

TABLE 9

Spin-lattice Relaxation Times (sec) of Egg Phosphatidyl-choline Vesicles Containing 5-Doxyl Cholesteryl Palmitate

Chain Position	25.15 MHz and 30 °C	100.6 MHz and 46 °C	
C1	0.49 (+/-0.05)	1.45 (+/-0.15)	0.53 (+/-0.05)
C2	0.15 (+/-0.02)		0.43 (+/-0.04)
C3	Not Resolved		0.52 (+/-0.05)
$(CH_2)_n$	0.32 (+/-0.03)		0.80 (+/-0.08)
C8 Oleic	0.30 (+/-0.03)		0.77 (+/-0.08)
C9 Oleic	0.40 (+/-0.04)		0.83 (+/-0.08)
C10 Lino	0.46 (+/-0.05)		0.97 (+/-0.10)
C11 Lino	0.32 (+/-0.03)		0.96 (+/-0.10)
w-2	0.43 (+/-0.04)		1.07 (+/-0.11)
w-1	0.77 (+/-0.08)		1.64 (+/-0.16)
w	1.31 (+/-0.13)		2.18 (+/-0.22)

relaxation rates in the presence and the absence of spin labelled cholesteryl ester. It should be noted that the error in $1/T_{1,SL}$ is appreciable if the values of $1/T_1^*$ and $1/T_1^\circ$ are both large relative to the difference in their magnitude.

As discussed in Chapter 3, ^{13}C spin-lattice relaxation is dominated by dipolar coupling between a nucleus and the (fluctuating) dipoles of nuclei in the surrounding lattice. The strength of such dipole-dipole interactions is determined, in part, by the magnitude of the magnetic moments of the interacting spins. The magnetic moment of an unpaired electron is 650 times greater than that of a proton (123), and 2600 times greater than that of a ^{13}C nucleus (219). As a consequence, in the presence of a paramagnetic centre, the ^{13}C spin-lattice relaxation time near the paramagnetic centre will be significantly reduced, and can be analyzed by direct analogy with equations 3.30 and 3.31 (52,197).

The spin label-induced longitudinal relaxation rate, $1/T_{1,SL}$, at 25.25 MHz and 30 °C is plotted against the approximate acyl chain position in Figure 36. Maximum enhancement of the relaxation rate is observed in the C1 (carbonyl)-C2 region. At chain positions beyond this region, extending toward the methyl terminus, the influence of the spin label is diminished and approximately constant within

Figure 36. ^{13}C NMR spin label-induced spin-lattice relaxation rate due to 1.7 mol% 5-doxyl cholesteryl palmitate at 25.25 MHz and 30 °C. Uncertainties were calculated from the square root of the sum of the squares of the absolute errors.

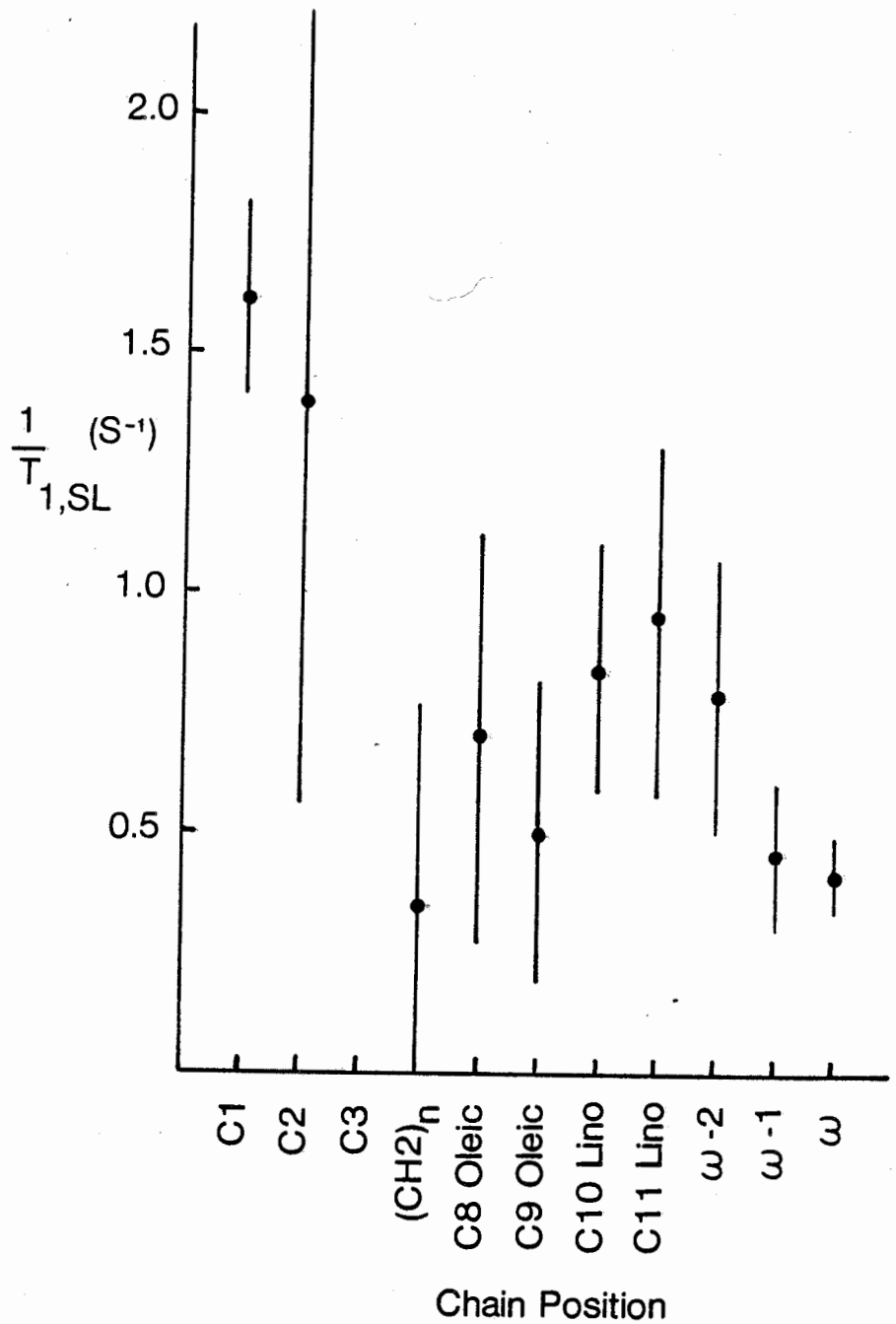
2.0
1.5
1.0
0.5
1/T1,SL (S-1)
C1
C2
C3
(CH2)n
C8 Oleic
C9 Oleic
C10 Lino
C11 Lino
ω -2
ω -1
ω
Chain Position

Figure 37. ^{13}C NMR spin label-induced spin-lattice relaxation rate due to 1.7 mol% 5-doxyl cholesteryl palmitate at 100.6 MHz and 46 °C. Uncertainties were calculated as in Figure 36.

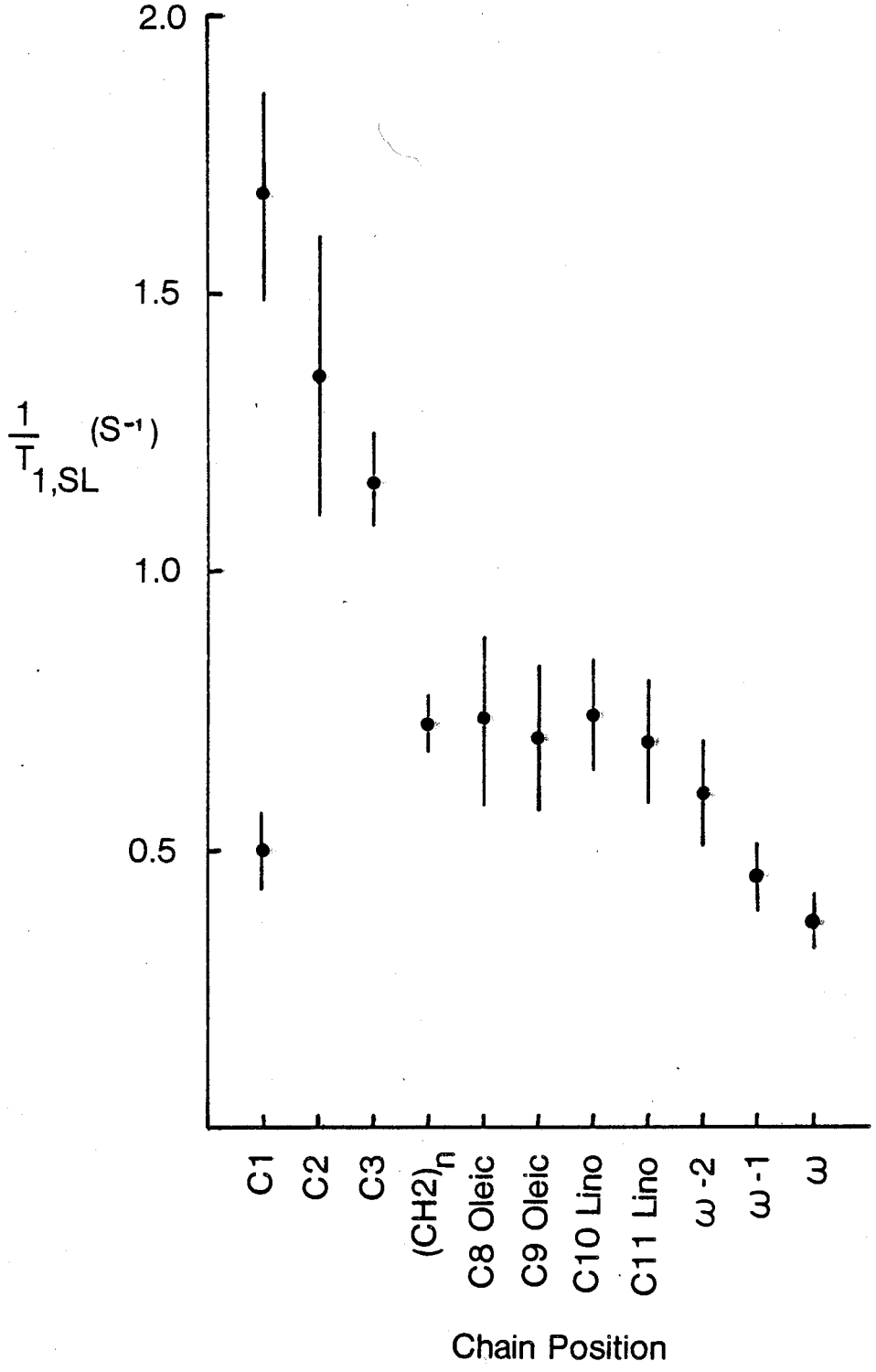
2.0
1.5
1.0
0.5
$\frac{1}{T_{1,SL}}$ (S^{-1})
C1
C2
C3
$(CH2)_n$
C8 Oleic
C9 Oleic
C10 Lino
C11 Lino
ω -2
ω -1
ω
Chain Position

experimental error. Figures 32B and 33B indicate that, as expected, the linewidths of the acyl chain resonances are increased by the presence of the spin label in qualitatively the same pattern.

A very similar profile of induced spin-lattice relaxation rate versus chain position, at 100.6 and 46 °C, is presented in Figure 37. Two important features distinguish this profile from that of Figure 36. Firstly, two carbonyl resonances, at 173.7 and 173.4 ppm, are resolved (Fig. 33). At 100.6 MHz and 30 °C these resonances are only poorly resolved, while at 25.2 MHz, in the presence of 5-doxyl cholesteryl palmitate, they are not resolved. Secondly, the relaxation rate of the downfield resonance is enhanced by a factor of approximately 4, while that of the upfield resonance is enhanced nearly 10-fold.

Assmann et al. (6) have assigned the two carbonyl resonances to magnetically non-equivalent acyl chains of phosphatidylcholine (see Figure 38). The downfield resonance was assigned to the carbonyl of the sn1-chain while the resonance to higher field was assigned to the carbonyl of the sn2-chain. More recent investigations indicate the carbonyl resonances originate from phospholipid molecules on the inside and outside of the vesicle (165,170,182,226).

When care is exercised to suppress the NOE effect, (see below) the intensity of each carbonyl resonance can be measured accurately (65). If the conclusion of Assmann et al. (6) is

Figure 38. Structure of dipalmitoyl phosphatidylcholine

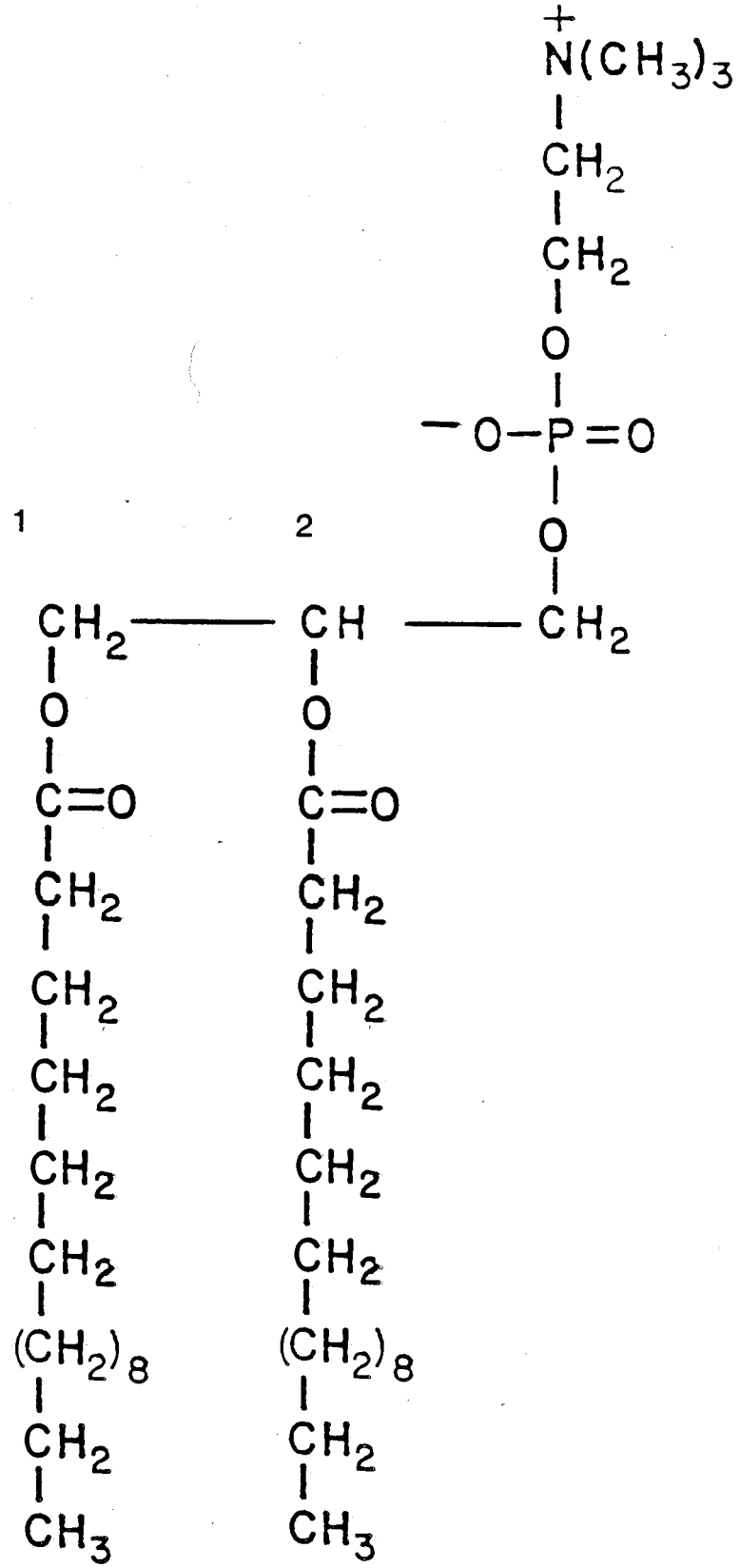

correct, the ratio of the relative intensities of the two carbonyl resonances should approach unity. However, at 100.6 MHz and 46 °C the ratio of the intensity of the downfield resonance to that of the upfield resonance is approximately 2:1 (see Figure 33). Moreover, at 100.6 MHz and 50 °C, the proton-decoupled ^{13}C spectrum of vesicles prepared from Bovine brain sphyngomyelin, a phospholipid containing only one carbonyl, reveals two carbonyl resonances, one at 177.4 and one at 177.8 ppm (spectrum not shown). Clearly, then, the possibility that the two carbonyl resonances arise from the magnetic non-equivalence of the acyl chains is remote.

The assignment of the carbonyl resonances was further investigated by the addition of Mn^{2+} ions (136) to freshly sonicated egg PC vesicles. Manganese ions enhance magnetic (spin-spin) relaxation rates thereby broadening the observed resonance (52). Owing to the strong inverse distance-dependence of such effects, carbonyls on the outside of the vesicles, in contact with the Mn^{2+} ions in the solvent, are expected to be selectively broadened.

Figure 39 demonstrates the effect of Mn^{2+} ions on the carbonyl resonances. When Mn^{2+} ions are added, to a concentration of 20 mM, to freshly prepared vesicles, the downfield resonance is selectively broadened so as to escape detection. The observation that the resonance at 173.4 ppm is

Figure 39. The effect of Mn^{2+} ions on the carbonyl peaks in the ^{13}C NMR spectrum of 20% W/V egg phosphatidylcholine vesicles at 100.6 MHz and 30 °C
Spectral parameters: sweep width = 20 kHz with quadrature detection; pulse width = 35 usec (90° flip angle); decoupling bandwidth = 4 kHz; dataset = 32 K; line broadening = 5 Hz. number of acquisitions = 1500. In order to supress NOE, the decoupler was gated on only during acquisition of the free induction decay with a 10 second delay between succesive pulses.

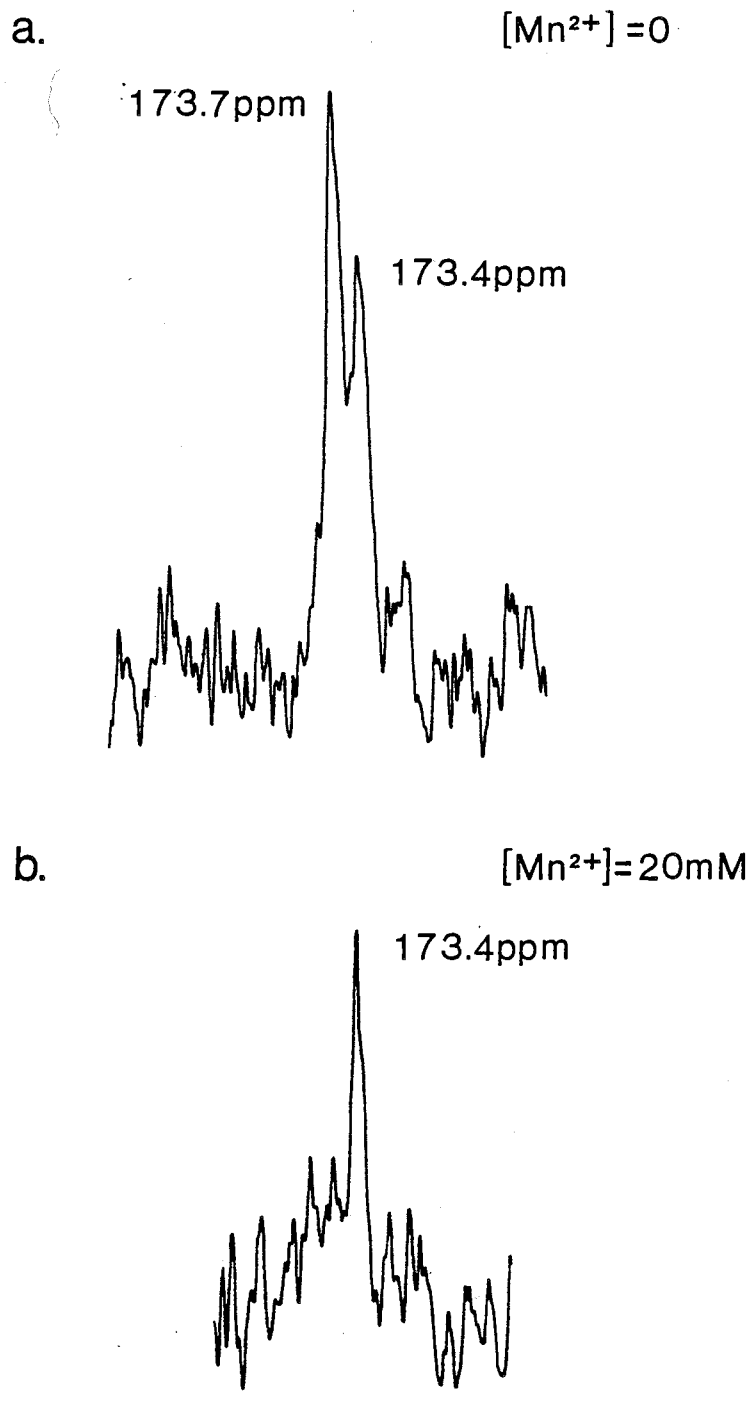
a.
[Mn²⁺] =0
173.7ppm
173.4ppm
b.
[Mn²⁺]= 20mM
173.4ppm

not broadened by the ions clearly demonstrates that, during the time course of the experiment, egg PC vesicles are essentially impermeable to the ions. Furthermore, since the effect of the Mn^{2+} ions is expected to be strongly distance-dependent, the downfield carbonyl resonance at 173.7 ppm is assigned to the outer half of the phospholipid vesicle. This assignment is in agreement with the results of experiments using lanthanide shift reagents (85,165,226). The opposite assignment has been reported by Shapiro et al. (182).

By inspection of equations 3.30 and 3.31, it is evident that the spin label-induced relaxation rate will increase significantly as the distance between the nitroxide moiety and phospholipid acyl chain decreases. When 1.7 mol% 5-doxyl cholesteryl palmitate is incorporated into egg PC vesicles, a maximum enhancement of the relaxation rate is observed in the C1-C2 region (Figures 35 and 36). This demonstrates that, on average, the nitroxide of 5-doxyl cholesteryl palmitate is embedded in the bilayer at a depth close to the carbonyl-C2 region. This is consistent with the cholesteryl ester adopting a "horseshoe" conformation as previously suggested by ^2H NMR (77) and EPR (79) experiments.

Comparison of the two carbonyl relaxation rates at 100.6 MHz and 46 °C in the absence of spin labelled cholesteryl ester indicates they are similar within experimental error. Incorporation of 1.7 mol% 5-doxyl cholesteryl palmitate into the

vesicles results in a selective enhancement of the relaxation rate of the carbonyls on the outside of the vesicles by a factor of ~4, while the relaxation rate for the carbonyls inside the vesicle are enhanced ~10-fold. This significant differential effect suggests either that ester incorporation is greater or that lipid packing is tighter in the inner layer than in the outer layer of the vesicle. A higher incorporation of ester would result in a given phospholipid having as its nearest neighbour a spin labelled cholesteryl ester more frequently. On the other hand, tighter lipid packing would decrease the distance separating the phospholipid from the nitroxide moiety. The result in either case, neglecting any possible accompanying differences in molecular motions between the inner and outer vesicle layers, is a larger enhancement of the spin-lattice relaxation rate in the inner vesicle layer.

Previous experimenters have proposed that there is preferential incorporation of the related lipid, cholesterol, into the inner monolayer of phosphatidylcholine vesicles (47). More recently, it has been demonstrated that as much as 5 mol% cholesteryl palmitate can be incorporated into the highly curved bilayer of vesicles containing egg PC (76) or dipalmitoyl-phosphatidylcholine (39). By way of contrast, less than 0.5 mol% can be incorporated into the much less curved bilayers of multilamellar liposomes of these same lipids (215). In view of this evidence, it is possible that more 5-doxyl cholesteryl

palmitate incorporates into the inner layer of vesicles where surface curvature is higher.

Asymmetric distribution of lipids across membranes has been reported previously (216), and current discussions (144) suggest this arrangement is important physiologically since it results in a suitable matrix for enzymes found only on one side of a membrane. In the case of cholesteryl esters, the possibility that there is preferential incorporation into the more highly curved regions of the bilayers may be relevant to an appreciation of the role of cholesteryl esters within the cell. Evidence indicates that some cholesteryl esters are formed inside the cell by enzymes bound to the endoplasmic reticulum (72). The endoplasmic reticulum is a highly convoluted network of tubes and cisternae, containing regions of very high curvature. If the cholesteryl esters exhibit preferential incorporation into the more highly curved regions of the endoplasmic reticulum, there would exist cholesteryl ester-rich regions adjacent to hydrolytic enzymes. Indeed, Goodman (75) has shown microsomes, derived from the endoplasmic reticulum, contribute as much as 32% of the total hydrolytic activity of liver homogenates.

It must also be considered that different packing densities may exist in the two opposing surfaces of the egg PC vesicles. Different lipid packing in the inner and the outer monolayers of the vesicle is a possible consequence of the difference in

the curvature of the two monolayers (166). Considering only geometric arguments, the opposite sign of curvature for the two monolayers predictably would lead to tighter packing near the aqueous interface, including the phospholipid carbonyl region, of the inner monolayer. On the other hand, near the centre of the bilayer it is predicted that the acyl chains of the inner monolayer would be subject to less motional restriction than in the outer monolayer.

One potential means of differentiating between asymmetric distribution of the spin-labelled ester and different packing densities on opposing vesicle surfaces is the addition of ascorbic acid to freshly sonicated vesicles containing the cholesteryl ester. If during the time span of the experiment the vesicles remain impermeable to ascorbic acid, only spin-labelled ester in the outer half of the vesicle will be reduced while the signal remaining from the cholesteryl ester on the inner half of the vesicle will reveal the amount of ester at the inner surface. This experiment was not attempted by the author.

The distance separating the nitroxide moiety and phospholipid acyl chain, at the nearest point, cannot be estimated through application of equations 3.30 or 3.31. The induced spin-lattice relaxation rate depends on both the distance separating the spin label from the phospholipid, r, and the number of spin labelled molecules, N. If one could assume a uniform distribution of 5-doxyl cholesteryl palmitate

throughout the vesicle, then N could be estimated, knowing the actual ratio of spin labelled ester to phospholipid. However, the observation of a differential enhancement of the spin-lattice relaxation rate of the carbonyl resonance inside the vesicle raises the possibility that distribution of the spin label is not uniform.

C. Spin-Lattice Relaxation in the Presence of 16-Doxyl Cholesteryl Stearate

Table 10 presents the spin-lattice relaxation times and the induced relaxation rates of the phospholipid acyl chain positions measured at 25.15 MHz in the presence of 16-doxyl cholesteryl stearate (II). When the nitroxide moiety is placed near the methyl terminus of the ester acyl chain, the magnitude of the induced relaxation rate is small. Within experimental error, $1/T_{1,GL}$ appears to be approximately constant over the length of the acyl chain as shown in Figure 40. In contrast to Figures 36 and 37, no apparent trend is visible nor are any maxima conspicuous.

The induced relaxation rate at a given chain positon depends on the juxtaposition of the spin label relative to a specific position as well as the number of spin labelled molecules incorporated into the vesicle. Solubility measurements of cholesteryl esters in egg PC vesicles

demonstrate that the incorporation of Label II is 30 to 50% less than Label I. The absence of any obvious pattern in Figure 40 may be the result of low incorporation of 16-doxyl cholesteryl stearate into the egg PC vesicles. As a consequence of reduced ester incorporation, the relaxation rates due to the presence of the spin label will be small, and experimental uncertainty may obscure any existing trend such that its detection is impossible.

An alternate explanation for the small but general influence of Label II may be rapid, large-amplitude motions of the ester acyl chain terminus. Accordingly, at any instant in time, the nitroxide moiety may be adjacent to any phospholipid chain position. As a consequence, the induced relaxation rate would be approximately constant.

This latter hypothesis is supported by the results of EPR experiments reported by Grover et al. (79). At 23°C the EPR spectra of egg PC multilayers containing Label II are characterized by sharp, well resolved lines indicating something close to isotropic motion. This high degree of motional freedom is further demonstrated by the low value of the order parameter, $S_{EPR} = 0.029$, determined from the spectra. Furthermore, ascorbic acid reduction of 16-doxyl cholesteryl stearate to the corresponding hydroxylamine occured with a half-life of ~16 minutes which was, within experimental error, identical to that observed with Label I.

Table 10

Spin-lattice Relaxation Times (sec) and Induced Relaxation Rates of Vesicles Containing 16-Doxyl Cholesteryl Stearate

Acyl Chain Position	Spin-lattice Relaxation Time	Induced Relaxation Rate
C1	1.06 (+/-0.11)	0.51 (+/-0.09)
C2	0.21 (+/-0.02)	0.00 (+/-0.72)
C3	0.23 (+/-0.02)	0.64 (+/-0.56)
$(CH_2)_n$	0.33 (+/-0.03)	0.25 (+/-0.40)
C8 Oleic	0.37 (+/-0.04)	0.07 (+/-0.37)
C9 Oleic	0.41 (+/-0.04)	0.44 (+/-0.31)
C10 Lino	0.57 (+/-0.06)	0.42 (+/-0.21)
C11 Lino	0.45 (+/-0.05)	0.05 (+/-0.31)
w-2	0.48 (+/-0.05)	0.54 (+/-0.26)
w-1	0.87 (+/-0.09)	0.30 (+/-0.14)
w	1.33 (+/-0.15)	0.40 (+/-0.08)

Figure 40. ^{13}C NMR spin label-induced spin-lattice relaxation rates due to 1.2 mol% 16-doxyl cholesteryl stearate in 20% w/v egg phosphatidylcholine vesicles at 25.15 MHz and 30 °C

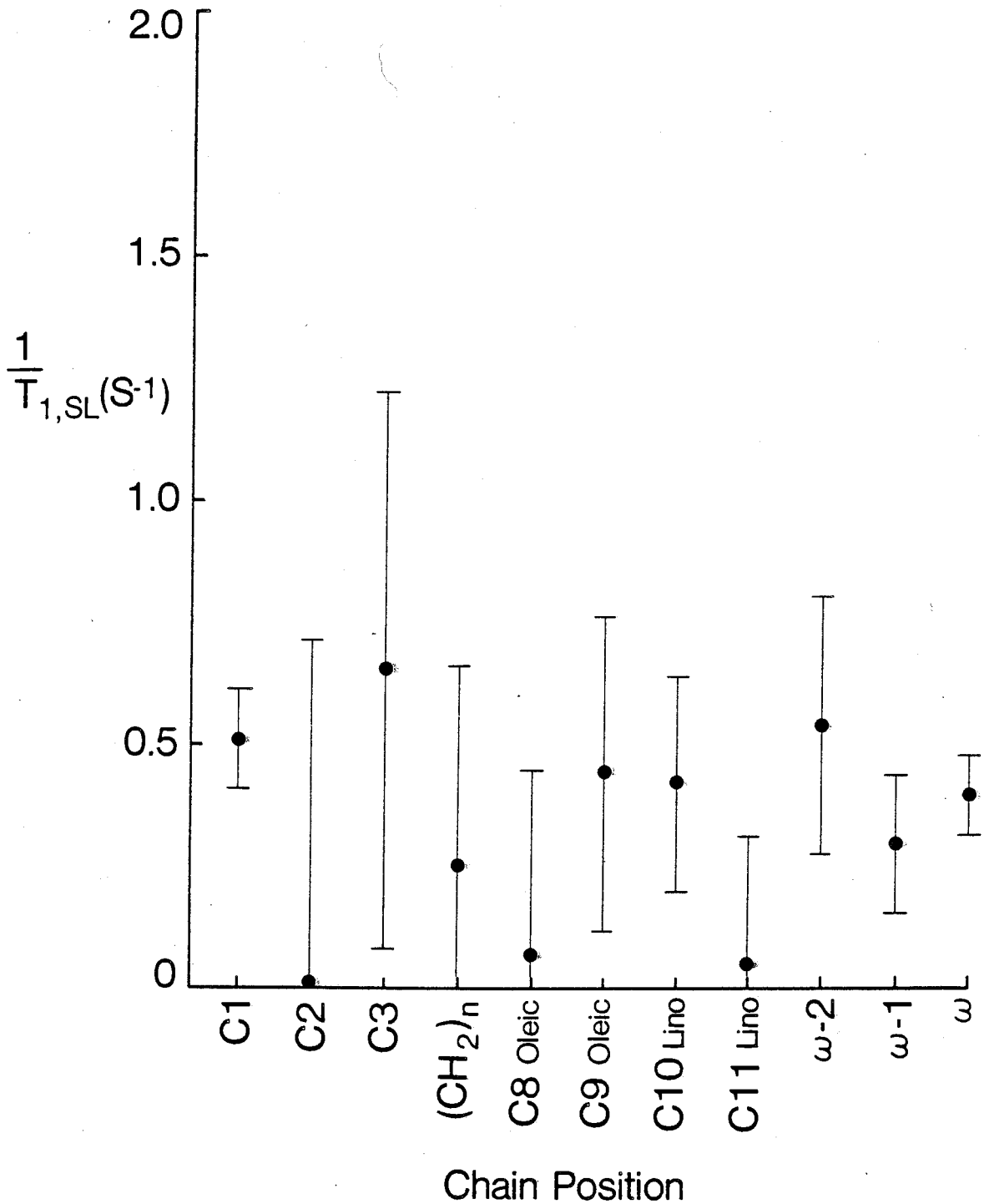
2.0
1.5
1.0
0.5
0
$\frac{1}{T_{1,SL}(S^{-1})}$
C1
C2
C3
$(CH_2)_n$
C8 Oleic
C9 Oleic
C10 Lino
C11 Lino
ω-2
ω-1
ω
Chain Position

Additional support for this postulate is provided by studies of monolayers composed of spin labelled palmitic or stearic acids where the nitroxide is attached to selected sites along the length of the acyl chain (31). In the strictest sense monolayers are not completely analogous to membranes (156). Nevertheless, to the extent that a monolayer represents one half of a bilayer, the comparison is valid. Surface pressure-area/molecule curves indicate a marked dependence on the position of the nitroxide ring along the acyl chain (31). When the carboxyl function of the fatty acid and the doxyl ring are close together, as in the case of 5-doxyl palmitic acid, they essentially form a single polar group. However, when the doxyl ring is shifted to the 12- or 16-position of stearic acid, the bipolar nature of the molecule becomes evident. In the case of fatty acids labelled near the methyl end of the chain, two different conformations are proposed. The first conformation is fully extended while the second is bent such that the nitroxide moiety is close to the aqueous interface. Similar behaviour has been observed using methyl esters of the respective fatty acids as well as spin labelled phospholipids (31). According to Cadenhead and Muller-Landau (31), the fully extended and bent conformations represent the two extremes of a dynamic equilibrium, and therefore all conformations between these extremes must also exist. In the case of methyl 12-doxyl stearate in egg PC these authors estimate that ~15% of the

molecules exist in the bent conformation.

Both the EPR evidence and monolayer studies suggest that rapid acyl chain motion occuring over a large amplitude is the more plausible explanation for the non-specific effect of 16-doxyl cholesteryl stearate on phospholipid relaxation rates. This interpretation runs counter to the observations of Godici and Landsberger (69). In analogous experiments to those reported here, Godici and Landsberger, using fatty acid labelled at the 16-position, report a clear maximum in $1/T_{1,SL}$ at the anti-penultimate (w-2) chain position. The authors report the effect of 16-doxyl stearic acid is more specific than that of 5-doxyl palmitic acid. It is difficult to reconcile the fatty acid results with the NMR data presented here. Moreover, Grover et al. (79) report an order parameter of 0.055 +/- 0.004 using 16-doxyl stearic acid while in the case of 5-doxyl palmitic acid, the order is 0.535 +/- 0.04. The effect of pH on the relative population of each conformer predicted by Cadenhead and Muller-Landau is unknown; however, it is known that the population of the bent conformer is temperature sensitive and decreases with increasing temperature (31). In this regard, it should be indicated that the experiments reported by Godici and Landsberger were performed at pH 8.0 (69) while the NMR experiments reported here, the monolayer studies (31) and the EPR investigations (79) were conducted in the range pH 6.0 to 7.4.

D. Spin-Lattice Relaxation in the Presence of Label IV

Label IV is the palmitic acid ester of the spin labelled sterol 1'-hydroxy-3β-di-n-propyl-17,17-aza-17a-D-homo(5α)-androstanoxyl-17a (label III). Steroid III is a reasonable analogue of cholesterol, and cholesterol has been shown previously to insert into bilayers such that the 3'-hydroxyl function is near the carbonyl region of the phospholipid, oriented toward the aqueous interface while the long molecular axis is approximately parallel to the phospholipid acyl chains (233). Unlike more frequently used spin labelled cholesterol analogues (30) which are labelled in the A-ring, Label III is labelled in the D-ring. The ^{13}C spin lattice relaxation times of egg PC acyl chains, measured in the presence of Label IV, and the induced relaxation rates are presented in Table 11.

Comparison of Table 11 with Table 10 or Figures 36 and 37 reveals that, in general, the magnitude of the induced relaxation rate, $1/T_{1,SL}$, is greater in the presence of Label IV than in the presence of 5-doxyl cholesteryl palmitate or 16-doxyl cholesteryl stearate. Measurement of the solubility of 5-doxyl cholesteryl palmitate in egg PC vesicles reveals that essentially all of the ester is incorporated into the vesicles. Clearly then. the incorporation of Label IV cannot be higher than that of 5-doxyl cholesteryl palmitate, and therefore the increment in the induced relaxation rate observed with Label IV

Table 11

Spin-lattice Relaxation Times (sec) and Induced Relaxation Rates of Vesicles containing Label IV

Acyl Chain Position	Spin-lattice Relaxation Time	Induced Relaxation Rate
C1	0.54 (+/-0.05)	1.42 (+/-0.19)
C2	0.15 (+/-0.02)	1.40 (+/-0.85)
C3	0.15 (+/-0.02)	2.96 (+/-0.75)
$(CH_2)_n$	0.16 (+/-0.02)	3.47 (+/-0.68)
C8 Oleic	0.15 (+/-0.02)	4.04 (+/-0.71)
C9 Oleic	0.35 (+/-0.04)	0.86 (+/-0.35)
C10 Lino	0.26 (+/-0.03)	2.51 (+/-0.40)
C11 Lino	0.22 (+/-0.02)	2.37 (+/-0.50)
w-2	0.24 (+/-0.02)	2.63 (+/-0.45)
w-1	0.34 (+/-0.03)	2.09 (+/-0.30)
w	0.57 (+/-0.06)	1.40 (+/-0.17)

over Label I cannot be the consequence of increased incorporation of Label IV. Inspection of equations 3.30 and 3.31 indicates that the spin-lattice relaxation rate of a ^{13}C nucleus varies directly with the correlation time t_c. For purposes of this discussion, consider t_c to be the average time interval before a nucleus is displaced laterally from a given lattice site. In the case of spin label induced relaxation, though, the correlation time in equation 3.30 and 3.31 is related to the length of time that the nitroxide moiety is adjacent a given nucleus. It is important to note that the definition here does not apply to rotational motion about the molecular axis of symmetry, since in the case of both the fatty acyl chain of the ester and the spin labelled sterol, this type of (rapid) motion is always present. The acyl chains of both Label I and II are very flexible. As a result, the correlation time may be much shorter near the methyl end of the chain than it is at the C1 or C2 position where the acyl chain is anchored to a bulky steroid. Steroid molecules composed of four fused rings, on the other hand, are rigid, and the correlation time in this case will be the time required for the lateral displacement of the entire molecule. Since the correlation time of the steroid portion of Label IV will be long, the spin label will spend more time adjacent to a given carbon nucleus.

When the induced relaxation rate is plotted against acyl chain position, as in Figure 41, a small maximum is evident at

Figure 41. ^{13}C NMR spin label-induced spin-lattice relaxation rates due to 1.7 mol% label IV in 20% W/V egg phosphatidylcholine vesicles at 25.15 MHz and 30 °C

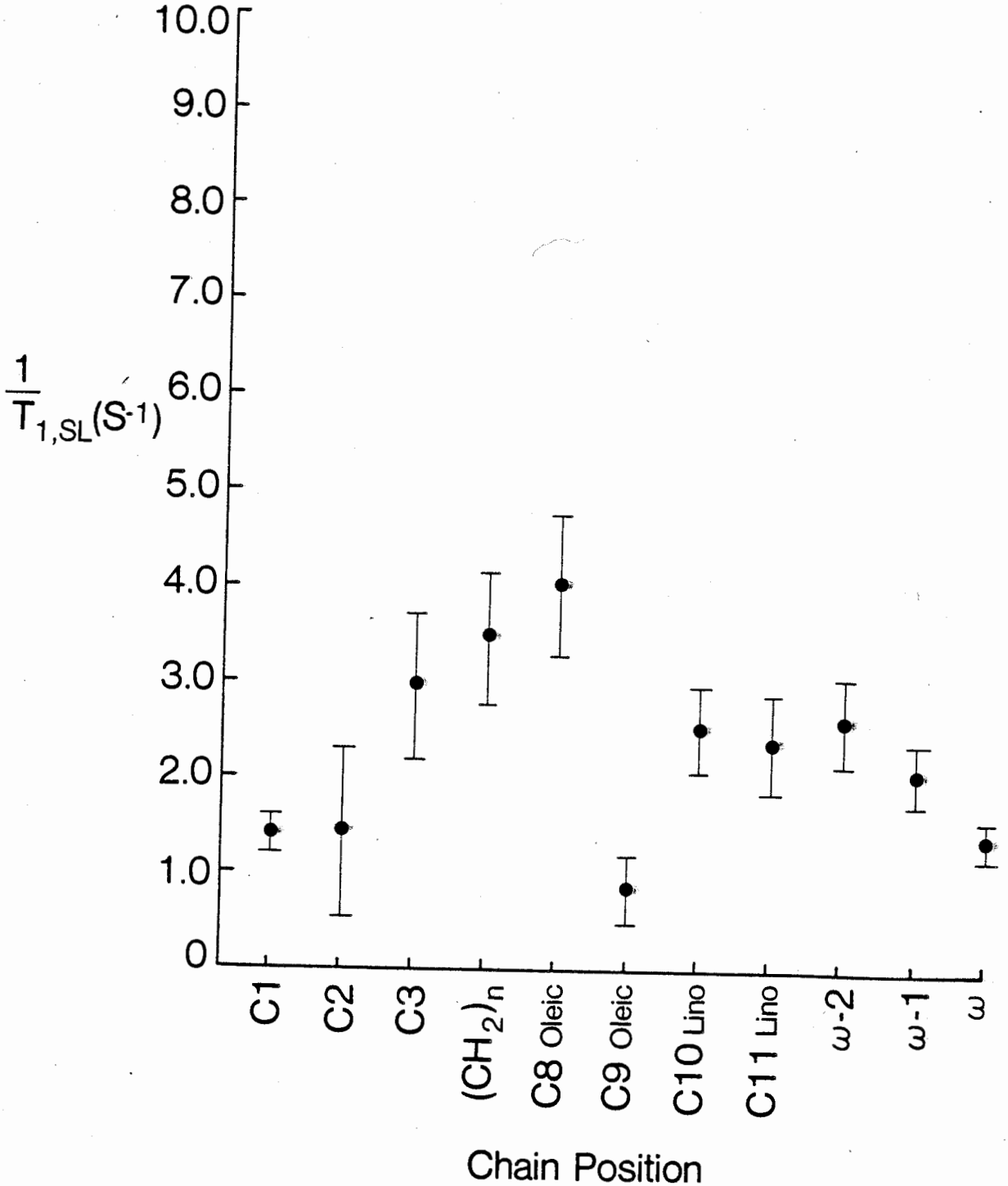
10.0
9.0
8.0
7.0
6.0
5.0
4.0
3.0
2.0
1.0
0
1/T1,SL(S-1)
C1
C2
C3
(CH2)n
C8 Oleic
C9 Oleic
C10 Lino
C11 Lino
ω-2
ω-1
ω
Chain Position

the C8 position. This suggests that the D-ring of label IV, on average is located at the same depth as C8 of the phospholipid acyl chains. It is also evident from Figure 41 that the distal methylene positions of the phospholipid chains are influenced to a greater extent than the carbonyl position. This suggests a pendulum-like swinging of the phospholipid acyl chains toward the D-ring of the ester. These results are consistent with an ester conformation which, on average, resembles a horseshoe.

E. Spin-Lattice Relaxation in the Presence of Label III

The precursor of Label IV, Label III, has been included in these studies for purposes of comparison. The spin-lattice relaxation times in the presence of Label III are presented in Table 12. The data are illustrated in Figure 42. A slight maximum may exist at C8 of the acyl chains. As demonstrated in Figure 42, the methylene positions near the methyl terminus are also affected by Label III indicating motion of the acyl chains. The trend between C2 and C8 is not well defined. This may be be due to reasons discussed earlier, i.e., one might predict the bipolar character of the sterol will produce motions in Label III such that the D-ring oscillates closer to the aqueous interface. If this prediction is accurate, it is clear that the sterol does not invert in the bilayer since the carbonyl of the phospholipid is the least affected by Label III.

Table 12

Spin-lattice Relaxation Times (sec) and Induced Relaxation Rates of Vesicles Containing Label III

Acyl Chain Position	Spin-lattice Relaxation Time	Induced Relaxation Rate
C1	0.56 (+/-0.06)	1.35 (+/-0.18)
C2	0.11 (+/-0.01)	3.82 (+/-1.05)
C3	0.14 (+/-0.01)	3.44 (+/-0.80)
$(CH_2)_n$	0.14 (+/-0.01)	4.36 (+/-0.76)
C8 Oleic	0.13 (+/-0.01)	5.06 (+/-0.81)
C9 Oleic	0.18 (+/-0.02)	3.56 (+/-0.59)
C10 Lino	0.30 (+/-0.03)	2.00 (+/-0.35)
C11 Lino	0.15 (+/-0.02)	4.49 (+/-0.70)
w-2	0.18 (+/-0.02)	4.02 (+/-0.36)
w-1	0.27 (+/-0.03)	2.85 (+/-0.38)
w	0.39 (+/-0.04	2.21 (+/-0.25)

Figure 42. ^{13}C NMR spin label-induced spin-lattice relaxation rates due to 1.7 mol% label III in 20% W/V egg phosphatidylcholine vesicles at 25.15 MHz and 30 °C

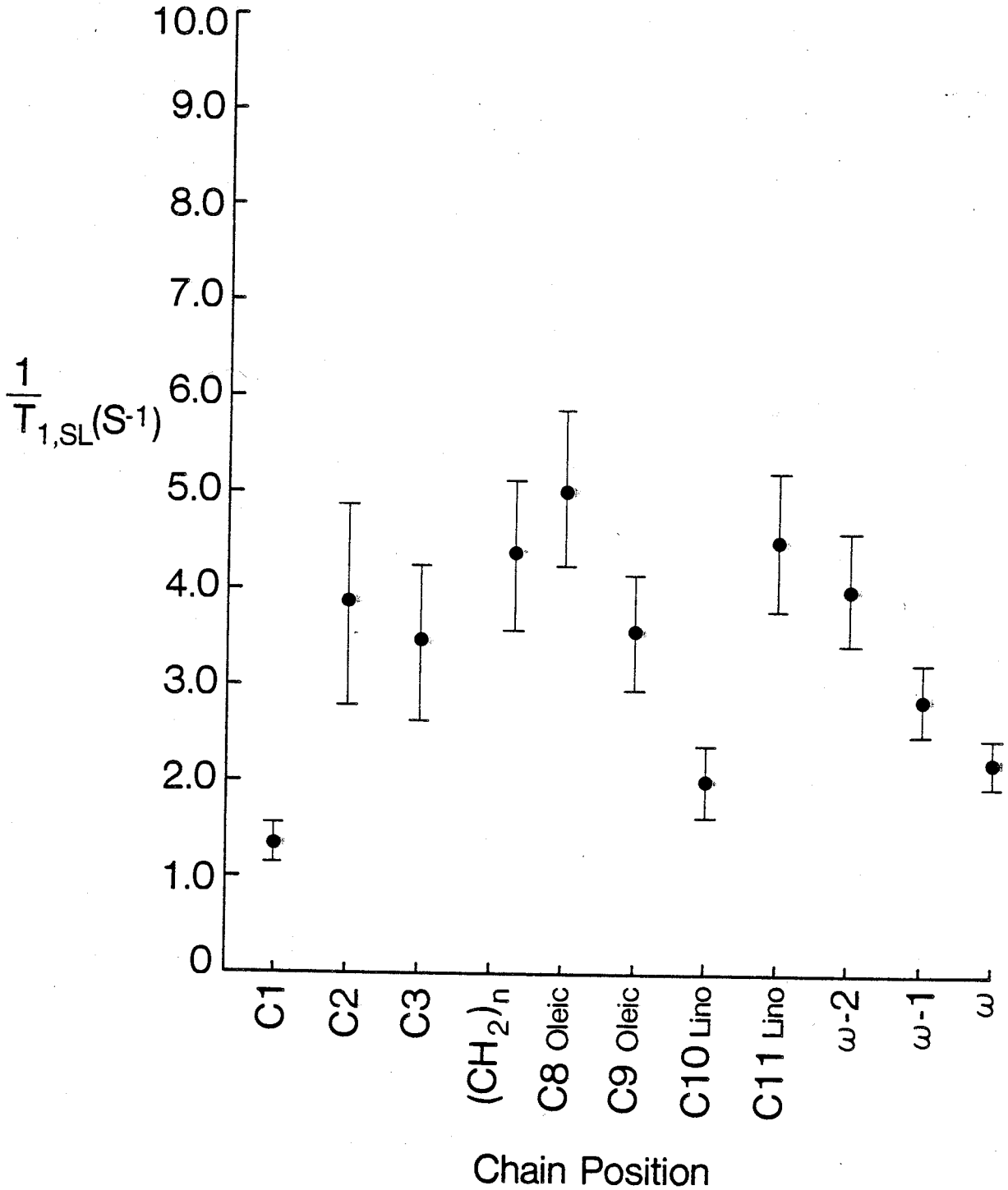
10.0
9.0
8.0
7.0
6.0
5.0
4.0
3.0
2.0
1.0
0
1/T1,SL(S-1)
C1
C2
C3
(CH2)n
C8 Oleic
C9 Oleic
C10 Lino
C11 Lino
ω-2
ω-1
ω
Chain Position

Chapter 5

Conclusions

The principal focus of the present investigations has been the study of the dynamics and organization of lipids in fresh human low density lipoprotein and model membranes. The investigation proceeded in three stages as follows:

A. Specifically Deuterated Cholesteryl Oleate in LDL_2

Specifically deuterated cholesteryl oleate has been successfully transferred into fresh human LDL_2, using lipid exchange proteins present in whole serum. Preliminary investigations using cholesteryl [1-^{14}C]oleate determined that ~8% of the cholesteryl esters in LDL_2 are exchanged using this technique. Gel permeation chromatography experiments indicate no protein-free structures are present in the isolated lipoprotein. Both native (unlabelled) and labelled LDL_2 were examined by negative staining electron microscopy, and no change was detected in the particle size of native LDL_2 during the cholesteryl ester exchange procedure.

The deuterium spin-lattice relaxation times T_1 for cholesteryl oleate in LDL_2 are shortest for segments close to the carbonyl group and increase progressively toward the

terminal methyl group of the cholesteryl ester acyl chain. This indicates that molecular motion increases toward the methyl terminus of the acyl chain.

Orientational order at the site of the deuterium nucleus was quantified by ^2H NMR through the order parameter, S_{CD}. In general, the order parameters decrease gradually as one progresses from chain positions near the sterol moiety toward the methyl terminus of the acyl chain. More importantly, the NMR spectra observed at the 2- and 5-positions of the cholesteryl ester acyl chain reveal a superposition of resonances indicating the coexistence of two distinct regions or domains of cholesteryl ester within the core of LDL_2. The order parameter values determined for the less ordered domain agree very closely with results of EPR experiments using cholesteryl 12-doxyl stearate in LDL_2 at 37 °C (114). By way of contrast, these order parameters are significantly lower than those observed using cholesteryl palmitate in reconstituted high density lipoprotein (HDL) at the same temperature (151). This is due, in part, to the fact that LDL_2 contains triglycerides whereas no triglycerides were present in reconstituted HDL. Upon storage of the labelled lipoprotein for periods of up to eight weeks, the mid-height linewidths of the observed spectra decrease 15-32% indicating a time-dependent change in orientational order within the core of LDL_2.

The linewidths observed at chain positions between the steroid moiety and the olefinic region decrease sharply with increasing temperature up to ~35 °C. This significant decrease cannot be fully explained as being the consequence of decreasing viscosity with rising temperature, and thus indicates a decrease in orientational order within the core of LDL_2. Above 35 °C, the linewidths remain relatively constant thus indicating completion of the phase transition. This behaviour is manifest in both cholesteryl ester domains. Therefore the linewidths indicate cholesteryl oleate is significantly less ordered, at physiological temperature, yet a finite amount of order is still present. At 15 °C the more ordered domain of cholesteryl oleate labelled at the 2-position constituted 60% of the total NMR signal attributed to the ester and, within experimental error, this figure remained constant with increasing temperature. However, at the 5-position, the domain of higher order decreased steadily as the temperature was increased. We are unable to conclude whether or not the relative population of the two domains is temperature sensitive. Positions near the methyl terminus of the cholesteryl ester acyl chain appear less sensitive to the phase behaviour of the lipoprotein core. At these chain positions the linewidths decrease monotonically with no inflection near 35 °C. This is in accord with calorimetric studies (10) indicating chain positions between the beginning of the olefinic region and the

methyl terminus contribute little to the phase behaviour of cholesteryl esters.

B. Selectively Deuterated Palmitic Acid in LDL_2

Selectively deuterated palmitic acid was incorporated into the outer monolayer of LDL_2. Gel permeation chromatography demonstrated that no protein-free structures were generated during the incorporation of the palmitic acid probe. The effect of fatty acid incorporation was monitored by ^{31}P NMR. The phosphorus NMR spectra of labelled and native LDL_2 were similar. In particular, the mid-height linewidths in both spectra were identical, within experimental error, indicating no change in the size of the lipoprotein particle upon incorporation of palmitic acid.

At chain positions 2 through 12, the ^2H NMR spectra reveal a superposition of resonances indicating clearly the coexistence of two regions of significantly different order within the outer shell of LDL_2. The order parameters determined for the less ordered region remain essentially constant from positions 2 through 12. In this region the S_{CD} values agree well with order parameters measured in phospholipid vesicles (152). In the more highly ordered domain, S_{CD} values remain approximately constant over at least the first 6 acyl chain positions. In this region,

the order parameter values are greater than those observed in phospholipid liposomes (153,175). The NMR data presented here, when considered in concert with NMR data on phospholipid vesicles (152), as well as the enzyme studies of both LDL_2 (2) and cultured cells (62) imply the less ordered phospholipid domain represents a sterol deficient region within the outer monolayer of LDL_2.

Spin-lattice relaxation times measured at selected acyl chain positions generally increase toward the methyl terminus of the acyl chain indicating increased motion away from the phospholipid-aqueous interface.

C. Spin Labelled Esters in Model Membranes.

The progressive development of atherosclerosis is characterized by the deposition of increased amounts of cholesteryl esters in membranes and, in later stages, the fatty streaks and plaques found in major arteries. The data presented here yield insight into the orientation and location of cholesteryl esters in model membranes.

The ^{13}C spin label-induced relaxation rate profile of egg PC vesicles in the presence of 5-doxyl cholesteryl palmitate shows a maximum at the C1-C2 region. This demonstrates that the 5-position of the cholesteryl ester acyl chain is adjacent to this region of the phospholipid acyl chains. The

increased resolution available at 100.6 MHz and 46 °C demonstrates that the enhancement of the relaxation rate of the carbonyl resonance from phospholipids inside the vesicle is ~2.5 times greater than that observed at the outer half of the vesicle. This is due to either a greater incorporation of cholesteryl ester molecules in the inner half of the bilayer, or to tighter packing in the inner half of the monolayer. The data presented here do not allow these two possibilities to be resolved.

In the presence of cholesteryl 16-doxyl stearate, the spin label-induced relaxation rate profile shows a small but general increase in the spin-lattice relaxation rate over the length of the phospholipid acyl chains. It is the opinion of this author that this is due to large-amplitude motions of the cholesteryl ester acyl chain. This interpretation is supported by the data presented in both monolayer studies (31) and EPR investigations (79).

In the presence of Label IV, the spin label-induced relaxation rate shows a maximum near C8 of the phospholipid acyl chain, indicating that, on average, the D-ring of the spin labelled sterol is located in the bilayer at a similar depth as the C8 position of the phospholipid.

When viewed in total, these data are consistent with a cholesteryl ester conformation which, on average, resembles a "horseshoe" such that the carbonyl group of the cholesteryl ester

is oriented toward the aqueous interface, while both the sterol moiety and the acyl chain extend into the hydrophobic interior of the vesicle bilayer. Moreover, the D-ring of the sterol is located near the C8 position of the phospholipid acyl chains while the C5 position of the cholesteryl ester acyl chain is located near the C1-C2 positions of the phospholipid. Positions on the cholesteryl ester acyl chain distal to the C5 position may undergo large-amplitude motions as indicated by the non-specific effect of cholesteryl 16-doxyl stearate on the spin-lattice relaxation rate of phospholipid acyl chains. It is also evident that phospholipid acyl chain positions near the centre of the bilayer undergo some "pendulum-like" motions as indicated by the enhanced relaxation rates in the presence of either Label III or Label IV.

Bibliography

1. Abragam, A. (1961), "The Principles of Nuclear Magnetism" Oxford University Press, Oxford.

2. Aggerbeck, L. P., Kezdy, F. J., and Scanu, A. M. (1976), J. Biol. Chem. 251, 3823-3830.

3. Alecio, M. R., Veatch, W. R., and Rands, R. R. (1982), Proc. Natl. Acad. Sci. U.S.A.

4. Allerhand, A., Doddrell, D., and Komoroski, R. (1971), J. Chem. Physics 55, 189-198.

5. Ames, B. N. (1966), "Methods in Enzymology" Vol. 8, (E. F. Neufeld, and V. Gimgurg, eds.) Academic Press, New York.

6. Assmann, G., Highet, R. J., Sokoloski, E. A., and Brewer, H. B. Jr. (1974), Proc. Natl. Acad. Sci. U.S.A. 71, 3701-3705.

7. Atkinson, D., Deckelbaum, R. J., Small, D. M., and Shipley, G. G. (1977), Proc. Natl. Acad. Sci. U.S.A. 74, 1042-1046.

8. Atkinson, D., Small, D. M., and Shipley, G. G. (1980), Annals N. Y. Acad. Sci. 348, 284-299.

9. Barnes, R. G. and Bloom, J. W. (1973), Molec. Phys. 25, 493-494.

10. Barrall, E. D. and Johnston, J. F. (1974), "Liquid and Plastic Crystals" Vol. 2, Chapter 10, (G. W. Gray, and P. A. Winsor eds.) Ellis Horwood Ltd. Chichester.

11. Batchelor, J. G., Prestegard, J. H., Cushley, R. J., and Lipsky, S. R. (1972), Biochem. Biophys. Res. Commun. 48, 70-74.

12. Bloch, F. (1946), Physical Review 70, 460-473.

13. Bloch, F., Hansen, W. W., and Packard, M. (1946), Physical Review 70, 474-485.

14. Bloembergen, N., Purcell, E. M., and Pound, R. V. (1948), Physical Review 73, 679-712.

15. Bloom, M. and Smith, I. C. P. (1984), in press.

16. Bloom, M., Burnell, E. E., MacKay, A. L., Nichol, C. P., Valic, M. I., and Weeks, G. (1978), Biochemistry 17, 5750-5762.

17. Bovey, F. A. (1972), "High Resolution NMR of Macromolecules" Academic Press, New York.

18. Brainard, J. R. and Cordes, E. H. (1981), Biochemistry 20, 4607-4617.

19. Brainard, J. R., and Szabo, A. (1981), Biochemistry 20, 4618-4628.

20. Brown, M. F. (1979), J. Magn. Reson. 35, 203-215.

21. Brown, M. F. (1982), J. Chem. Phys. 77, 1578-1599.

22. Brown, M. S., Deuel, T. F., Basu, S. K., and Goldstein, J. L. (1978), J. Supramolec. Struct. 8, 223-224.

23. Brown, M. S., Faust, J. R., and Goldstein, J. L. (1975), J. Clin. Invest. 55, 783-793.

24. Brown, M. S. and Goldstein, J. L. (1976), Science 191, 150-154.

25. Brown, M. S., Kovanen, P. T., and Goldstein, J. L. (1980), Ann. N. Y. Acad. Sci. 348, 48-67.

26. Brown, M. F., Ribeiro, A., and Williams, G. D. (1983), Proc. Natl. Acad. Sci. 809, 4325-4329.

27. Brown, M. F., Seelig, J., and Habrien, U. (1979), J. Chem. Phys. 70, 5045-5053.

28. Burnell, E. E., Cullis, P. R., and de Kruijff B. (1980), Biochim. Biophys. Acta. 603, 63-69.

29. Burnett, L. J., and Muller, B. H. (1971), J. Chem Phys. 55, 5829-5831.

30. Butler, K. W. and Smith, I. C. P. (1978), Can. J. Biochem. 56, 117.

31. Cadenhead, D. A. and Muller-Landau, F. (1975), "Monolayers" (E. D. Goddard, editor), Am. Chem. Soc., Washington, D. C.

32. Cameron, D. G., Casal, H. L., Gudgin, E. F., and Mantsch, H. H. (1980), Biochim. Biophys. Acta. 596, 463-467.

33. Carrington, A. and McLachlan, A. D. (1967), "Introduction to Magnetic Resonance" Harper & Row, New York.

34. Chapman, D. (1975), Quart. Rev. Biophys. 8, 185-235.

35. Cornwell, D. G., Geer, J. C., and Panganamala, R. V. (1975), "International Encyclopedia of Pharmacology and Therapeutics" (E. J. Masaro, and G. Peters eds) Pergamon Press, Oxford.

35A. Craig, I. F., Via, D. P., Sherrill, B. C., Sklar, L. A., Mantulin, W. W., Gotto, A. M., and Smith, L. C. (1982), J. Biol. Chem. 257, 330-335.

36. Craven, B. M. and Guerina, N. G. (1979), Chem. Phys. Lipids 29, 91-98.

37. Curatolo, W., Verma, S. P., Sakura, J. B., Small, D. M., Shipley, G. G., and Wallach, D. F. A. (1978), Biochemistry, 1802-1807.

38. Cushley, R. J. and Forrest, B. J. (1977), Can. J. Chem. 55, 210-226.

39. Cushley, R. J., Gorrissen, H., and Wassall, S. R. (1980), Can. J. Chem. 58, 2433-2441.

40. Davis, J. H. (1983), Biochim. Biophys. Acta, 737, 117-171.

41. Davis, J. H., Maraviglia, W., Weeks, G., and Godin, D. V. (1979), Biochim. Biophys. Acta 550, 362-366.

42. Deckelbaum, R. J., Shipley, G. G., Small, D. M., Lees, R. S., and George, P. K. (1975), Science 190, 392-394.

43. Deckelbaum, R. J., Shipley, G. G., and Small, D. M. (1977), J. Biol. Chem. 252, 744-754.

44. Derbyshire, W., Govin, T., and Warner, D. (1969), Molec. Phys. 17, 401-417.

45. Delmelle, M., Butler, K. W., and Smith, I. C. P. (1980), Biochemistry 19, 698-704.

46. De Kruijff, B., Cullis, P. R., and Radda, G. K. (1975), Biochim. Biophys. Acta 406, 6-20.

47. De Kruijff, B., Cullis, P. R., and Radda, G. K. (1976), Biochim. Biophys. Acta 436, 729-740.

48. Deveaux, P. and McConnell, H. M. (1972), J. Am. Chem. Soc. 94, 4475-4481.

49. Dluhy, R. A., Mendolsohn, R., Casal, H. L., and Mantsch, H. H. (1983), Biochemistry 22, 1170-1177.

50. Dobretsov, G. E., Spirin, M. M., Chekrygin, O. V., Karamansky, I. M., Dmitriev, V. M., and Vladimirov, Yu. A. (1972), Biochim. Biophys. Acta 710, 172-180.

51. Doddrell, D., Glushko, V., and Allerhand, A. (1972), J. Chem. Phys. 56, 3683-3689.

52. Dwek, R. A. (1973), "Nuclear Magnetic Resonance (NMR) in Biochemistry" Claredon Press, Oxford.

53. Eisenberg, S. (1980), Ann. N. Y. Acad. Sci. 348, 30-47.

54. Eisenberg, S., Bilheimer, D. W., Levy, R. I., and Lindgren, F. T. (1973), Biochim. Biophys. Acta 326, 361-377.

55. Eisenberg, S. and Levy, R. I. (1975), "Advances in Lipid Research" Vol. 13, 10-12, (R. Paoletti, and D. Kritchevsky eds.) Academic Press, New York.

56. Eisenberg, S. and Olivecrona, T. (1979), J. Lipid Res. 20, 614-623.

57. Farrar, T. C. and Becker, E. D. (1971), "Pulse and Fourier Transform NMR Introduction to Theory and Methods" Academic Press, New York.

58. Finer, E. G. (1974), J. Magn. Reson. 13, 76-86.

59. Finer, E. G., Flook, A. G., and Hauser, H. (1972), Biochim. Biophys. Acta 260, 49-58.

60. Finer, E. G., Flook, A. G., and Hauser, H. (1972), Biochim. Biophys. Acta 260, 59-69.

61. Finer, E. G., Henry, R., Leslie, R. B., and Robertson, R. W. (1975), Biochim. Biophys. Acta 380, 320-337.

62. Fisher, G. J., Freter, C. E., Ladenson, R. C. and Sibert, D. F. (1983), J. Biol. Chem. 258, 11705-11712.

63. Fogelman, A. M., Hokom, M. M., Haberlund, M. E., Tanaka, R. D., and Edwards, P. A. (1982), J. Biol Chem. 257, 14081-14086.

64. Forrest, B. J. and Cushley, R. J. (1977), Atherosclerosis 28, 309-318.

65. Freeman, R., Hill, H. D. W., and Kaptein, R. (1972), J. Magn. Reson. 7, 327-329.

66. Forte, T. M. and Nichols, A. V. (1972), Adv. Lipid Res. 10. 1-41.

67. Gally, H. U., Pluschke, G., Overath, P., and Seelig, J. (1979), 5605-5609.

68. Gent, M. P. N. and Prestegard, J. H. (1977), J. Magn. Reson. 25, 243-262.

69. Godici, P. E. and Landsberger, F. R. (1974), Biochemistry 13, 362-368.

70. Godici, P. E. and Landsberger, F. R. (1975), Biochemistry 14, 3927-3934.

71. Goldstein, J. L., and Brown, M. S. (1974), J. Biol. Chem. 249, 5153-5162.

72. Goldstein, J. L., Dana, S. E., and Brown, M. S. (1974), Proc. Natl. Acad. Sci. U.S.A. 71, 4288-4292.

73. Goldstein, J. L., Dana, S. E., Brunschede, G. Y., and Brown, M. S. (1975), Proc. Natl. Acad. Sci. U.S.A. 72, 1092-1096.

74. Goldstein, J. L., Kita, T., and Brown, M. S. (1983), New Engl. J. Medicine 309, 288-296.

75. Goodman, D. S. (1965), Physiol. Rev. 747-838.

76. Gorrissen, H., Tulloch, A. P., and Cushley, R. J. (1980), Biochemistry, 19, 3422-3429.

77. Gorrissen, H., MacKay, A. L., Wassall, S. R., Valic, M. I., Tulloch, A. P., and Cushley, R. J. (1981), Biochim. Biophys. Acta 644, 266-272.

78. Grover, A. K. and Cushley, R. J. (1979), Atherosclerosis 32, 87-91.

79. Grover, A. K., Forrest, B. J., Buchinski, R. K., and Cushley, R. J. (1979), Biochim. Biophys. Acta 550, 212-221.

80. Gulik-Krzywicki, T., Yates, M., and Aggerbeck, L. P. (1979), J. Mol. Biol. 131, 475-484.

81. Handley, D. A., Arbeeng, C. M., Witte, L. D., Goodman, D. S., and Chien, S. (1983), J. Ultrastructure Res. 83, 43-47.

82. Hamilton, J. A., Cordes, E. H., and Glueck, C. J. (1979), J. Biol. Chem. 254, 5435-5441.

83. Hamilton, J. A., Oppenheimer, N. J., Addleman, R., Clouse, A. P., Cordes, E. H., Steiner, P. M., and Glueck, C. J. (1976), Science 194, 1424-1427.

84. Hamilton, J. A., Oppenheimer, N.J., and Cordes, E. H. (1977), J. Biol. Chem. 252, 8071-8080.

85. Hamilton, J. A. and Small, D. M. (1981), Proc. Natl. Acad. Sci. 78, 6878-6882.

86. Hamilton, J. A. and Small, D. M. (1982), J. Biol. Chem. 257, 7318-7321.

87. Hamilton, J. A., Talkowski, C., Childers, R. F., Williams, E., Allerhand, A., and Cordes, E. H. (1974), J. Biol. Chem. 249, 4872-4878.

88. Hatch, F. T. and Lees, R. S. (1968), "Advances in Lipid Research" Vol. 6, (R. Paoletti, and D. Kritchevsky eds.) Academic Press, New York.

89. Havel, R. J., Elder, H. A., and Bragdon, J. H. (1955), J. Clin. Invest. 34, 1345-1353.

90. Henderson, T. O., Kruski, A. W., Davis, L. G., Glonek, T., and Scanu, A. M. (1975), Biochemistry 14, 1915-1920.

91. Heitman, E. (1982), "Regulation of Serum Lipids by Physical Exercise" CRC Press, Boca Raton, Florida.

92. Hoffer, M. (1981), "Transport Across Biological Membranes" Pitman Advanced Publishing Program, Boston.

93. Hoff, H. F., Bradley, W. A., Henderson, C. L., Gaubatz, J. W., Karagus, M. D., and Gotto, A. M. Jr. (1979), Biochim. Biophys. Acta. 573, 361-374.

94. Hoff, H. F., Heideman, C. L., and Gaubatz, J. W. (1979), "Atherosclerosis V Proceedings of the Fifth International Symposium" Springer-Verlag, New York.

95. Hoff, H. F., Jackson, R. L., Mao, S. J. T., and Gotto, A. M. Jr. (1974), Biochim. Biophys. Acta 351, 407-415.

96. Hoff, H. F., Lee, J. T., Titus, J. L., Jackson, R. L., De Bakey, M. E., and Gotto, A. M., Jr. (1974), Circulation 50, III-6-16.

97. Hsiao, C. Y. Y., Ottaway, C. A., and Wetlaufer, D. B. (1974), Lipids 9, 913-915.

98. Huang, C. (1969), Biochemistry 8, 344-351.

99. Hubbel, W. L. and McConnell, H. M. (1971), J. Am. Chem. Soc. 93, 314-326.

100. Jacobs, R. E. and Oldfield, E. (1981), Prog. NMR Spectrosc. 14, 113-136.

101. Jahnig, F. (1979), Proc. Nat. Acad. Sci. U.S.A. 76, 6361-6365.

102. Jahnig, F., Harlos, K., Vogel, H., and Eibl, H. (1979), Biochemistry 18, 1459-1468.

103. James, E., Wooten, R., Nicoll, A., Turner, P., and Lewis, B. (1977), Circulation 56, Sup. III, p. 21.

104. Janiak, M. J., Loomis, C. R., Shipley, G. G., and Small, D. M. (1974), J. Mol. Biol. 86, 325-339.

105. Janiak, M. J., Small, D. M., and Shipley, G. G. (1976), Biochemistry 15, 4575-4580.

106. Janiak, M. J., Small, D. M., and Shipley, G. G., (1979), J. Lipid Res. 20, 183-199.

107. Janiak, M. J., Small, D. M., and Shipley, G. G. (1979), J. Biol. Chem. 254, 6068-6078.

108. Jarrell, H. C. and Smith, I. C. P. (1983), "The Multinuclear Approach to NMR Spectroscopy", (J. B. Lambert and F. G. Riddell eds.), D. Reidel Publishing Co.

109. Jonas, A. (1977), Biochim. Biophys. Acta 486, 10-22.

110. Kang, S. Y., Gutowsky, H. S., and Oldfield, E. (1979), Biochemistry 18, 3268-3271.

111. Kang, S. Y., Gutowsky, H. S., Hsung, J. C., Jacobs, R., King, T. E., Rice, D., and Oldfield, E. (1979), Biochemistry 18, 3257-3267.

112. Katz, S. S., Shipley, G. G., and Small, D. M. (1976), J. Clin. Invest. 58, 200-211.

113. Katz, S. S., Small, D. M., Shipley, G. G., and Rogers, E. L. (1974), Circulation 50, III-6, 15.

114. Keith, A. D., Mehlhorn, R. J., Freeman, N. K., and Nichols, A. V. (1973), Chem. Phys. Lipids 10, 223-236.

115. Kelusky, E. C., Duforc, E. J., and Smith, I. C. P. (1983), Biochim. Biophys. Acta 735, 302-304.

116. Keough, K. M., Oldfield, E., Chapman, D., and Benyon, P. (1973), Chem. Phys. Lipids 10, 37-50.

117. Keough, K. M. W. and Davis, P. J. (1979), Biochemistry 18, 1453-1459.

118. Kolata, G. (1983), Science 221, 1164-1166.

119. Kreiger, M., Peterson, J., Goldstein, J. L., and Brown, M. S. (1980), J. Biol. Chem. 255, 330-333.

120. Kroon, P. A. (1981), J. Biol. Chem. 256, 5332-5339.

121. Kroon, P. A. and Kreiger, M. (1981), J. Biol. Chem. 256, 5340-5349.

122. Kroon, P. A., Quinn, D. M., and Cordes, E. H. (1982), Biochemistry 21, 2745-2753.

123. Krugh, T. R. (1976), "Spin Labeling Theory and Applications" (L. J. Berliner, editor) Academic Press, New York.

124. Laggner, P. and Muller, K. W. (1978), Quart. Rev. Biophys. 11, 371-425.

125. Laggner, P. and Kostner, G. M. (1978), Eur. J. Biochem. 84, 227-232.

126. Laggner, P., Kostner, G. M., Rakusch, U., and Worcester, D. (1981), J. Biol. Chem. 256, 11832-11839.

127. Lang, P. D. and Insull, W. Jr. (1970), J. Clin. Invest. 49, 1479-1488.

128. Langer, T., Strober, W., and Levy, R. I. (1972), J. Clin. Invest. 51, 1528-1536.

129. Lee, A. G., Birdsall, N. J. M., and Metcalfe, J. C. (1974), "Methods in Membrane Biology" Vol. 2 (E. Korn editor) Plenum Press, New York, p. 2-156.

130. Lewis, B. A. and Engleman, D. M. (1983), J. Mol. Biol. 166, 211-217.

131. Levine, Y. K., Birdsall, N. J. M., Lee, A. G., and Metcalfe, J. C. (1972), Biochemistry 11, 1416-1421.

132. Lichtenberg, D., Peterson, N. O., Giradet, J., Kainosho, M., Kroon, P. A., Seiter, C. H. A., Feigenson, G. W., and Chan, S. I. (1975), Biochim. Biophys. Acta 382, 10-21.

133. Lichtenberg, D. and Zilberman, Y. (1979), J. Magn. Reson. 34, 491-497.

134. Lipari, G. and Szabo, A. (1982), J. Am. Chem. Soc. 104, 4546-4558.

135. Lipari, G. and Szabo, A. (1982), J. Am. Chem. Soc. 104, 4559-4570.

136. Longmuir, K. J. and Dahlquist, F. W. (1976), Proc. Nat. Acad. Sci. 73, 2716-2719.

137. Lowry, O. H., Rosebrough, N. J., Farr, A. L., and Randall, R. J. (1951), J. Biol. Chem. 193, 265-273.

138. Luzzati, V., Tardieu, A., and Aggerbeck, L. P. (1979), J. Mol. Biol. 131, 453-473.

139. MacDonald, G. G. and Leigh, J. S. (1973), J. Magn. Reson. 9, 358-362.

140. MacKay, A. L., Burnell, E. E., Nichol, C. P., Weeks, G. I., Bloom, M., and Valic, M. I. (1978), FEBBS Lett. 88, 97-100.

141. Mantsch, H. H., Saito, H., and Smith, I. C. P. (1977), "Progress in NMR Spectroscopy" (J. W. Emsley, J. Feeney, and J. Sutcliffe eds.), Pergamon Press, London.

142. Metcalfe, J. C., Birdsall, N. J. M., and Lee, A. G. (1973), Ann. N. Y. Acad. Sci. 222, 460-467.

143. Metzler, D. E. (1977), "Biochemistry: The Chemical Reactions of Living Cells" Academic Press, New York.

144. Michaelson, D. M., Horwitz, A. F., and Klein, M. B. (1973), Biochemistry 12, 2637-2645.

145. Miller, N. E., Weinstein, D. B., and Steinberg, D. (1978), J. Lipid Res. 19, 644-653.

146. Nichols, A. V. (1978), "The Lipoprotein Molecule" (H. Peeters editor) Plenum Press, New York.

147. Oldfield, E., Gilmore, R., Glaser, M., Gutowsky, H. S., Hsung, J. C., Kang, S. Y., King, T. E., Meadows, M. and Rice, D. (1978), Proc. Natl. Acad. Sci. U.S.A. 75, 4657-4660.

148. Pace, R. J. and Chan, S. I., (1982), J. Chem. Phys. 76, 4217-4227.

149. Pace, R. J. and Chan, S. I., (1982), J. Chem. Phys. 76, 4228-4240.

150. Pace, R. J. and Chan, S. I., (1982), J. Chem. Phys. 76, 4241-4247.

151. Parmar, Y. I., Gorrissen, H., Wassall, S. R., and Cushley, R. J. (1983), J. Biol. Chem. 258, 2000-2004.

152. Parmar, Y. I., Wassall, S. R., and Cushley, R. J. (1984), J. Am. Chem. Soc. 106, 2434-2435.

153. Pauls, K. P., MacKay, A. L., and Bloom, M. (1983), Biochemistry 22, 6101-6109.

154. Peterson, N. O. and Chan, S. I. (1977), Biochemistry 16, 2657-2667.

155. Phair, R. D., Hammond, M. G., Bowden, J. A., Fried, M., Fisher, W. R., and Bernieu, M. (1975), Fed. Proc. Am. Soc. Exp. Biol. 34, 2263-2270.

156. Philips, M. C. and Chapman, D. (1968), Biochim. Biophys. Acta 163, 301-313.

157. Quinn, P. J. (1981), Prog. Biophys. Molec. Biol. 38, 1-104.

158. Rice, D. and Oldfield, E. (1979), Biochemistry 18, 3272-3279.

159. Richter, H., Srey, C., Winter, K., and Fuerst, W. (1977), Pharmazie 32, 164-169.

160. Rudel, L. L. and Morris, M. D. (1973), J. Lipid Res. 14, 364-366.

161. Sackmann, E. and Trauble, H. (1972), J. Am. Chem. Soc. 94, 4482-4491.

162. Scanu, A. M. (1979), "The Biochemistry of Atherosclerosis" (A. M. Scanu Jr. editor) Marcel Dekker Inc., New York.

163. Scanu, A. M. and Hirz, R. (1968), Nature 218, 200-201.

164. Scanu, A. M., Pollard, H., and Reader, W. (1968), J. Lipid Res. 9, 342-349.

165. Schmidt, C. F., Barenholz, Y., Huang, C., and Thompson, T. E. (1977), Biochemistry, 16, 3948-3953.

166. Schuh, J. R., Banerjee, U., Muller, L., and Chan, S. I. (1982), Biochim. Biophys. Acta 687, 219-225.

167. Sears, B. (1975), J. Memb. Biol. 20, 59-73.

168. Sears, B., Deckelbaum, R. J., Janiak, M. J., Shipley, G. G., and Small, D. M. (1976), Biochemistry 15, 4151-4157.

169. Sears, B., Hutton, W. C., and Thompson, T. E. (1974), Biochem. Biophys. Res. Commun. 60, 1141-1147.

170. Sears, B., Hutton, W. C., and Thompson, T. E. (1976), Biochemistry 15, 1635-1639.

171. Seelig, J. (1977), Quart. Rev. Biophys. 10, 353-418.

172. Seelig, J. and Browning, J. L. (1978), FEBS. Lett. 92, 41-44.

173. Seelig, J., Limacher, H., and Bader, P. (1972), J. Am. Chem. Soc. 94, 6364-6371.

174. Seelig, J. and Niederberger, W. (1974), Biochemistry 13, 1585-1588.

175. Seelig, A. and Seelig, J. (1974), Biochemistry 13, 4839-4845.

176. Seelig, J. and Seelig, A. (1974), Biochem. Biophys. Res. Commun. 57, 406-411.

177. Seelig, J. and Seelig, A. (1980), Quart. Rev. Biophys. 13, 19-61.

178. Seelig, J. and Waespe-Sarcevic, N. (1978), Biochemistry 17, 3310-3315.

179. Seiter, C. H. A. and Chan, S. I. (1973), J. Am. Chem. Soc. 95, 7541-7553.

180. Semenkovich, C. F., Ostlund, R. E., Levy, R. A., and Osa, S. R. (1982), J. Biol. Chem. 257, 12857-12865.

181. Serralach, E. N., de Haas, G. H., and Shipley, G. G., (1984), Biochemistry 23, 713-720.

182. Shapiro, Yu. E., Viktorov, A. V., Volkova, V. I., Barsukov, L. I., Bystrov, V. F., and Bergelson, L. D. (1975), Chem. Phys. Lipids 14, 227-232.

183. Sheetz, M. P. and Chan, S. I. (1972), Biochemistry 11, 4573-4581.

184. Shepherd, J., Bicker, S., Lorimer, A. R., and Packard, C. J. (1979), J. Lipid Res. 20, 999-1006.

185. Singer, S. J. and Nicholson, G. L. (1972), Science 175, 720-731.

186. Singleton, W. S., Gray, M. S., Brown, M. L., and White, J. L. (1965), J. Am. Oil Chem. Soc. 42, 53-56.

187. Slicter, C. P. (1963), "Principles of Magnetic Resonance" (F. Seitz editor) Harper and Row, New York.

188. Sklar, L. A., Craig, I. F., and Pownall, H. J. (1981), J. Biol. Chem. 256, 4286-4292.

189. Sklar, L. A., Matulin, W. W., and Pownall, H. J. (1982), Biochem. Biophys. Res. Commun. 105, 674-680.

190. Smaby, J. M., Baumann, W. J., and Brockman, H. L. (1979), J. Lipid Res. 20, 789-795.

191. Smaby, J. M. and Brockman, H. L. (1981), Biochemistry 20, 118-123.

192. Smaby, J. M. and Brockman, H. L. (1981), Biochemistry 20, 724-730.

193. Small, D. M. (1977), J. Coll. Interface Sci. 58, 581-602.

194. Small, D. M. and Shipley, G. G. (1974), Science 185, 222-228.

195. Smith, E. B. (1979), "Atherosclerosis V Proceedings of the Fifth International Symposium" (A. M. Goto Jr, L. C. Smith, and B. Allen eds.) Springer-Verlag, New York.

196. Smith, I. C. P., Stockton, G. W., Tulloch, A. P., Polnaszek, C. F., and Johnson, K. G. (1977), J. Coll. Interface Sci. 58, 439-451.

197. Solomon, I. (1955), Phys. Rev. 99, 559-565.

198. Soutar, A. K., Myant, N. B., and Thompson, G. R. (1977), Atherosclerosis 28, 247-256.

199. Stein, J. M., Edner, O. J., and Bargoot, F. G. (1968), Science 162, 909-911.

200. Steinberg, D. (1979), Prog. Biochem. Pharmacol. 15, 166-199.

201. Stockton, G. W., Johnson, K. G., Butler, K. W., Tulloch, A. P., Boulanger, Y., Smith, I. C. P., Davis, J. H., and Bloom. M. (1977), Nature 269, 267-268.

202. Stockton, G. W., Polnaszek, C. F., Leitch, L. C., Tulloch, A. P., and Smith, I. C. P. (1974), Biochem. Biophys. Res. Commun. 60, 844-850.

203. Stockton, G. W., Polnaszek, C. F., Tulloch, A. P., Hazan, F., and Smith, I. C. P. (1976), Biochemistry 15, 954-966.

204. Stockton, G. W. and Smith, I. C. P. (1976), Chem. Phys. Lipids 17, 251-263.

205. Stoeffel, W., Tungal, B. D., Zierenberg, O., Schreiber, E., Binczek, E. (1974), Hoppe-Seyler's Z. Physiol. Chemistry 355, 1367-1380.

206. Stuhrmann, H. H., Tardieu, A., Mateu, L., Sardet, C., Luzzati, V., Aggerbeck, L. P., and Scanu, A. M., Jr. (1975), Proc. Natl. Acad. Sci. 72, 2270-2273.

207. Sturtevant, J. M. (1974), Ann. Rev. Biophys. Bioeng. 3, 35-49.

208. Suckling, K. E., Blair, H. A. F., Boyd, G. S., Craig, I. F., and Malcom, B. R. (1979), Biochim. Biophys. Acta 551, 10-21.

209. Tall, A. R., Small, D. M., Atkinson, D., and Rudel, L. L. (1978), J. Clin. Invest. 62, 1354-1363.

210. Tardieu, A., Mateu, L., Sardet, C., Weiss, B., Luzzati, V., Aggerbeck, L., and Scanu, A. M. Jr. (1976), J. Mol Biol. 101, 129-153.

211. Taylor, M. G. and Smith, I. C. P. (1980), Biochim. Biophys. Acta 559, 140-149.

212. Thompson, G. and Sigurdson, G. (1974), Circulation 50, Sup. III, p 272.

213. Tien, H. Ti. (1974), "Bilayer Lipid Membranes (BLM) Theory and Practice" Marcel Dekker, Inc. New York.

214. Treleaven, W. D., Wassall, S. R., and Cushley, R. J. (1983), Chem. Phys. Lipids 33, 223-231.

215. Valic, M. I., Gorrissen, H., Cushley, R. J., and Bloom, M. (1979), Biochemistry 18, 854-859.

216. Van Deenan, L. L. M. (1981), FEBS Lett. 123, 3-13.

217. Vold, R. L., Waugh, J. S., Klein, M. P., and Phelps, D. E. (1968), J. Chem. Phys. 48, 3831.

218. Wassall, S. R., Treleaven, W. D., Parmar, Y. I., and Cushley, R. J. (1982), Biochem. Biophys. Res. Commun. 107, 429-434.

219. Weast, R. C. (1978), "CRC Handbook of Chemistry and Physics" CRC Press Inc. Boca Raton, Florida.

220. Wilkins, M. H. F., Blaurock, A. E., and Engleman, D. M. (1971), Nature New Biology 230, 72-76.

221. Wissler, R. W. (1979), "Atherosclerosis V Proceedings of the Fifth International Symposium" (A. M. Goto Jr., L. C. Smith, and B. Allen eds.) Springer-Verlag, New York.

222. Woessner, D. E. (1962), J. Chem. Phys. 36, 1-4.

223. Worcester, D. L. and Franks, N. P. (1976), J. Mol. Biol. 100, 359-378.

224. Wolber, P. K. and Hudson, B. S., (1981), Biochemistry 20, 2800-2810.

225. Yeagle, P. L., Langdon, R. G., and Martin, R. B. (1977), Biochemistry, 16, 3487-3491.

226. Yeagle, P. L. and Martin, R. B. (1976), Biochem. Biophys. Res. Commun. 69, 775-780.

227. Yeagle, P. L., Martin, R. B., Pottinger, L., and Langdon, R. G. (1978), Biochemistry 17, 2707-2710.